EXPLOSIVE-FREE BREAKAGE OF BIAXIALLY LOADED ROCK USING SOUNDLESS CHEMICAL DEMOLITION AGENTS

By

Tuo Chen

Department of Mining and Materials Engineering

McGill University, Montreal.

May 2023

A thesis submitted to McGill University in partial fulfillment of the requirements of the degree of Doctor of Philosophy

Table of Contents

List of Figures

List of Tables

Abstract

The method of drilling and blasting with explosives is widely used in mining and civil engineering projects such as subsurface space construction and mine development and production. Nevertheless, there has been a global move in the last two decades to transition to low-carbon economies and green mining in response to climate change. This is because blasting with explosives creates by-products such as hazardous gases, strong ground vibrations, fly rocks, noise, and dust. As a result, there has been a growing research interest in developing rock fragmentation techniques that do not rely on explosives. Soundless Chemical Demolition Agents (SCDA) are one of the alternatives to explosives in underground mining operations. SCDA are powdery cementitious products containing primarily calcium oxide (CaO). Once mixed with water, and poured into a borehole in the rock, significant expansion is generated as CaO gradually transforms into portlandite crystals ($Ca(OH)_2$) during the curing process, causing the borehole to fracture under the influence of expansive pressure.

This thesis is part of a multi-phase project focusing on the development of SCDA technique to achieve large-scale hard rock fragmentation in underground mines. More specifically, it involves the investigation of SCDA performance in hard rock environment under biaxial confinement, which is the natural stress condition of a mining front. The thesis begins with a critical review of the history and development of SCDA including its composition, physical properties, fracturing performance, relevant numerical modelling techniques, and current applications in the field. Following the literature review, a number of numerical models of biaxially loaded panels with different SCDA hole patterns were built and examined with using finite difference codes PFC2D and FLAC3D. Five panel models were analyzed and compared, and the optimum designs were retained for further examination with laboratory testing.

The experimental program was carried out on large 1 m x 1m panels made from high-strength concrete and Standstead granite. The concrete panels were subjected to constant biaxial stresses of 15 MPa and 23 MPa, whereas the granite panels were subjected to 26 MPa and 40 MPa. Panels were placed in a biaxial loading frame, which was built specifically for this project. It has a capacity of 10 MN and 6 MN in the vertical and horizontal directions, respectively. All panels are instrumented to monitor applied loads and planar and out-of-plane displacements. The concrete tests were repeated on panels from Stanstead granite.

Various SCDA borehole patterns were examined using discrete-element code PFC2D. Once calibrated against the mechanical properties of the panel material, the PFC model is used to examine and compare different possible borehole patterns in a panel subjected to biaxial stress – a scenario that is analogous to a mining front. The optimum PFC model helped design the borehole pattern for the first concrete panel test with the so-called diamond-shaped hole pattern. In laboratory, such borehole pattern successfully fractured and created craters in the center of concrete and rock panels in 11.8 hours and 3.5 hours, respectively. The relatively short breakage time of hard rock panel shows the promise of using SCDA as an alternative to explosives in underground mining condition. In addition, SCDA induces dominant out-of-plane fractures in biaxially loaded panels, which is further confirmed and analyzed by finite-difference modelling using FLAC3D code. The failure mechanism analysis revealed that the concrete panel experienced ductile tensile failure and eventual shear failure, whereas the granite panel only had brittle tensile failures.

A second series of large-scale experiments was carried out on two granite panels with V-cut hole pattern, where the drill holes are 45° inclined with respect to the panel face. FLAC3D models show that the V-cut pattern can overcome the biaxial confinement and demolish hard rock panel. This

was further confirmed with laboratory testing on a granite panels. Two Panel collapses was observed after 11 hours 53 minutes and 7 hours 29 minutes, respectively, however, it used significantly fewer SCDA holes than the diamond pattern. Thus, the V-test also demonstrates the promise of using SCDA as alternative to explosive-free rock breakage.

The next step in this research dealt with the method of SCDA loading into drill holes. A novel loading method for SCDA slurry loading into horizontal and up-tilted boreholes was developed using 3D-printed cartridges. Four host materials for SCDA, namely thermoplastic polyurethane (TPU), polylactide (PLA), polyethylene terephthalate glycol (PETG), and acrylonitrile butadiene styrene (ABS) are tested in laboratory for rock slab demolition with a single SCDA hole. The best candidate PLA cartridge was selected and implemented in a field trial in an underground mine. This developed loading approach can be utilized for subsurface SCDA applications where pouring SCDA into downhole under gravity cannot be applied.

Finally, to set the stage for the next phase of this multi-phase project involving in-situ tests, a set of guidelines is proposed to serve as a basis for the implementation of SCDA method in underground mining applications.

Résumé

La méthode de forage et de dynamitage avec des explosifs est largement utilisée dans les projets miniers et de génie civil tels que la construction souterraine et le développement et la production de mines. Néanmoins, il y a eu un intérêt croissant pour les méthodes de fragmentation de roche sans explosifs au cours des deux dernières décennies en raison de la transition vers des économies à faible émission de carbone et de l'exploitation minière verte en réponse au changement climatique. En effet, le dynamitage avec des explosifs crée des sous-produits tels que des gaz dangereux, de fortes vibrations au sol, des projections de roches, du bruit et de la poussière. Les agents de démolition chimique silencieux (SCDA) sont l'une des alternatives aux explosifs pour la fragmentation de roche. Les SCDA sont des produits cimentaires pulvérulents qui contiennent principalement de l'oxyde de calcium (CaO). Une fois mélangé avec de l'eau et versé dans un trou de forage dans la roche, une expansion importante est générée lorsque CaO se transforme progressivement en cristaux de portlandite ($Ca(OH)_2$) pendant le processus de durcissement, provoquant la fracture du trou de forage sous l'influence de la pression expansive.

Cette thèse fait partie d'un projet en plusieurs phases axé sur le développement de la technique SCDA pour réaliser une fragmentation à grande échelle de la roche dure dans les mines souterraines. Plus précisément, il s'agit d'étudier les performances du SCDA dans un environnement de roche dure sous confinement biaxial, qui est la condition de contrainte naturelle dans un front minier. La thèse commence par un examen critique de l'histoire et du développement du SCDA, y compris sa composition, ses propriétés physiques, ses performances de fracturation, les techniques de modélisation numérique pertinentes et les applications actuelles dans le domaine. Suite à la revue de la littérature, plusieurs modèles numériques de panneaux chargés biaxialement avec différents modèles de trous SCDA ont été construits et examinés avec le code d'éléments

discrets PFC2D et le code de différences finies FLAC3D. Cinq modèles de panneaux ont été analysés et comparés, et les conceptions optimales ont été retenues pour un examen plus approfondi avec des tests en laboratoire.

Le programme expérimental a été réalisé sur des panneaux de 1 m x 1 m en béton à haute résistance et granit Standstead. Les panneaux de béton ont été soumis à des contraintes biaxiales constantes de 15 MPa et 23 MPa, tandis que les panneaux de granit ont été soumis à 26 MPa et 40 MPa. Les panneaux ont été placés dans un cadre de chargement biaxial, qui a été conçu et construit spécifiquement pour ce projet. Le châssis de chargement a une capacité de 10 MN et 6 MN dans les directions verticale et horizontale, respectivement. Tous les panneaux sont instrumentés pour surveiller les charges appliquées ainsi que les déplacements plans et hors plan. Les essais de béton ont été répétés sur des panneaux de granite de Stanstead.

Divers modèles de trous de forage SCDA ont été examinés à l'aide du code PFC2D. Une fois calibré par rapport aux propriétés mécaniques du matériau du panneau, le modèle PFC est utilisé pour examiner et comparer différents modèles de trous de forage possibles dans un panneau soumis à une contrainte biaxiale - un scénario analogue à un front minier. Le modèle PFC optimal a aidé à concevoir le modèle de trou de forage pour le premier test de panneau de béton avec le modèle de trou dit en forme de losange. En laboratoire, un tel modèle de trou de forage s'est fracturé avec succès et a créé des cratères au centre des panneaux de béton et de roche après 11,8 heures et 3,5 heures, respectivement, à partir du moment où le SCDA est appliqué. Le temps de rupture relativement court du panneau de roche dure montre la promesse d'utiliser le SCDA comme alternative aux explosifs dans les conditions d'exploitation minière souterraine. De plus, le SCDA a induit des fractures hors du plan dans le panneau chargé biaxialement, ce qui est ensuite confirmé et analysé avec la modélisation FLAC3D. L'analyse du mécanisme de rupture a révélé que le

panneau de béton a subi une rupture de traction ductile et éventuellement une rupture de cisaillement, tandis que le panneau de granit n'a présenté qu'une rupture de traction fragile.

Une deuxième série d'expériences à grande échelle a été réalisée sur deux panneaux de granit avec un motif de trous en forme de V, où les trous de forage sont inclinés à 45° par rapport à la face du panneau. Les modèles FLAC3D montrent que le modèle de coupe en V peut surmonter le confinement biaxial et démolir le panneau de roche dure. Cela a été confirmé par des tests en laboratoire sur du granit. On a observé que deux panneaux s'effondraient après 11 heures 53 minutes et 7 heures 29 minutes, cependant, ces tests utilisaient beaucoup moins de trous SCDA que le modèle en losange. Ainsi, le motif en forme de V démontre également la promesse de SCDA en tant que méthode potentielle de rupture de roche sans explosif.

L'étape suivante de cette recherche a porté sur la méthode de chargement de la boue SCDA dans un trou de forage qui ne peut donc pas être rempli par gravité. Une nouvelle méthode de chargement SCDA dans des trous horizontaux et inclinés vers le haut a été développée à l'aide de cartouches imprimées en 3D. Quatre matériaux hôtes pour SCDA, à savoir le polyuréthane thermoplastique (TPU), le polylactide (PLA), le polyéthylène téréphtalate glycol (PETG) et l'acrylonitrile butadiène styrène (ABS) sont testés en laboratoire pour la démolition de dalles rocheuses avec un seul trou SCDA. Le meilleur candidat - la cartouche PLA - a été sélectionné et mis en œuvre avec succès lors d'un essai sur le terrain dans une mine souterraine. Cette méthode peut être utilisée pour les applications SCDA souterraines où il n'est pas possible de verser du SCDA dans un trou de forage.

Enfin, pour se préparer pour la prochaine étape de ce projet comprenant plusieurs phases, un ensemble de lignes directrices est proposé pour servir de base à la mise en œuvre de la méthode SCDA dans les applications minières souterraines.

Acknowledgements

I would like to begin by expressing my deep gratitude to Professor Hani S. Mitri, my supervisor, for his unwavering support, guidance, and instruction throughout the past several years. During my Ph.D. studies, his dedicated mentorship enabled me to explore and advance in the field of mining engineering. Thanks to the countless conversations and discussions with my supervisor, I was able to finish my research project satisfactorily and obtain this degree.

My Ph.D. thesis was financially supported by my supervisor's grant from Natural Resources Canada, Clean Growth Program, Grant No. CGP-17-1003 and industry partner Newmont Corporation. Their support and permission to publish my work are gratefully acknowledged.

I would like to express my sincere gratitude to CanmetMINING for their dedication in conducting large-scale experiments and providing valuable test data. In particular, I want to acknowledge the outstanding efforts of Mr. Ian Bedard and Mr. William Render, whose hard work was crucial to the successful completion of the experiment.

I would like to express my gratitude to my colleagues at the Mine Design Lab - Dr. Isaac Vennes, Dr. Kelly Habib, and Yizhuo Li - for their collaboration, teamwork, and companionship during our time working together and traveling. Additionally, I would like to extend my thanks to Dr. Shahe Shnorhokian for his valuable contributions to the project.

Lastly, I would like to express my heartfelt gratitude for the love, understanding, and unwavering support of my parents. Their dedication has been a constant source of encouragement throughout my life, and I am truly grateful for their guidance and presence in my journey.

Contributions of Authors

The author of this thesis is the primary and corresponding author for all manuscripts listed below. Prof. Hani Mitri is the supervisor of the Ph.D. candidate and the co-author of these manuscripts.

Chapter 3

Chen, T., Vennes, I., & Mitri, H. S. (2022). Investigation into Rock Breakage with Expansive Cement Under Biaxial Confinement. Rock Mechanics and Rock Engineering, 55(10), 6263-6277. https://doi.org/10.1007/s00603-022-02988-4

Chapter 4

Chen, T., Vennes, I., & Mitri, H. S. (2023). Biaxially confined rock breakage with SCDA: large-scale tests and numerical modelling. Rock Mechanics and Rock Engineering, https://doi.org/10.1007/s00603-023-03332-0

Chapter 5

Chen, T., Vennes, I., & Mitri, H. S. (2023). Explosive-free rock breakage under biaxial loading condition using V-cut drill hole pattern, International Journal of Rock Mechanics and Mining Sciences (Under review).

Chapter 6

Chen, T., Habib, K., Li, Y., & Mitri, H. S. (2023). Development of a novel cartridge for expansive cement application to hard rock breakage. CIM Journal (Under review).

List of Abbreviations

ABS:	Acrylonitrile Butadiene Styrene
AE:	Acoustic Emission
BTS:	Brazilian Tensile Strength
DEM:	Discrete Element Method
EC:	Expansive Cement
FEM:	Finite Element Method
FDM:	Finite Difference Method
FLAC3D:	Fast Lagrangian Analysis of Continua in Three Dimensions
GHG:	Green House Gas
MDT:	Minimum Demolition Time
PETG:	Polyethylene Terephthalate Glycol
PFC2D:	Particle Flow Code in Two Dimensions
PLA:	Polylactic Acid
SCDA:	Soundless Chemical Demolition Agents
TFC:	Time of First Crack
TPU:	Thermoplastic Polyurethane

UCS:	Uniaxial Compressive Strength
XRD:	X-Ray Diffraction
σ_1:	Maximum Principal Stress
σ_2:	Intermediate Principal Stress
σ_3:	Minimum Principal Stress
p_i:	Internal Expansive Pressure
E:	Elastic Modulus
r_i:	Inner Radius
r_o:	Outer Radius
ε_θ:	Tangential Strain
p_{Peak}:	Peak Pressure.
μ:	Poisson's Ratio

Chapter 1: Introduction

1.1 Background

The need for natural resources such as oil, gas, and minerals is predicted to grow exponentially over the next few decades (D' Hugues et al., 2022). This is owing to the world's population growth and rapid expansion of construction, manufacturing, and technology (Christmann & Lefebvre, 2022). The continuation of subsurface rock excavation activities will be inevitable to industries such as mining, oil and gas, and subsurface space construction. Drilling & blasting is currently the dominant method for rock fragmentation in mining and civil engineering projects. However, this method is known to be associated with the production of uncontrollable vibrations, toxic fumes including green house gas (GHG) emissions, fly rocks, noise, and dust. Therefore, the practice of drilling & blasting method must follow stringent design, safety, and occupational safety and health regulations. With concern over climate change due to the production of GHG emissions, interest in explosive-free rock fracturing techniques has captured the interest of many researchers in the past decade. This Ph.D. thesis is part of a multi-phase project which is aimed at developing a reliable explosive-free method for hard rock fragmentation in underground mining using the so-called soundless chemical demolition agents (SCDA).

SCDA is a powdery cementitious material made from Portland cement and expansive additives – primarily calcium oxide (CaO), which expands during the curing process of the slurry. When the hydration reaction occurs in a confined borehole in rock or concrete, high expansive pressure is generated causing the borehole to fracture. SCDA was firstly commercialized in 1970s, but failed to attain broad adoption due to limited published guidelines and product manufacturers. A large number of competitive products are available 40 years later until the patents expired (Huynh &

Laefer, 2009). Over the last decade, both laboratory and field research has been undertaken on SCDA usage, leading to some practical recommendations on its surface applications, such as non-explosive concrete demolition and rock quarrying.

1.2 Research Problem

Currently, SCDA is being used occasionally to split rock blocks in dimension stone quarries to obtain vibration-free fracture resulting in clean-cut blocks, which can be further sawn into slabs for commercial use without much material loss. Due to complex stress environment and higher material strength that are typical in deep underground environments, SCDA usage has been barely studied to fracture subsurface hard rock. Therefore, further research and investigation are needed to develop SCDA methods for rock fracturing underground, such as in an underground mine, particularly for situations when explosives are not the best option for rock fragmentation. Interest is drawn towards the use of SCDA in underground mines to mitigate the environmental risks associated with the generation of toxic fumes. The currently used blasting method in underground mines requires additional ventilation to exhaust blast-induced fumes after each blast. Besides, the use of explosives creates ground vibrations, which could affect the integrity of the wall rock – a factor that is well known as blast damage (Sainoki & Mitri, 2014). The development of explosives-free rock excavation such as SCDA is of interest to eliminate the safety risks and environmental impacts associated with blasting.

The challenges encountered when implementing SCDA in underground hard rock mines can be summarized as follows. First, there is a lack of knowledge and prior hands-on experience with in-situ trials involving the use of SCDA underground where rock is presumably stiffer and stronger than rocks encountered in surface applications. Apart from a few pilot trials underground on

boulder fragmentation (Habib, 2022) and coal mining roof fracturing (Xu et al., 2019), there is no well-documented trials for underground hard rock fragmentation with SCDA.

Secondly, if SCDA is to be used to fracture a rock face in an underground mine, the host rock around the SCDA borehole will be subjected to lateral confinement in the form of biaxial compressive stress [maximum principal stress (σ_1) and intermediate principal stress (σ_2)] in a plane that is parallel to the rock face, as illustrated in Figure 1-1. As the SCDA borehole is drilled perpendicular to the rock face, the biaxial compression stress condition would hamper the development of SCDA fracturing into the surrounding rock. In this case, the SCDA pressure must overcome not only the tensile strength of the host rock, but more importantly the mining-induced compressive stress behind the rock face.

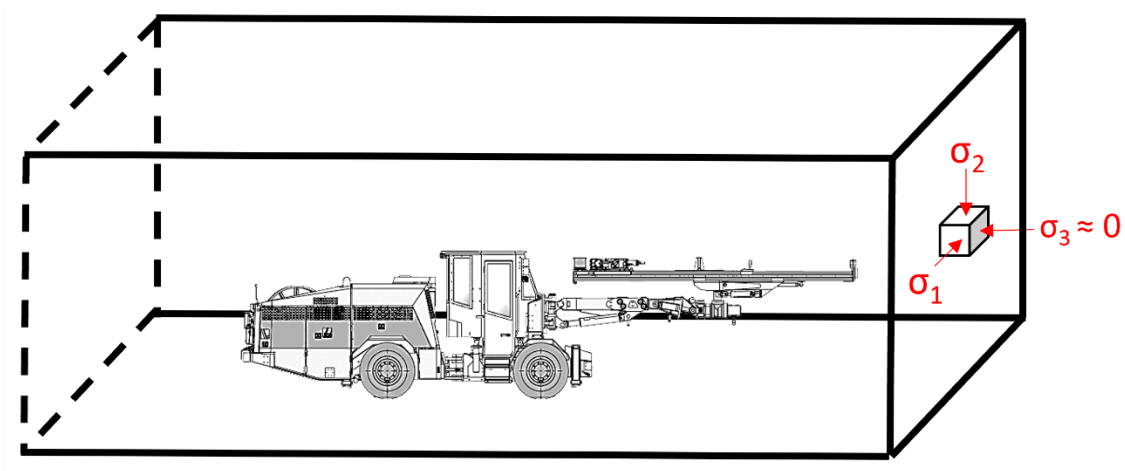

Figure 1.1: Biaxial compression state of stress in a rock face.

SCDA slurry can be poured downhole by gravity when loading vertically oriented boreholes. However, underground mining applications may necessitate the use of boreholes that are horizontal or up-tilt. To date, such methods have not been fully developed. It is noteworthy that unlike cement grout, SCDA borehole loading cannot be implemented with slurry pumps as this

could risk damaging the pump components if the pump is not flushed clean immediately after each use, to avoid damage to pump components.

The abovementioned challenges are the subject of this study.

1.3 Scope of Work

The scope of this research is focused on the development of methodologies and practical guidelines for using SCDA to break hard rock in underground mines. A series of large-scale laboratory tests is conducted under biaxial loading to investigate SCDA performance to break an underground hard rock face with proposed SCDA drill hole patterns. Discrete-element and finite-difference numerical modeling methods are used to optimize the drill hole pattern and explore rock face fracturing mechanism due to SCDA. Viable SCDA cartridge loading approach is designed and tested for charging SCDA slurry into horizontal, uptilted, or wet boreholes that could present in underground applications.

1.4 Research Objectives

The long-term goal of this multi-phase project is to ultimately develop a feasible and reliable method for explosive-free rock breakage in underground mines using SCDA. To help achieve such goal, several specific objectives have been set for this thesis. They are:

- Conduct a state-of-the art literature review of research on the development and applications of SCDA technique.
- Investigate – by ways of appropriate numerical modelling techniques – the potential for SCDA to break a hard rock panel representing a mining front subjected to biaxial stress conditions.

- Based on numerical modelling, propose SCDA optimum borehole patterns that are likely to produce maximum fracturing.
- Design a large-scale experimental program for testing the performance of SCDA to break panels from high strength concrete and granite, subjected to biaxial loading conditions.
- Validate the proposed SCDA borehole patterns from numerical modelling by comparison with experimental results of the concrete panels then the panels from granite.
- Design and implement feasible SCDA borehole loading methods for vertical, horizontal, and up-tilted boreholes.
- Make recommendations for field applications of SCDA, particularly for face advance in mine development projects.

1.5 Thesis Outline

The thesis is structured into the following eight chapters. The first chapter presents a summary of this study, including its background, scope, and objectives. Chapter 2 presents a comprehensive review of the history, development and current application field of SCDA technique. The merits and performance of SCDA are highlighted for a potential alternative to explosives in rock breakage applications. Chapter 3 reports an optimized diamond-shaped SCDA hole pattern that results in the most fractures based on discrete-element PFC2D simulation. The large-scale panel tests under biaxial confinement are designed and carried out on two high-strength concrete panels, and their results are consistent with those of the PFC2D models. Chapter 4 presents large-scale panel test results of granite hard rock with diamond-shaped hole pattern, which confirms the ability of SCDA for hard rock breakage under high confinement. Both concrete and rock panel demolitions due to SCDA are back analyzed using finite-difference FLAC3D codes, and the panel fracturing mechanisms are revealed using FLAC3D modelling. Chapter 5 proposes a V-cut SCDA hole

pattern for rock panel demolition, where the drill holes are 45° angled with regard to the rock panel, allowing the component of the SCDA expansive pressure to go against the panel free surface. The results of large-scale tests and FLAC3D modelling of the V-cut pattern are presented. Chapter 6 develops and implements viable SCDA borehole loading methods for horizontal and up-tilted boreholes. Laboratory test and field trial results in an underground mine are presented. In Chapter 7 summarizes the main research findings and recommends future field work to implement the SCDA method into underground practice. The set of methodologies proposed in this work could guide the SCDA applications for subsurface hard rock face breakage.

Chapter 2: Literature Review

2.1 Overview of rock fracturing techniques

Since the Paris Agreement, a global trend to transition to low-carbon economies in response to climate change has been initiated (Vrontisi et al., 2020). According to Odell et al. (2018), climate change has become a critical driver of mining policy, e.g., El Salvador banned metal mining due to the country's vulnerability to water resources in 2017 under climate change. As the political and environmental restraints are increasing in mining and natural resource industries, a large and growing body of literature has investigated non-explosive and environmentally friendly rock fracturing methods in recent years, hoping to avoid the undesired by-products from traditional drilling and blasting method.

Rock fragmentation is an important part of mining and civil engineering projects. Black powder was first tried to blasting rock in mining industry in Hungary in 1627, and then gradually spread and became the most common rock excavation method in mining projects. Mechanical excavation methods were first used about 120 years ago (Buffington, 2000). Despite the rapid growth of mining and construction industries, the traditional drill and blast method is still the first choice for rock fragmentation as it is the more realistic solution considering production cost and efficiency (Al-Bakri and Hefni, 2021). However, rock breakage using traditional explosives has some immediate negative effects, such as flying rocks, ground vibration, noise, air overpressure, and toxic gas emissions. Blasting undermines the stability of the remaining rock mass as it could lead to degradation of the surrounding rock quality. It could also affect the surrounding structures such as rock pillar, backfill, mine facilities, or surface structures (Gad et al., 2005; Huo et al., 2020; Wang et al., 2022a). As a safety measure, the mine is evacuated prior blasting and additional

ventilation is used to exhaust blast-induced fumes. As illustrated in Figure 2-1, a typical underground drift advance cycle using conventional blasting method includes six steps (Habib et al., 2022). The third step of blasting and ventilation between shifts normally lasts for two hours in Canadian mines to vent out toxic fumes generated from blasting from the working area.

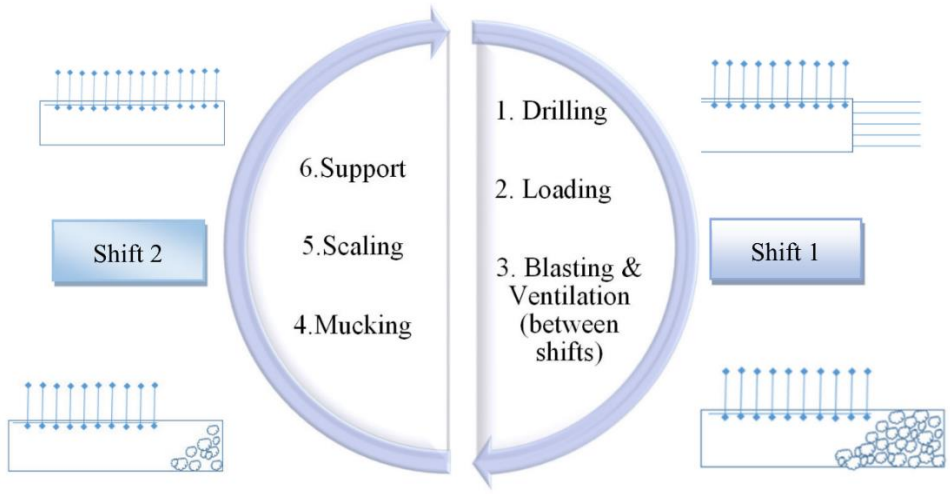

Figure 2.1: Typical tunnel development cycle with drilling and blasting during two shifts per day (Habib et al., 2022).

With world energy consumption set to increase by a further 56% by 2040 (Conti et al., 2016), the necessity to develop more efficient alternative rock fragmentation methods is clear given the adversities using traditional explosive methods. In recent decades, many efforts have been made on developing explosive-free rock breakage methods to overcome the abovementioned drawbacks of conventional blasting. Many researchers conducted extensive studies on water jet cutting method for rock fracturing, but it has certain deficiencies such as significant waste of water and temperature limitation in cold environment (Liu et al., 2014; Stoxreiter et al., 2018). To overcome these drawbacks, some recent studies explored and developed waterless high-pressured gas fracturing, liquid nitrogen fracturing, and foam fracturing systems (Zhao et al. 2019; Huang et al.

2020; Liu et al., 2021). Besides, other methods such thermal fragmentation, plasma blasting, and expansive cements are developed for hard rock fracturing in mining field (Habib et al., 2022). The thermal fragmentation method was applied in narrow-vein mining to reduce ore dilution. It relies on a strong burner that is inserted into borehole to break wall rock. This method requires high temperature up to 800 ℃ and the induced rock fragmentation spalling can enlarge the borehole from 152 mm to a maximum of 1200 mm (Drake et al., 2020). The plasma blasting method utilizes pulsed electrical discharge for rock breakage (Ikkurthi et al., 2002; Kuznetsova et al., 2022). The plasma blasting probe in a water-filled borehole generates expansive plasma and pressure waves in the water. When the wave is transmitted to the rock medium, it causes the rock to fracture. The Soundless Chemical Demolition Agents (SCDA) – used in this study – was developed more than 30 years ago (Fig 2-2a). Its commercial applications started after a decade in civil engineering projects such as the block splitting in quarries and concrete fracturing (Jiang et al. 2021; Kim et al., 2021). An application example for concrete demolition is shown in Figure 2-2b.

a) SCDA powder b) Concrete block demolished with SCDA

Figure 2.2: Soundless Chemical Demolition Agents (SCDA) (Kim et al., 2021).

In recent years, there has been an increasing interest in implementing SCDA in underground mining, but the performance and potential applications of SCDA in subsurface conditions

involving strong and hard rocks and high in-situ stresses has not been fully investigated. In the following sections, the SCDA is reviewed, and its development, performance, and applications are highlighted.

2.2 Soundless Chemical Demolition Agents (SCDA)

2.2.1 Introduction

SCDA, also known as expansive cements or static cracking agents, refers to chemically-based powdery compound that is an alternative to rock fracturing without explosives. The SCDA slurry swells during the curing process, and when it is poured into a borehole in rock or concrete, the swelling process may cause the host medium to crack silently after a period of chemical reaction.

SCDAs are made up of mainly Portland cement and expansive additives. Portland cement is the most common type of cement for general applications worldwide. Portland cement is made by heating a chemical mixture of lime, silica, alumina and iron to 1400–1600 °C in a kiln in the first step, where the raw materials interact and form a new phase known as clinker. After cooling and crushing, gypsum is added to adjust the setting time, and the mixture is ground exceedingly fine to become Portland cement. Depending on expansive additives, SCDA is classified into three categories according to ASTM C 845 Standard (ASTM, 2004): Type K, Type M, and Type S.

- Type K: Anhydrous calcium sulfoaluminate ($4CaO \cdot 3Al_2O_3 \cdot SO_3$), calcium sulfate ($CaSO_4$), and calcium oxide (CaO);
- Type M: Calcium aluminate ($CaO \cdot Al_2O_3$) and Anhydrite ($CaSO_4$);
- Type S: Tricalcium aluminate ($CaO \cdot Al_2O_3$) and Anhydrite ($CaSO_4$).

Regardless of the source of aluminate component, all types of SCDA produce ettringite crystals as the main driver for SCDA expansion (ASTM, 2004). Another popular type of expansive cement is Type G, whose expansive ability comes from the production of Portlandite (Arshadnejad, 2011). The expanding spheres model of SCDA is demonstrated in Figure 2-3 (Manatunga et al., 2021).

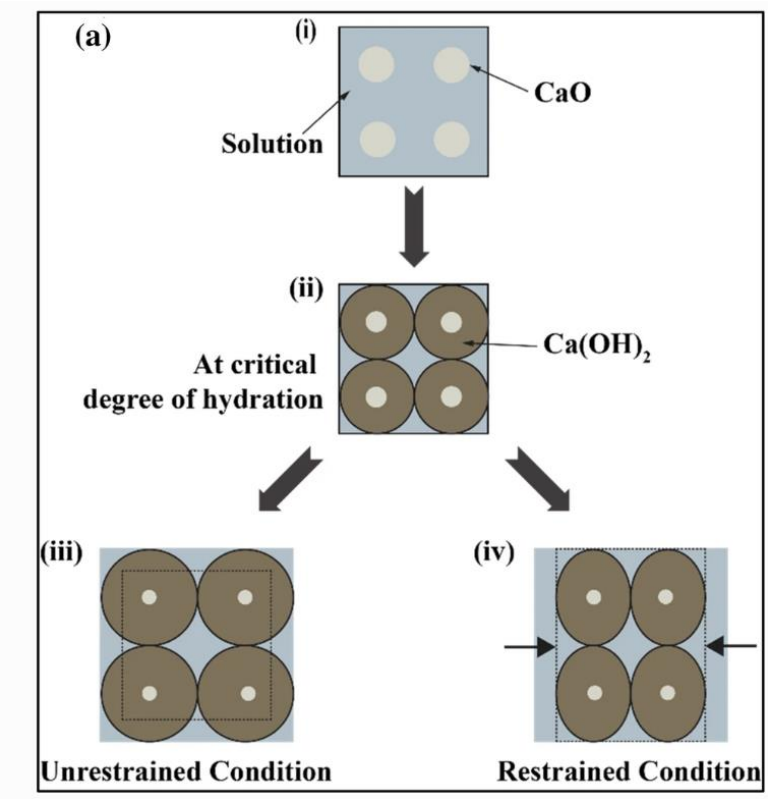

Figure 2.3: Expanding spheres model of SCDA (Manatunga et al., 2021).

Although there are many variances in the composition of different SCDA products, a common chemical composition with the predominant amount of CaO accounting for 81% to 95% can be found in any form of SCDA, as shown in Table 2-1 (De Silva et al., 2016).

Table 2.1: Chemical composition of SCDA (De Silva et al., 2016).

Chemical Components	Percentage by Mass (%)

SiO_2	1.5 – 8.5
Al_2O_3	0.3 – 5.0
Fe_2O_3	0.2 – 3.0
CaO	81 – 96
MgO	0 – 1.6
SO_3	0.6 – 4.0

The expansion of SCDA is primarily induced by the hydraulic reaction that generates ettringite crystals and Portlandite during the curing of SCDA mixture. Both lead to a progressive increase in radial and tangential tensile pressure in a confined borehole in rock or concrete. As shown in Figure 2-4, a fracture is formed at the weakest location along the inner surface of hole. The fracture will begin to propagate when the tensile stress surpasses the tensile strength of the host medium. The tension created by the SCDA is decreased in proportional to the square of the distance from the hole boundary. Consequently, the tensile stress produced by the SCDA expansion is the main driving force for the rock to fracture (Harada et al.,1989), which indicates the tensile strength is most crucial rock property in determining whether the rock medium surrounding the SCDA borehole will fracture due to SCDA.

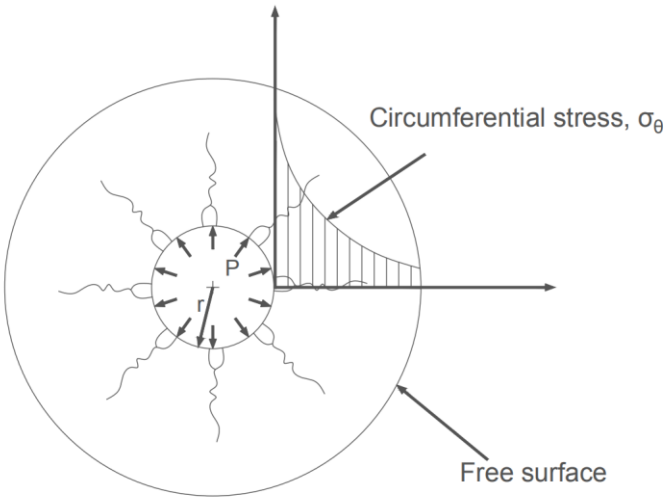

Figure 2.4: SCDA-induced borehole fracturing (modified based on Harada,1989).

2.2.2 SCDA mechanical properties and physical capacity

Even though SCDA has been applied in civil engineering projects for more than 20 years, the mechanical properties and application capacity of SCDA have not been fully explored so far. There have been several research efforts undertaken to investigate the mechanical properties and physical characteristics of SCDA in laboratory conditions. The primary scientific challenge that concerns the application of SCDA is how to quantify the maximum pressure that SCDA can generate from the chemical reaction in actual rock fracturing applications, where rock cracking is initiated by SCDA expansion, and the SCDA material loses its confinement, thus the pressure drops significantly before reaching its potential peak value. To measure the peak expansive pressure of SCDA, the thick-walled cylinder method, also referred as the steel pipe method is mostly used in the literature (Hinze and Brown, 1994; Habib et al., 2023; Kim et al., 2021). This method involves pouring SCDA into a thick-walled cylinder and monitoring the tangential or circumferential strain on the outer surface of the cylinder (as seen in Figure 2-5).

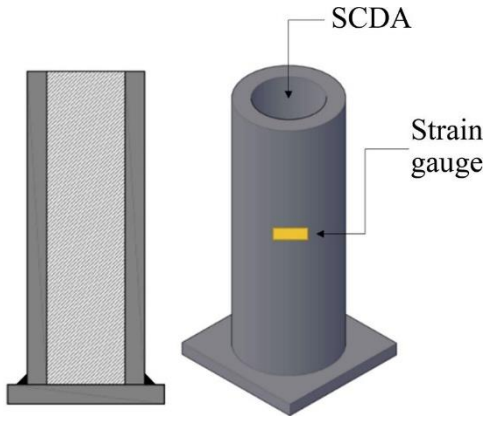

Figure 2.5: Schematic configuration for the SCDA peak pressure estimation using thick-walled cylinder (Habib et al., 2023)

Based on the measured tangential strain on the cylinder surface, the SCDA pressure is estimated analytically as follows (Timoshenko and Goodier, 1951).

$$p_i = E\varepsilon_\theta \frac{(r_o^2 - r_i^2)}{2r_i^2} \tag{2-1}$$

where p_i is the internal expansive pressure in MPa, E is the elastic modulus of the steel cylinder in MPa. r_i and r_o are the inner and outer radii of cylinder in mm, respectively. ε_θ is the circumferential or tangential strain measured on the external surface of the cylinder.

Some researchers attempted to modify the original steel cylinder method for SCDA peak pressure estimation. Laefer et al. (2018) reported that the pipe testing does not provide an effective heat sink which is the large rock mass in real life. Therefore, the authors compared the SCDA performance by placing the host pipe in water bath (as illustrated in Figure 2-6) and chamber at the same ambient temperature of 10 °C. They found out that the pipe testing in the chamber had 5°C higher hydration heat and a sixfold increase in expansive pressure compared with the one in water bath after 4 days. This implies that the host medium temperature plays a key role; reported

pipe test results cannot be directly used to forecast SCDA field performance in a cool host temperature of 10 ℃. Li et al. (2021) also placed SCDA-filled steel pipe in a water tank with a constant temperature of 15 ℃ for heat dissipation. The influences of pipe parameters and surrounding metal constraint on the development of SCDA expansive pressure were tested. It was found that when the pipe was placed in water, the SCDA peak temperature reduced by 85% and the onset time of peak temperature was delayed compared to the typical procedure of placing the steel pipe in room temperature. An enhanced steel pipe approach called the upper end surface method was put forward by Xu et al. (2022). Based on their test results, a mathematical model of SCDA expansive pressure that incorporates the radial pipe strain was created via numerical simulation. Habib et al. (2023) employed a high-capacity pressure sensor to measure the SCDA pressure directly in the borehole, and the results are then used to obtain a correction factor between directly measured pressure and the estimated SCDA pressure from the analytical equation (2-1).

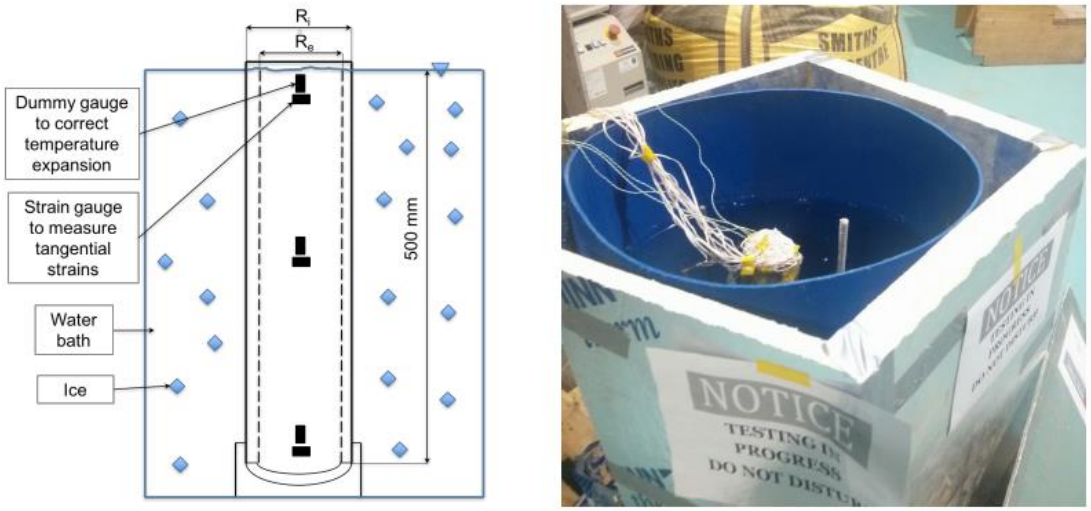

(a) Steel pipe dimensions and strain gauge orientations

(b) Photograph of 76.2 mm sample in the water bath

Figure 2.6: Testing configuration for large steel pipes in a water bath (Laefer et al., 2018).

Apart from quantifying SCDA expansive pressure, researchers also carried out studies on SCDA expansion mechanism, chemical composition analysis, physical property testing, expansive capacity optimization, and the influence of hydration and temperature, et al. Hinze and Brown (1994) studied the influence of water to cement ratio in SCDA, ambient temperature, and hole diameter on the expansive pressure development. Their test results showed that larger water content in SCDA leads to less expansive pressure, while higher ambient temperature results in greater expansive pressure. Low water content, on the other hand, makes cement more viscous and difficult to flow while high temperature may increase the risk of SCDA spout-out. De Silva et al. (2017) examined how the hydration process affects the mechanical characteristics and microstructure of SCDA using the scanning electron microscopy and X-ray diffraction (XRD). Figure 2-7 illustrates how the weight fraction of phases in SCDA varies during the hydration process (De Silva et al., 2017). The expansion of SCDA is primarily caused by the forms of Portlandite ($Ca(OH)_2$) and Ettringite, even though the Portlandite is the dominant source. Their study also indicates that SCDA might be more effective to fracture the surrounding rock masses under high confinement.

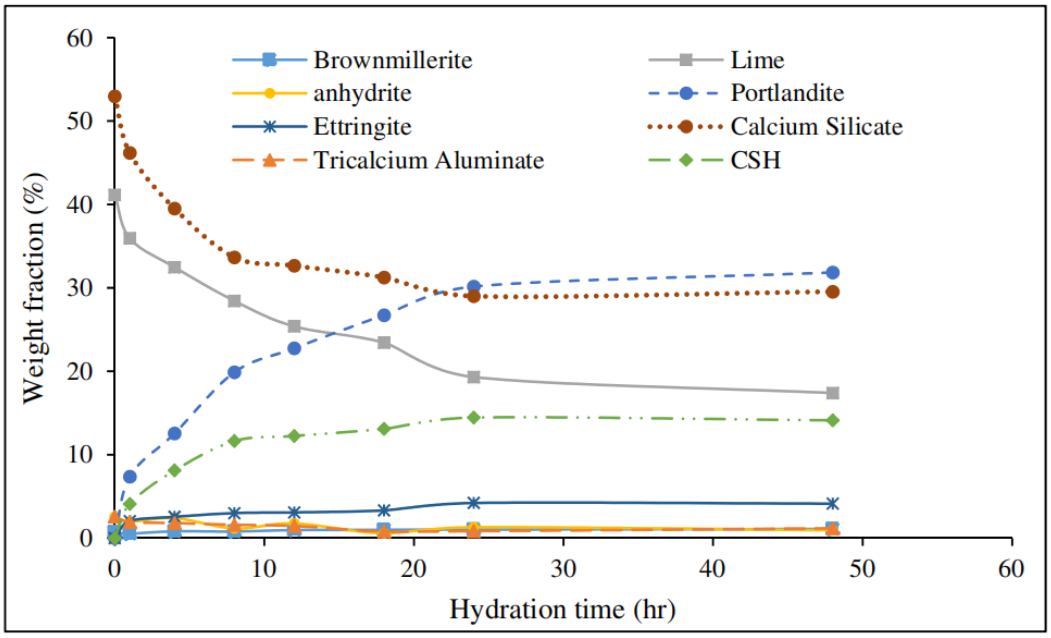

Figure 2.7: Weight fraction of components in SCDA with hydration time (De Silva et al., 2017)

De Silva et al. (2018) continued a study on improving the applicability of SCDA in saturated rockmass. They added $CaCl_2$ to accelerate the expansive pressure and discovered that a combination of 0.1% welan gum and 2% $CaCl_2$ by weight of SCDA to be the most effective accelerator. Such a combination increases the pressure generation rate by 44% and accelerate the onset of expansion pressure by 52% compared with unmodified SCDA. The effect of saturation conditions on SCDA performance to fracture geological reservoir rock formations was then examined by De Silva et al. (2019a). The findings demonstrated that saline conditions and reduced pore-water both improve SCDA's fracturing performance. Qiu et al. (2021) monitored the axial and radial expansive pressures generated by SCDA contained in a steel cylinder sealed by a servo-controlled piston. The elastic modulus and Poisson's ratio are obtained during SCDA hydration under constant volume condition. A mathematical model was also constructed for variation of elastic modulus with the major principal stress. Natanzi et al. (2016) tested SCDA pressure

development and peak hydration heat under different ambient temperatures in steel pipes. The experimental investigation revealed a 350% rise in pressure when the ambient temperature was adjusted from 2 °C to 19 °C, as demonstrated in Figure 2-8.

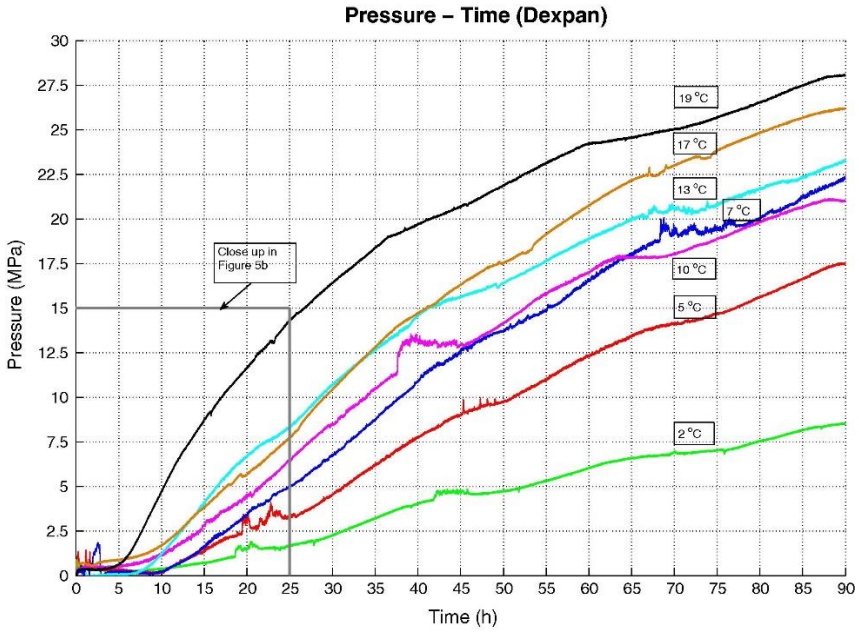

(a) Expansive pressure development over 4 days

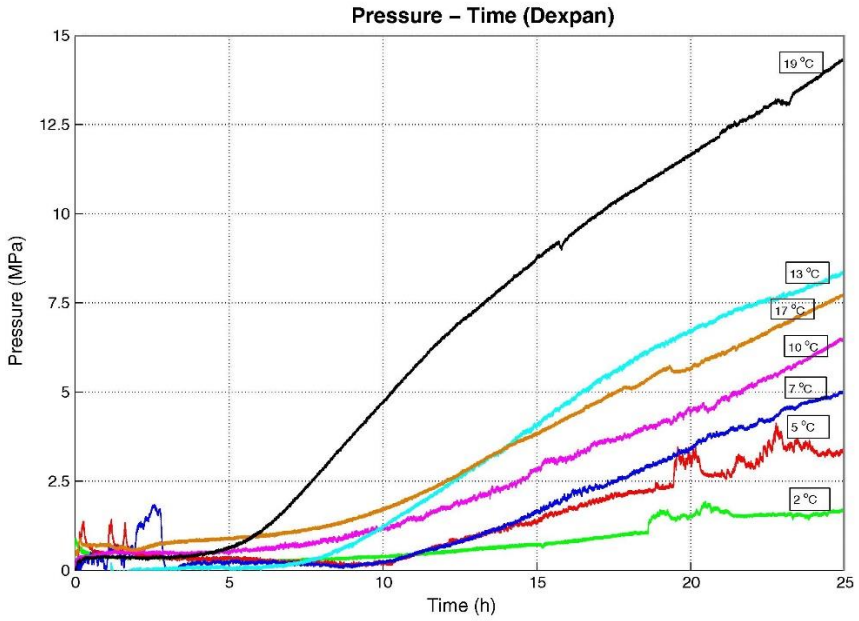

(b) Expansive pressure development in first day

Figure 2.8: Development of expansive pressure at different ambient temperatures (Natanzi et al., 2016).

Natanzi et al. (2019) also examined the effect of ambient temperature (2°C–19°C) on SCDA chemical alterations in steel pipe using two SCDA products namely Dexpan and Bristar. The results showed that SCDA produced larger expansive pressure accompanied with higher $Ca(OH)_2$ and lower concentrations $CaCO_3$ at higher ambient temperatures. Wang et al. (2022b) tested small granite blocks fracturing using SCDA under low biaxial confinements (0 ~ 6 MPa), and the test setup is illustrated in Figure 2-9. Their findings indicate that SCDA fracturing efficiency is highly influenced by the biaxial loading ratios, and the highest fracturing efficiency is achieved when two boreholes align the maximum principal stress direction.

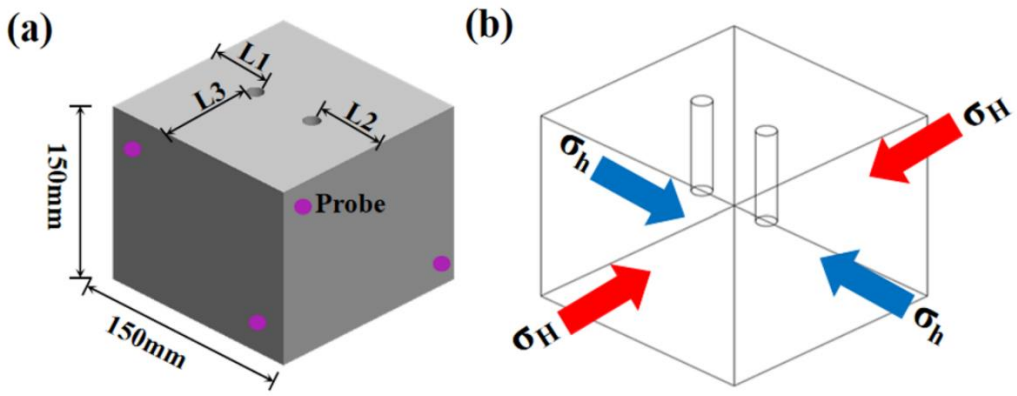

Figure 2.9: Block fracturing test under biaxial confinement (Wang et al., 2022b). (a) Sample with two SCDA holes: L1, L2 and L3 are 50 mm, 50 mm, and 75 mm, respectively; (b) Biaxial loading direction.

Liu et al. (2022) explored the usage of microwave to accelerate SCDA reaction, as shown in Figure 2-10a. Their study results showed that microwave could make the SCDA reaction more complete by enhancing the hydration reaction of CaO, and the onset time of peak expansive pressure is

significantly advanced using the microwave heating method compared to no heating or conventional heating condition, as shown in 2-10b. However, these experiments were carried out on small cubic rock samples (15 cm) with 10 cm deep SCDA holes in a microwave oven. When SCDA is injected deep into the rock and there is a big area of SCDA holes, it would be difficult to apply microwave heating in the field application.

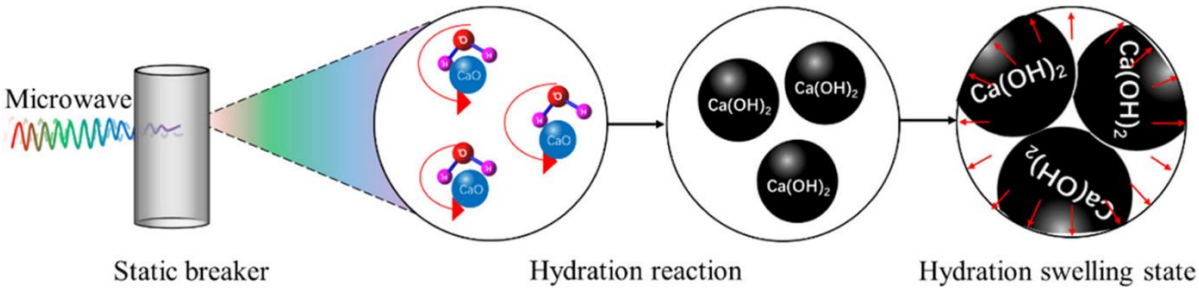

(a)

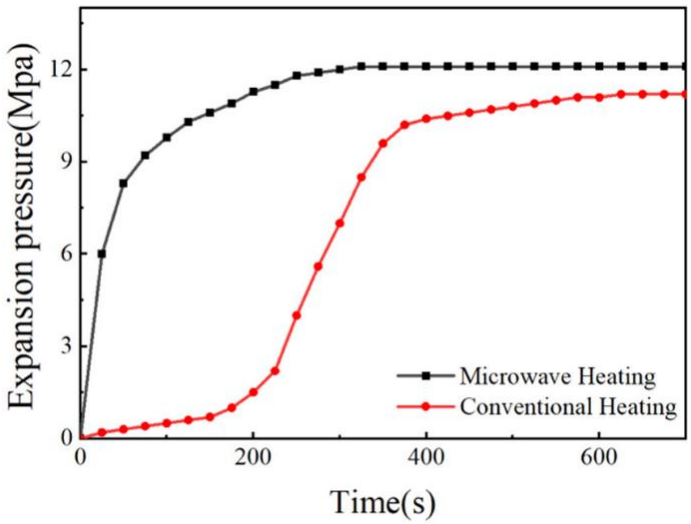

(b)

Figure 2.10: Microwave irradiation mechanism to speed up SCDA expansion (a) and comparison between microwave and conventional heating methods (b) (Liu et al., 2022).

2.2.3 Numerical simulation of SCDA

Numerical simulation offers clear benefits when physical experiments are challenging and costly to conduct under certain circumstances. In recent years, several publications concerned themselves with rock fracturing estimation due to SCDA expansion using numerical simulation approaches such as finite element method (FEM), finite difference method (FDM), and discrete element method (DEM). Habib et al. (2023) conducted axisymmetric simulation of thick-walled steel cylinder test using ABAQUS software. The modelling work, combined with direct pressure measurement, led to the determination of the peak elastic modulus of SCDA material when it is at peak pressure. Based on an iterative process, it was found the SCDA peak modulus of elasticity ranges from 8.1 GPa and 8.35 GPa. This is useful in future SCDA modelling studies, such as SCDA pattern design or fracturing estimation in practical mining applications. The SCDA expansion behaviour in axial-output tests were back analyzed by Qiu et al. (2021) using FEM, as shown in Figure 2-11a. In the experiments, both radial stress and axial stress can be measured by the testing system. It was found that a linear model cannot simulate the observed ratio between axial stress and radial stress in the steel cylinder test. Then, the authors studied the effects of varying elastic modulus and Poisson's ratio on the axial pressure value while keeping radial pressure a constant. A relationship was built between elastic modulus and principal stresses (as seen in Figure 2-11b) and input in the model, which allows the modelled radial and axial pressures in line with the test data.

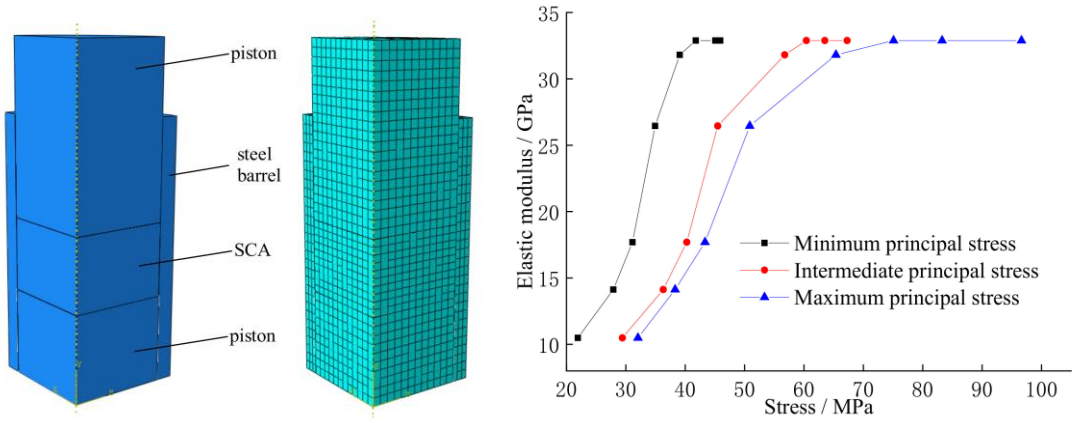

(a) Finite element model (b) Relation between principal stresses and SCDA elastic modulus

Figure 2.11: Numerical modelling study by Qiu et al. (2021).

Wang et al. (2018) modified a cohesive element approach in ABAQUS software using python codes to simulate the rock fracturing process. In their work, a two-dimensional rock panel fracturing under confinement induced by a SCDA hole with a directional notch of 0°, 45° or 90° are examined numerically, as shown in Figure 2-12. Quasi-static pressures from 0 to 150 MPa were applied to the borehole to examine the influences of deviatoric stresses and notch direction on crack initiation pressure. The results showed that the minimum principal stress σ_3 is the main factor controlling crack initiation pressure. It is also reported that both deviatoric stress and notch direction affect crack propagation direction.

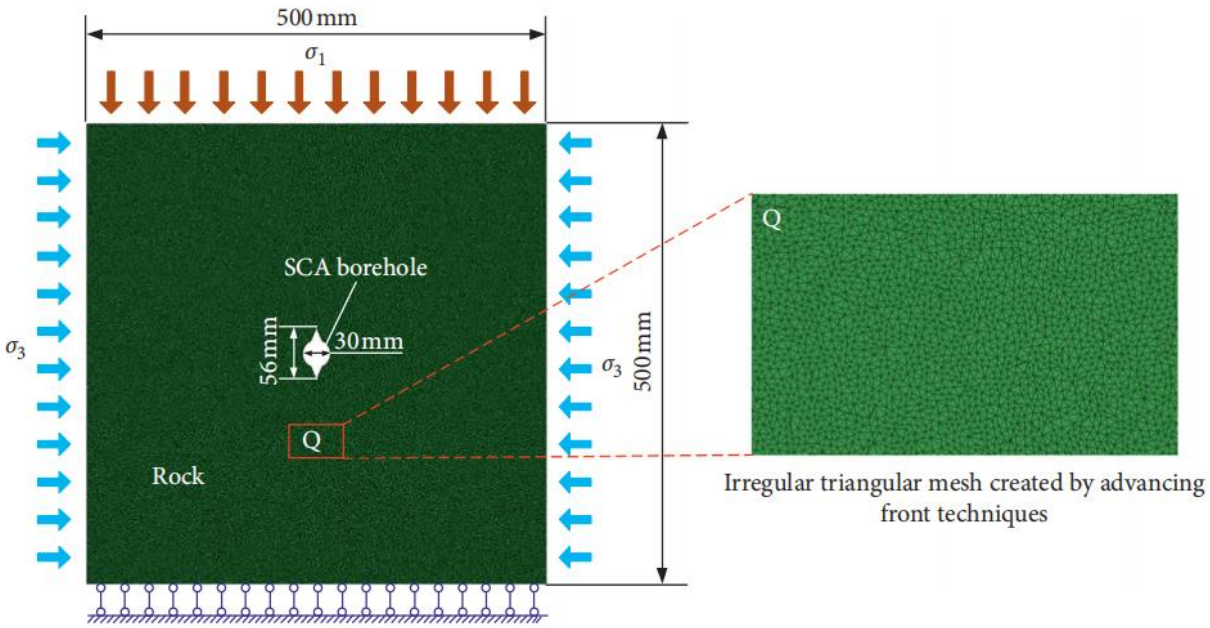

Figure 2.12: FEM modelling of notched SCDA hole under biaxial stress confinement and (Wang et al., 2018).

Cho et al. (2018) modelled fractures in concrete panel induced by SCDA in ABAQUS software. The thermal expansion approach is employed for the expansive pressure simulation with a minimal thermal expansion coefficient (1×10^{11}/°C), and the temperature induced SCDA pressure was set to rise linearly. Additionally, the authors used the proposed modelling techniques to investigate the minimum required SCDA pressure to form a U-shaped crack with nine SCDA holes, as shown in Figure 2-13 (only the results from the half of the symmetric panel with five SCDA holes is presented). The results indicated that the minimum expansion pressure need was 68.02 MPa at the central hole A-1.

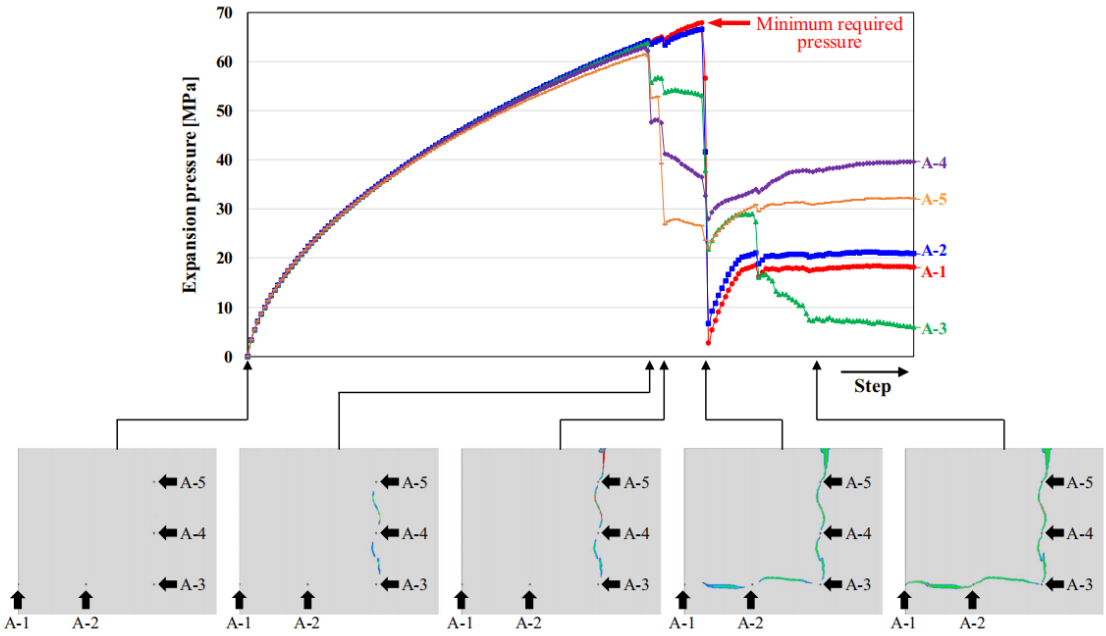

Figure 2.13: Crack development from a nine-SCDA hole pattern with expansion pressure variation (Cho et al., 2018).

Apart from FEM, some scholars attempted to use another continuum modelling approach such as FDM for SCDA expansion simulation (Tang et al., 2021; Xu et al., 2022). In such studies, stress boundary is used on the SCDA borehole wall to create the expansive pressure. Thus, this method can be used to analyze the stress-strain relations in the surrounding medium caused by the input pressure, also material yielding can be checked to represent fracturing zone if plastic model is assigned, as shown in Figure 2-14. Although continuum modelling techniques have the advantage of modelling large scale domains such as mine wide models, they have certain inherent limitations in terms of modelling fracture propagation explicitly. Additionally, experimental measurements of the stress boundary conditions from steel pipe tests are normally used as input boundary conditions, which is challenging to reflect the pressure variation during the rock fracturing process. This is due to the fact that borehole cracking induces expansive pressure reduction.

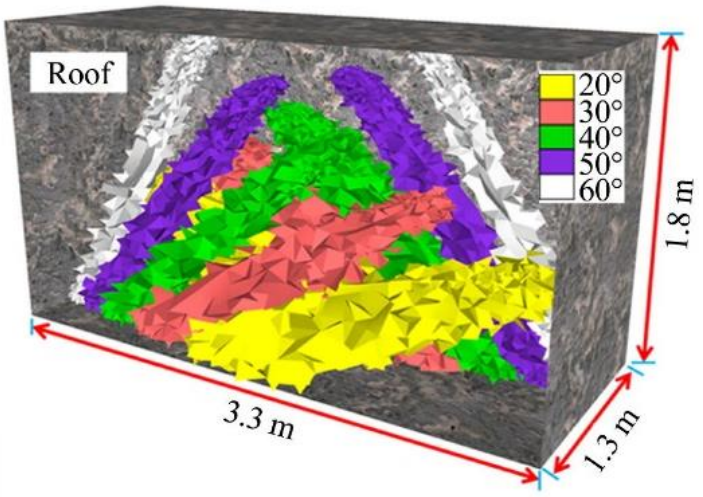

Figure 2.14: Plastic zones induced by SCDA (Tang et al., 2021).

Another option for the simulation of cracks induced by SCDA expansion is the DEM (De Silva and Ranjith, 2019b; De Silva and Ranjith, 2020). The primary distinction between DEM and continuum numerical approaches is that the contacts between system components are updated with the deformation and separation process in DEM but are stationary in FEM. Traditional continuum approaches require a high-quality mesh domain to have good accuracy and solution convergence. In the case of DEM, there is no convergence difficulty when the discrete blocks or particles are treated as rigid as the computation is conducted by shifting the boundary condition and modifying the block contacts. Therefore, DEM can support and simulate significant displacements, rotation, and separation between elements. Generally, for the simulation of SCDA expansion using DEM, a cylindrical rigid wall is placed in the borehole, and the expansion pressure of the SCDA is produced by providing the expansive velocity of the wall, as shown in Figure 2-15 (De Silva and Ranjith, 2020). While this is feasible, such modelling technique inherently ignores the influence of the host medium stiffness its state of stress since the rigid wall will expand uniformly in the radial direction regardless of the applied state of stress and deformation. Tang et al. (2022) also tried the simulation of the SCDA expansion process by combining the finite difference approach

with the DEM. The effect of different model parameters on the expansion pressure was investigated and the model was calibrated based on the experiments.

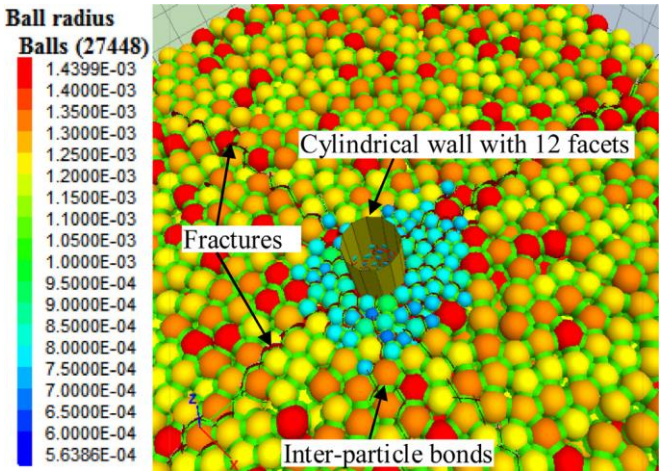

Figure 2.15: Numerical simulation of SCDA expansion using cylindrical wall in PFC3D modelling software (De Silva and Ranjith, 2020).

2.3 Current application field of SCDA

The extension of the SCDA application in the field beyond the traditional civil engineering uses like concrete demolition has increasingly attracted researchers in the past decade. The use of SCDA is presently anticipated for hard rock roof breaking in coal mines, in-situ leaching, rock fracturing in oil and gas reservoirs, and underground metal mines. For instance, due to the fact that SCDA produces no vibrations that might harm nearby structures, Natanzi & Laefer (2014) combined SCDA method with highly limited blasting and hydraulic hammer to demolish and replace old structures in a historic site. The rocks were removed by air hoist after SCDA fracturing, which assists in demolition acceleration without producing exceptionally high vibration to the surrounding subway and water tunnels. Natanzi et al. (2020) also tested the selective demolition of masonry unit wall using SCDA. After demolition, masonry units above the diagonally arranged

SCDA holes could be removed without causing additional damage to the units below the band. SCDA was used by Shang et al. (2017) to investigate discontinuity persistence. As shown in Figure 2-16a, the SCDA boreholes are drilled along the discontinuity line of rock blocks. Thus, the pre-existing persistent area and rock bridge area can be directly revealed and observed on the splitting surface after SCDA splitting, allowing the discontinuity persistence to be quantified (See Figure 2-16b).

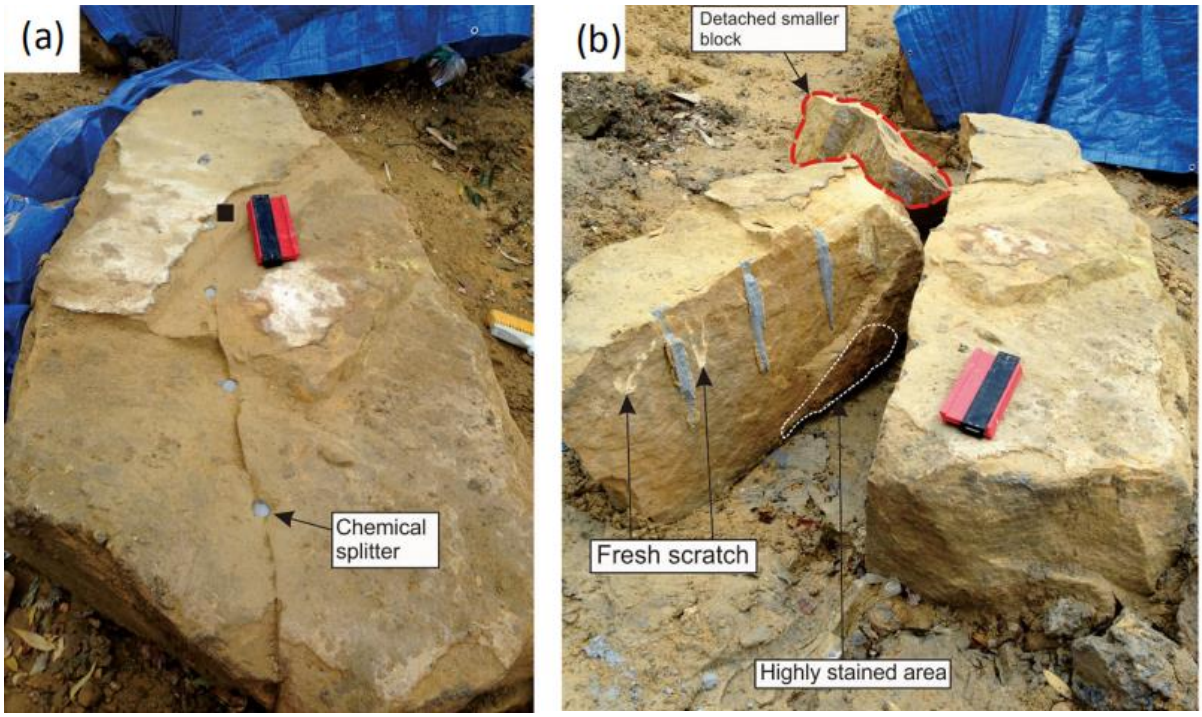

(a) SCDA holes along a discontinuity (b) Splitting blocks due to SCDA

Figure 2.16: Discontinuity persistence investigation using SCDA method (Shang et al., 2017).

Through laboratory experiments and discrete element simulations, De Silva et al. (2018) investigated how SCDA might be used for in-situ leaching (Figure 2-17a). The findings suggest that SCDA could create a controllable fracture network in rock mass that is impervious (Figure 2-17b). De Silva et al. (2019b) also studied application of intermittent charging and multistage

charging as shown in Figure 2-17c. They found out that intermittently charged SCDA can reduce the amount of SCDA to achieve the same fracturing performance. Multistage charging can increase the fracturing density (Figure 2-17d) without the need of multiple drillholes filled with SCDA. Hydrochloric acid could be considered for acid digestion of SCDA residual product between each charging stage, although the residual SCDA was removed manually to prevent rock mineral dissolution for the test purposes in this study.

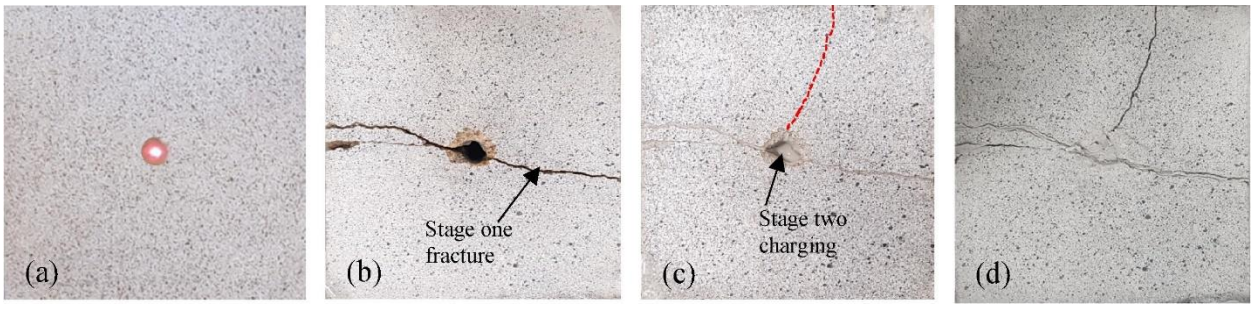

Figure 2.17. Sandstone specimen during two-stage fracturing, (a) first SCDA injection, (b) after first stage fracturing, (c) second injection, and (d) after second stage fracturing (De Silva et al., 2019b).

Tang et al. (2017) carried out an experimental study on fracturing coal briquettes using SCDA to improve coal permeability, with the aim of increasing the permeability of the coal seam layer for better gas extraction. The ideal ratio of CaO, naphthalene-based water reducer, sodium gluconate, and silicate cement in SCDA was found to be 90:3:5:7 using orthogonal experiments. Xu et al. (2019) investigated the application of SCDA for coal mine roof caving. A multi-stage SCDA loading scheme for boreholes with different inclination angle was proposed as shown in Figure 2-18a, aiming to excavate new free surfaces step-by-step until the entire rock mass demolished as shown. The boreholes were charged in the following order: 30° holes first, 45° holes second, and 60° holes at the end, with one hour interval, as shown in Figure 2-18b. After the test, some cracks

were generated from the SCDA holes and propagated to the empty pilot holes, as shown in Figure 2-18c.

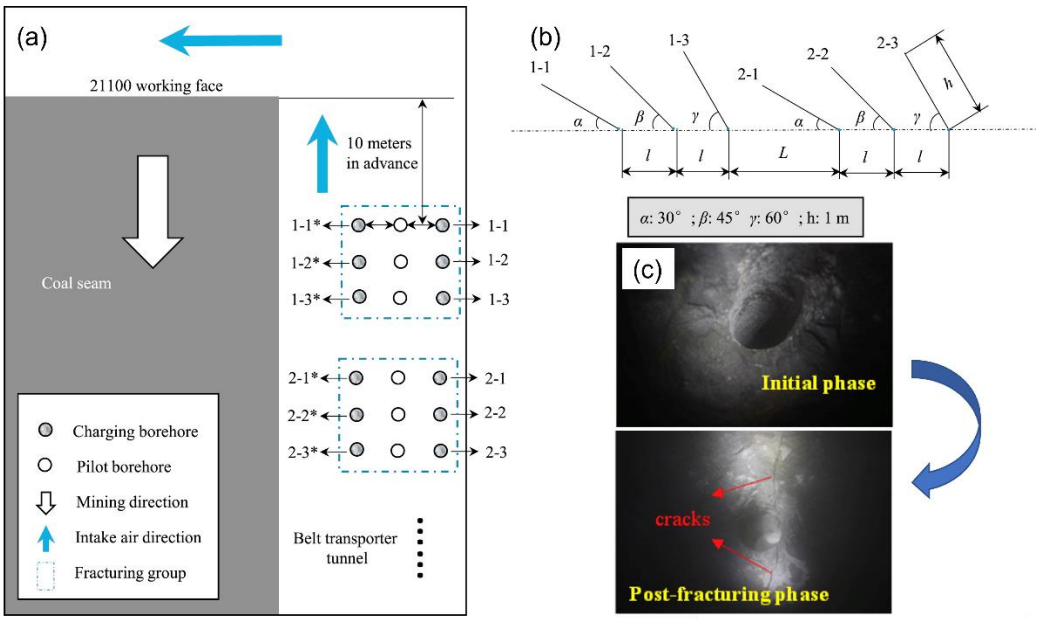

Figure 2.18: Diagram of borehole layout design in coal seam roof (a); SCDA hole depth and incline angles (b); test results (c)

Tang et al. (2021) also attempted to apply SCDA method for weakening the hard rock on the roof of a coal mine. They inserted coiled SCDA cartridges into the limestone roof with drilling elevation angle ranging from 20˚ to 60˚. The influence of the borehole angle on the displacement and plastic failure volume was examined using numerical modelling, showing that the greater the drilling elevation angle, the less effective the SDCA. Xu et al. (2021) designed a self-swelling SCDA cartridge (see Figure 2-19a) composed of sponge, kraft paper, and thread rod, etc. The appearance of the product is presented in Figure 2-19b. The authors attempted to expand the potential application of SCDA when loading in upper tilted or horizontal hole is required, however, the expansion pressure produced by self-swelling cartridge was found highly sensitive to the packing density, cartridge diameter the insertion gap between the cartridge and the borehole wall. Besides,

SCDA powders are preloaded into this special cartridge, which is inserted into borehole after being immersed in water for a certain time. Hence, in order to load the most popular form of liquid SCDA, new and cost-effective loading methods still need to be developed for the subsurface applications where SCDA mixture cannot be poured into boreholes under gravity.

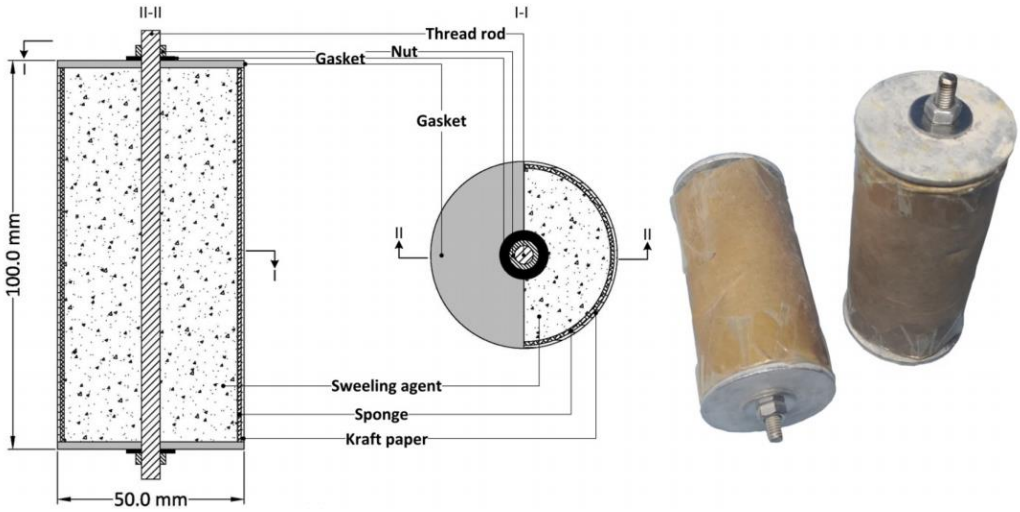

(a) Cartridge structure (b) Examples

Figure 2.19: Self-swelling cartridge design (Xu et al., 2021)

2.4 Summary

In this chapter, an overview of non-explosive rock fracturing methods is presented with a focus on the merits of SCDA over other methods. This is followed by a detailed and critical review of the SCDA technique and its applications. The review describes the chemical composition and the fundamental fracturing mechanism of expansive cements. A detailed account is given to the experimental research efforts done over the past two decades on the mechanical behaviour and physical properties of SCDA. Numerical simulation using FEM and DEM are reviewed and their

features and limitations are outlines. Finally, current and potential applications of SCDA in practice are highlighted.

Bridging text between Chapter 2 and Chapter 3

The previous chapter comprehensively reviews the development and applications of SCDA as an alternative to explosives for concrete and rock breakage. It shows that SCDA has a great potential to be used for rock breakage applications in underground mines, such as mine drift face advancing. However, several challenges encountered in the underground environment must first be addressed to achieve such applications. These include biaxial confining stress at a mining front, and the high strength and stiffness of hard rock. Both factors could inhibit the effectiveness of the SCDA expansive pressure. The mechanical performance of SCDA under biaxial loading conditions has been barely studied in literature. Therefore, the first step in this research is to investigate the performance of SCDA under high biaxial confinement. A large-scale testing program is reported in the following chapter. High-strength concrete panels of dimensions 1 m ×1 m × 0.25 m are loaded to 15 MPa and 23 MPa in a biaxial loading system. This setup mimics the stress condition of a mine drift front in the field. PFC2D modelling is conducted on different SCDA drillhole patterns to help predict and optimize the SCDA fracturing efficiency due to SCDA. Two drillhole patterns simulated in PFC2D are selected for the large-scale experiments and the experimental results are compared with the model predictions.

The parallel bond model (PBM) in PFC2D is used in the numerical modelling study reported in Chapter 3. The idea behind the PBM is that it can transmit both force and moment between the particles rather than force only as in the conventional Linear Model or Unbonded Model. The PBM uses two parallel interfaces acting over a small rectangular area defining the contact between two particles. The first interface carries a force, whereas the second interface carries a force and a moment due to relative rotation between particles. Both interface models are linear and use elastic

normal and shear springs. The components of a bonded PBM model are shown in Figure B.1a, and those of the Unbonded Model in Figure B.1b.

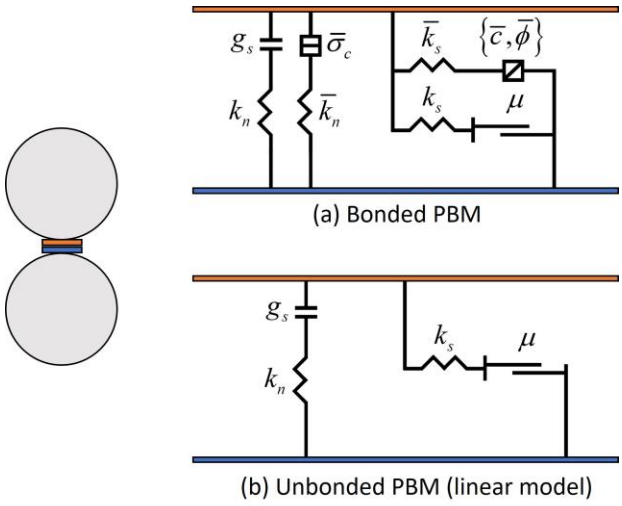

Figure B.1: Rheological components of PBM

In Figure B.1a, g_s represents the surface gap. When $g_s \leq 0$, the first interface is active and resists applied load through linear normal stiffness in compression k_n, and shear stiffness k_s . If $g_s > 0$, all forces at the interface are removed. In Figure B.1a, $\bar{k}_n$ and $\bar{k}_s$ represent the normal and shear stiffnesses of the second interface that carries force and moment. If the strength of the second interface is exceeded (e.g., using Coulomb strength model with cohesion $\bar{c}$ and friction angle $\bar{\emptyset}$.), it can no longer resist rotation and the PBM reduces to the linear elastic or Unbonded Model (Figure B.1b) with only force calculations. Thus, PBM is active if it is bonded or if the surface gap $g_s \leq 0$. The unbonded model is non-tension. More details on the PBM can be found in Itasca Consulting Group, Inc. (2021).

The following chapter is a published paper in the Rock Mechanics and Rock Engineering, 2022, 55 (10), 6263-6277.

Chapter 3: Investigation into rock breakage with expansive cement under biaxial confinement

Author:

Tuo Chen*, Isaac Vennes, Hani S. Mitri

Affiliation:

Department of Mining and Materials Engineering, McGill University, Montreal, Canada H3A 0E8

Address: 3450 University Street, Montreal, Quebec, Canada H3A 0E8

*Corresponding author. Tel.: +14388662473; E-mail address: tuo.chen@mail.mcgill.ca (T. Chen)

Abstract

While drilling and blasting with explosives is widely used for rock fragmentation in mining and civil engineering, its use is associated with rigorous safety and environmental constraints as blasting creates toxic fumes, vibrations and dust. In recent years, there has been a growing interest in transitioning from blasting with explosives to rock fragmentation without explosives. In this study, the potential of expansive cement (EC) as an alternative to explosives to break hard rock under confinement is explored through a comprehensive experimental and numerical modelling study. To do so, two large-scale tests have been designed and carried out on 1 m x 1 m x 0.25 m panels made from high-strength concrete and subjected to planar, biaxial loading conditions. Such test configuration is designed to mimic a mining front subjected to biaxial stresses. Different EC drill hole patterns were tested and compared. The fragmentation behaviour due to EC was first examined with five particle flow code (PFC2D) models simulating different EC drill hole patterns. Two panel designs were retained for the large-scale experiment. It is found that rock breakage with EC under confinement is feasible and promising, especially when the optimized drill pattern from numerical modelling is adopted. It is demonstrated that discrete element modeling with PFC2D can be used effectively to design and optimize the EC drill hole pattern under biaxial confinement. The findings of this study could set the stage for numerous future applications of EC for rock fragmentation of subsurface hard rock excavations such as shafts, tunnels, and mine openings.

Keywords: Expansive cement; Hard rock fragmentation; PFC model; Large-scale biaxial tests

3.1 Introduction

Drilling and blasting with explosives is widely used for rock fragmentation in mining and civil engineering projects. However, the use of explosives is associated with rigorous safety and environmental constraints as blasting creates toxic fumes, ground vibrations and dust. Moreover, underground mining blasts are often accompanied by damage of the wall rocks causing overbreak and requiring additional ground supports. Due to these factors, there has been a growing interest in transitioning from blasting with explosive energy to rock fragmentation without explosives. In this study, the potential of expansive cement (EC) as an alternative to explosives to break hard rock is explored through a comprehensive experimental and numerical modelling study. The work is part of a multi-phase project which ultimately aims to rationalize a robust methodology for the practice of advancing mining fronts under confinement with EC.

Expansive cement, also known as soundless chemical demolition agents or EC is a commercially available product. Its current primary use is in the construction industry whereby old foundations are demolished by injecting EC into drill holes in the foundation. EC is also used in dimension stone quarries as a means for boulder or large block splitting (Shang et al., 2017). More details on the chemical composition of EC and the exothermal reaction leading to the expansion behaviour are found elsewhere (Habib, 2019).

Injected in a drill hole, and once cured, EC gradually exerts increasing pressure on the drill hole perimeter eventually overcoming the tensile strength of the drill hole host medium and creating fractures in the radial direction. With this feature, EC has successfully seen many practical applications where the confining pressure or in-situ stress is low or non-existent. The challenge with the use of EC in subsurface projects such as underground mines is the presence of confining

pressure due to in-situ stress. At the boundary of a mine opening, the state of stress in the plane of the boundary is biaxial, i.e., $\sigma_1 > \sigma_2$ and the stress perpendicular to it is zero, i.e., $\sigma_3 = 0$ (Brown, 1974, Mitri et al., 2005, Yun et al., 2010). As illustrated in Figure 1, an EC drill hole in the mining face would be subjected to biaxial stress representing the confinement. Thus, the challenge with the successful application of EC in underground mining is that the EC expansion pressure must overcome not only the tensile strength of the rock, but also the confining pressure around the drill hole. It is therefore not surprising that EC has rarely been attempted in underground metal mines to break hard rock under high confinement pressure. In this study, such challenge is being addressed for the first time. To do so, five large-scale tests have been designed and carried out on 1 m x 1 m x 0.25 m panels made from high strength concrete under planar, biaxial loading conditions. This test configuration is designed to mimic a mining front subjected to biaxial confining stress as illustrated in Figure 3.1. Different EC drill hole patterns were tested and compared. The fragmentation behaviour due to EC drill holes subjected to confinement was first examined with numerical modelling, more specifically, particle flow code (PFC2D), to help with the design of experiments. Below is a brief literature review focusing on the use of discrete element method (DEM) for the simulation of fracturing process.

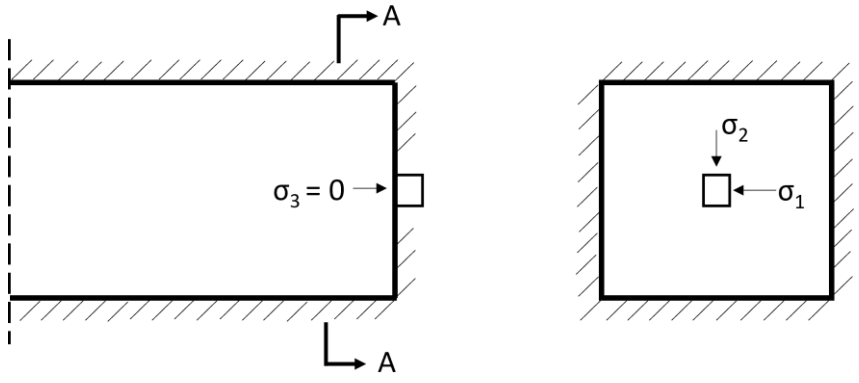

(a) Longitudinal section (b) Section A-A

Figure 3.1: Biaxial state of stress at an excavation face.

With the aim of predicting EC behavior under confinement, numerical modelling approaches are adopted in this research. Since the early 1980s, there has been a growing interest in sophisticated and powerful numerical methods that can be applied to the fracture initiation and propagation processes in rock and concrete materials (Hoek & Martin, 2014). A well-calibrated discontinuum model could predict the rock fracturing process and help us understand the rock fracturing mechanisms induced by EC expansion. Most importantly, modelling can be conducted to optimize the EC drill hole pattern and stress relief hole arrangement, depth, and spacing in the rock panel to boost the fragmentation efficiency, which could save time, cost, and labor when conducting in-situ tests. As a discontinuum approach, discrete element method (DEM) is a robust tool to model cracking and separation processes of rock. In this work, DEM is used to simulate rock fracture initiation and propagation processes induced by EC pressure.

The basic difference between DEM and continuum numerical methods is that the contact patterns between components of the system are continuously changing with the deformation process for the former but are fixed for the latter. Traditional continuum methods such as finite elements and finite difference rely on high quality meshing of the domain to improve the accuracy and in the case of finite difference to also ensure solution convergence when explicit method is used. For the DEM, unless the discrete element is treated as deformable and divided into a mesh of continuum elements, there is no convergence problem as the calculation is processed by moving boundary condition and changing contact. Besides, DEM can support and model large displacements, rotation, and frictional sliding between particles (Jing, 2003).

Wanne and Young (2008) conducted a numerical modeling study of rock failure due to thermal expansion using the discrete element code PFC2D. The numerical model was validated with

laboratory experiments of granite cylinders that fractured due to a heat source placed in a central borehole. The numerical models showed similar failure behavior to that observed in laboratory experiments. Lan et al. (2010) studied developed fracture initiation and propagation in intact brittle rock using the DEM code UDEC. The program UDEC is developed by Itasca (2015) and was used in the study to model a deformable polygonal grain-like structure (see Figure 3.2) which closely simulates the mineral grain structure of brittle rock.

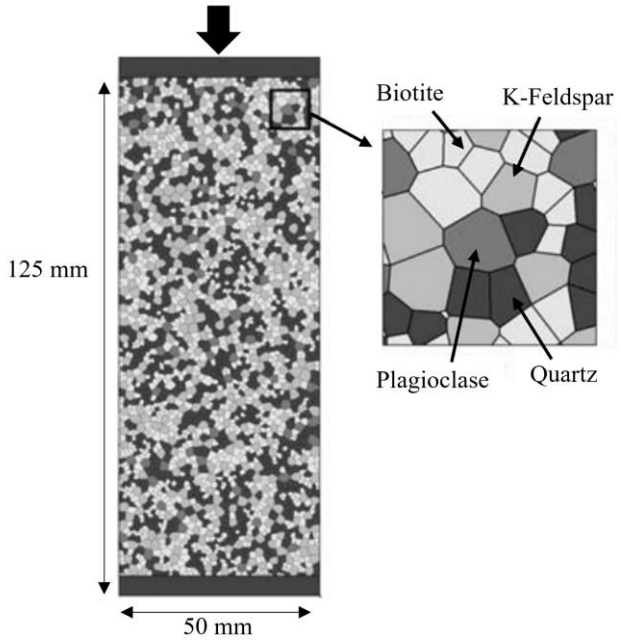

Figure 3.2: Layout for an unconfined compression test for a granite sample using GBM-UDEC model. (Reproduced from Lan et al., 2010).

Haeri et al. (2018) simulated crack separation of concrete disc specimens under Brazilian tensile tests using DEM code PFC2D. The tested disc specimens contained one or two pre-existing non-persistent joints and showed different fracturing paths when the joints length is different. It is found that these fracturing path differences are in very good agreement with the DEM modelling results. Cho et al. (2007) introduced a clumped particle model to simulate the failure envelope and

behaviour of rock using PFC2D code. In a bonded particle model, particles are grouped into many clumps with designated radius by a stamping logic, as shown in Figure 3.3. For each formed clump, the group of glued particles behaved as a single rigid body and could not be broken apart. Hence, irregularly shaped clumps increase the dilatancy and frictional resistance within rock model. After calibration, the clumped-particle model accurately predicted both the stress–strain behavior and the complete nonlinear failure envelope for both Lac du Bonnet granite and a weak synthetic rock under uniaxial loading. Ye et al. (2019) proposed a more advanced clump logic that can be used for both 2D and 3D bonded particle models. Different with stamping logic in Figure 3.3, this method revolves around the idea of growth from a seed particle, which is similar to the mineral crystallization process. The DEM rock model generated using this clump logic resulted in higher interlocking and properly predicted high compressive to tensile strength ratios and nonlinear strength envelope. Ivars et al. (2011) proposed a synthetic rock mass approach for jointed rock mass modelling in bonded particle model using PFC3D. As shown in Figure 3.4, the intact rock is represented by bonded particle model and joints are represented by the smooth joint model. The concept of synthetic rock mass was also used by Castro-Filgueira et al. (2020) for the simulation of intact and fissured granite samples. In this research, flat-joint contact model was applied for the intact rock, and the smooth-joint contact model is applied for artificial fissures. The modelled pre-peak behavior of rock is quite similar to laboratory tests, but post-failure volumetric strain is typically larger than actual test values. Overall, it is shown that a well-calibrated DEM model can simulate the fracturing process of rock and concrete materials explicitly, all while considering pore pressure and/or thermal expansion when modelling multi-physics behaviour.

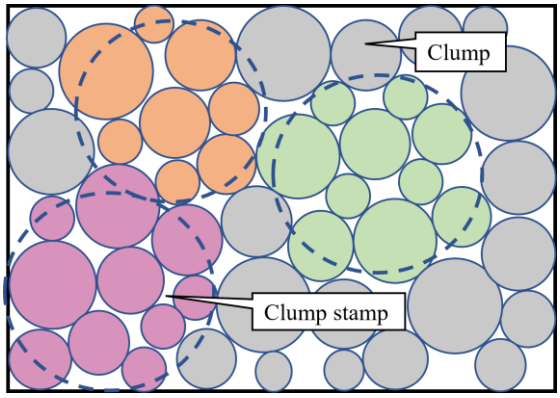

Figure 3.3: Illustration of stamping logic to control clump size (Reproduced from Cho et al., 2007).

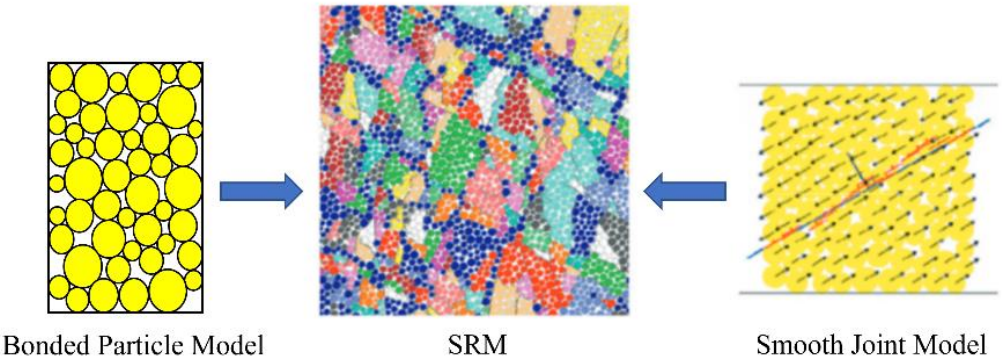

Figure 3.4: Synthetic rock mass basic components (Reproduced from Ivars et al., 2011).

3.2 Mechanical property calibration models

3.2.1 Model design

Rock mechanics is one of the disciplines from which the DEM developed (Burman, 1971; Cundall, 1971; Chappel, 1972; Cundall & Strack, 1979). Cundall & Strack (1979) first showed that DEM can also be used to model granular assemblies of 2D discs and 3D spheres. DEM has become increasingly popular in the field of rock engineering since Potyondy et al. (1996) demonstrated that this computational method could be used for simulating deformation and fracturing of rock. The basic formulation of DEM includes the equations of motion of rigid/deformable elements,

such as blocks, particles, or other shapes of bodies. The contacts between bodies in the model domain are identified and updated during the computation process until convergence is obtained. The response of contacts and deformable bodies are represented by suitable constitutive models. In the case of deformable bodies in general DEM method, implicit or explicit continuum methods can be used to discretize and calculate stress-strain relations within the discrete bodies and the contacts between them can be seen as continuously updated boundary conditions.

According to the in-situ stress survey in the Canadian shield (Arjang and Herget, 1997), the maximum horizontal-to-vertical stress ratio usually ranges from 1 to 3 at depths between 1000 m to 500 m. That said, the induced stress around the excavation is even higher than the in-situ stress if the surrounding rocks are assumed to be homogeneous (Brady and Brown, 1993). In this study, large panels of 1 m x 1 m x 0.25 m will be placed in a biaxial loading setup as will be discussed later. The applied loads will result in a biaxial confinement of 23 MPa and 15 MPa. Such level of confinement represents a virgin far-field stress at approximately 500 m below surface in the Canadian shield, where the minor stress (13 MPa) is vertical, and the major stress (25 MPa) is horizontal.

To predict the EC drill hole pattern performance under biaxial loading, a panel is modelled under biaxial stress with PFC2D. A well-calibrated DEM model is capable of simulating crack initiation and orientation as well as the separation process of the material explicitly. The first step is to apply in-situ confinements to the model boundaries. Subsequently, the holes are drilled off in the panel before injecting EC into the holes. Clearly, the EC drill hole arrangement is critical as it will dictate the rock fracturing pattern and the efficiency of EC. Hence, the main objective of the numerical modelling study is to predict and optimize the EC drilling pattern before carrying out the physical experiment.

Once different drilling patterns are modelled and compared, the large-scale tests are conducted, and the efficiency of EC drill hole patterns is assessed. The test results will also be useful in validating the PFC2D models. Considering the labour work and expense incurred to prepare large-scale intact rock blocks, it was decided to test panels made from high-strength concrete instead used in the current stage of the research project. The concrete panels should provide an indication of EC behaviour in hard rock.

3.2.2 Calibration models

To calibrate the parameters of PFC2D model, uniaxial and Brazilian tests are conducted on cylindrical specimens that are cored from the prepared concrete block to determine the mechanical properties of the high-strength concrete; see concrete cores in Figure 3.5. The UCS tests are completed using axial displacement control at 0.0009 mm/s and the Brazilian tests are completed using axial load control at 0.10 kN/s. The results are shown in Table 3.1 for the UCS tests and Table 3.2 for the Brazilian test. For the purposes of numerical model calibration, the average values of UCS = 54.6 MPa, E = 24.2 GPa, and BTS = 4.9 MPa, were used in the PFC2D model.

Figure 3.5: High-strength concrete cores.

Table 3.1: UCS test results for concrete

Specimen ID	Specifications			Strength and Elastic Properties			
	Diameter (mm)	Length (mm)	Bulk Density (g/cm^3)	Peak Strength (MPa)	Confinement (MPa)	Young's Modulus E (GPa)	Poisson's Ratio
STAC-C-U1	74.92	169.98	2.32	54.7	0.0	24.6	0.08
STAC-C-U2	74.91	169.98	2.32	51.8	0.0	23.7	0.05
STAC-C-U3	74.92	170.02	2.33	57.4	0.0	24.3	0.07
Average				UCS: 54.6		24.2	0.07

Table 3.2: Brazilian test results for concrete

Specimen ID	Specifications			Strength and Elastic Properties	
	Diameter (mm)	Length (mm)	Bulk Density (g/cm^3)	Failure Load (kN)	Brazilian Tensile Strength (MPa)
STAC-C-B1	74.82	49.80	2.30	32.20	5.50
STAC-C-B2	74.95	49.78	2.29	14.06	2.40
STAC-C-B3	74.89	49.82	2.29	28.42	4.85
STAC-C-B4	74.63	50.00	2.28	27.35	4.67
STAC-C-B5	74.94	49.98	2.28	29.86	5.08
STAC-C-B6	74.91	49.79	2.30	29.32	5.00
Average (Excluding Max and Min values)					4.90

To perform model calibration, two basic PFC2D models were first created – one for UCS simulation and calibration and another for tensile strength. A trial-and-error calibration procedure was employed in the PFC2D models where the microscopic parameters of the particles and bonds are varied until the uniaxial and direct tensile tests yield strength results converge to experimental

ones. In this way, the proper input microscopic parameters are decided and the PFC2D model for high-strength concrete material is calibrated. The specimens are modelled in PFC2D using parallel-bonded model, as shown in Figure 3.6a. Parallel-bonded model provides an interface with a pair of springs with constant normal and shear stiffnesses between each pair of particles, and is suitable to simulate solid materials such as rock, concrete, coal, etc. (Liu et al., 2019; Haeri et al., 2018). These two springs have specified tensile and shear strengths when the interface is bonded. Once the shear or tensile stress acting on the interface exceeds the specified strength, the bond breaks creating a shear or tension crack as shown in Figure 3.6a. The relation between particle motion and the acting forces is based on Newton's law (Potyondy and Cundall, 2004).

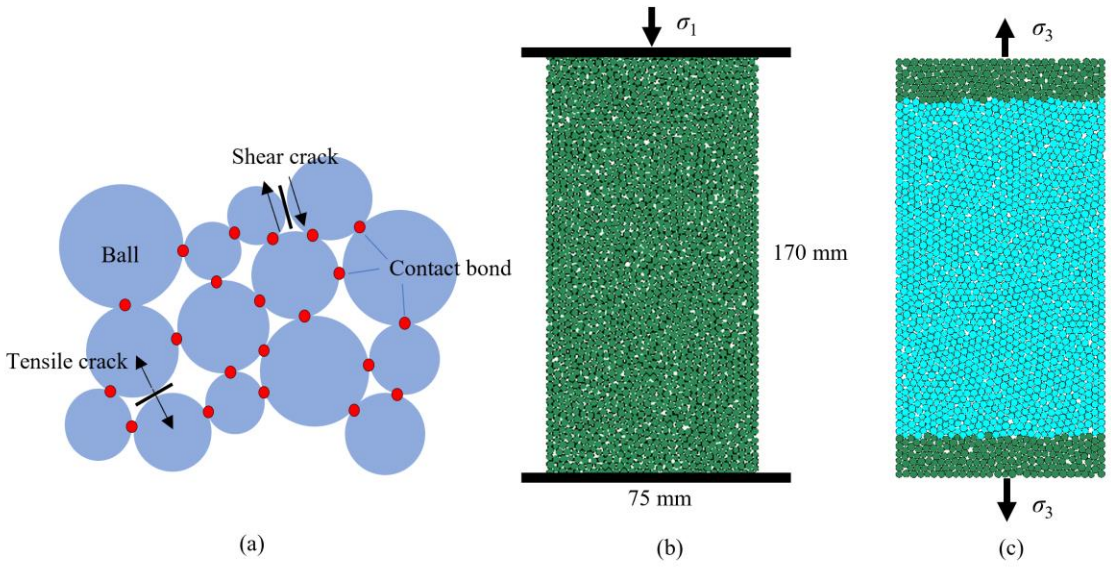

Figure 3.6: PFC2D calibration models. a) Parallel-bonded assembly, b) UCS model, c) direct tension model.

Dimensions of the PFC2D models for uniaxial and direct tensile tests are shown in Figure 3.6b and 3.6c. These simplified models are deemed representative for mechanical property calibration purposes. Particle size or resolution of the DEM model is an important parameter as the particles

must be small enough to let the crack propagate through its desired path but decreasing the diameter of the smallest ball D_{min} in the assembly will significantly increase the computation time. Also, if model has been calibrated with respect to certain D_{min} and D_{max}/D_{min} ratio, it should not be changed, or the calibration process needs to be repeated. The maximum and minimum radii of the particles are 2 mm and 3 mm in this modelling work to allow for a satisfactory resolution and reasonable computation time.

During the calibration process, the microscopic parameters of the bonded particles are changed until a suitable stress-strain curve is obtained as shown in Figure 3.7. As can be seen, the axial stress-strain plot indicates that the UCS is 54.5 MPa, the Young's Modulus is 24.3 GPa, and the Poisson's ratio is 0.07. This is consistent with the concrete lab test results. Meanwhile, the simulated direct tensile strength test shows the tensile strength is 4.9 MPa, which is in line with the Brazilian test results. Figure 3.8 shows the simulated failure modes in terms of shear and tension cracks. Considering the purpose of the study, tensile strength is the most critical property in the simulation as it determines whether the rock around the EC drill hole will break (Hanif et al, 2007). The calibrated microscopic parameters are listed in Table 3.3.

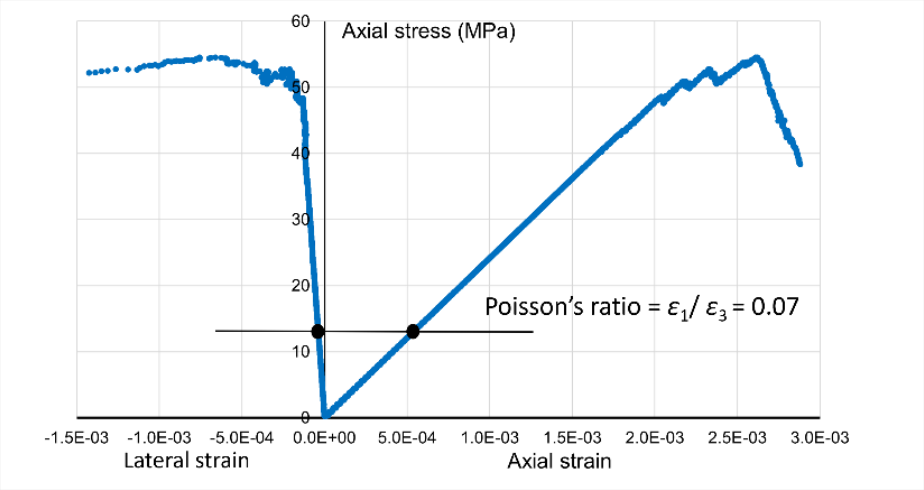

Figure 3.7: Simulated stress-strain curve as produced by the calibration models.

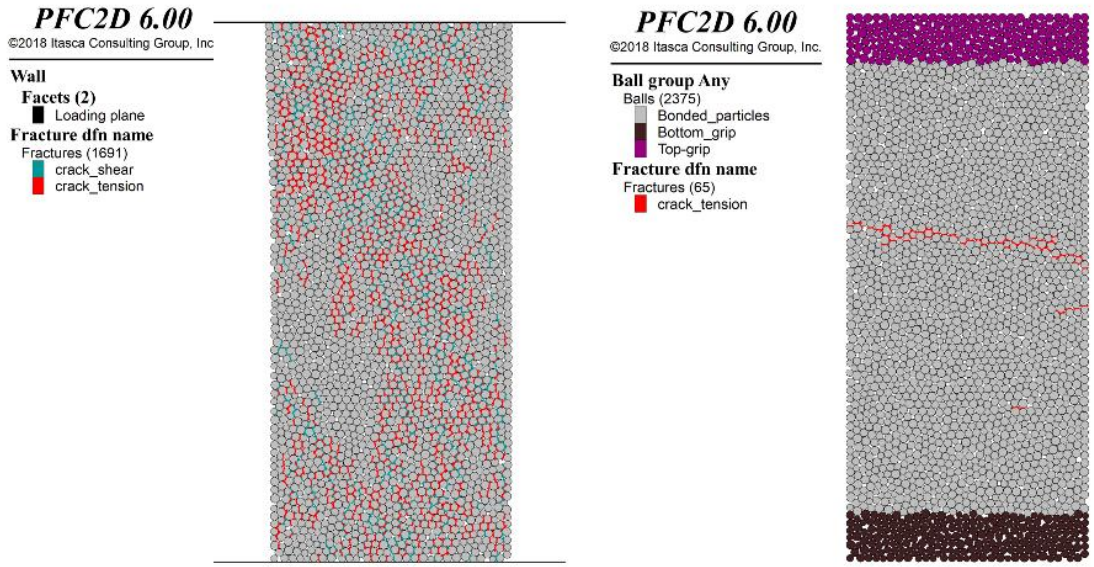

Figure 3.8: Simulated failure modes. (a) UCS model, b) Direct tension model.

Table 3.3: Calibrated microscopic parameters in PFC2D model.

Bond stiffness		Bond Strength		
Effective Modulus E^*	k^* (k_n to k_s ratio)	Tensile Strength σ_t	Cohesion c	Frictional Angle φ
10 GPa	0.9	5 MPa	16 MPa	45°

3.3 PFC2D models for EC drill hole patterns

3.3.1 Model setup

With the aim of simulating panel fracturing due to EC pressure and comparing different drill hole patterns, the parallel-bonded particles are assembled as two-dimensional panels with dimensions of 60 cm × 60 cm in PFC2D. The calibrated parameters in Table 3.3 are used with the same particle size (2 to 3 mm) to ensure that the physical behaviour of the modelled panels is close to reality. Five numerical models with different drilling patterns are examined as shown in Figure 3.9. The

drill pattern in Model #1 was previously proposed by Alvarez De la Garma (2021) who found it to be more effective than the staggered hole pattern based on ABAQUS modelling results. Similar to blasting, relief holes are introduced in each pattern. In drilling and blasting, the purpose of the void hole is to provide a free face for the movement of the fragmented material. Void holes in EC method pattern serve to shield the EC hole from the biaxial stress field, facilitating rock fracturing around the EC hole by releasing the confining stress. As can be seen in Figure 3.9, the EC holes are 38 mm (1.5”) in diameter, and the relief holes are 101 mm (4”) in diameter. The distance between centers of stress relief and EC holes is 10 cm.

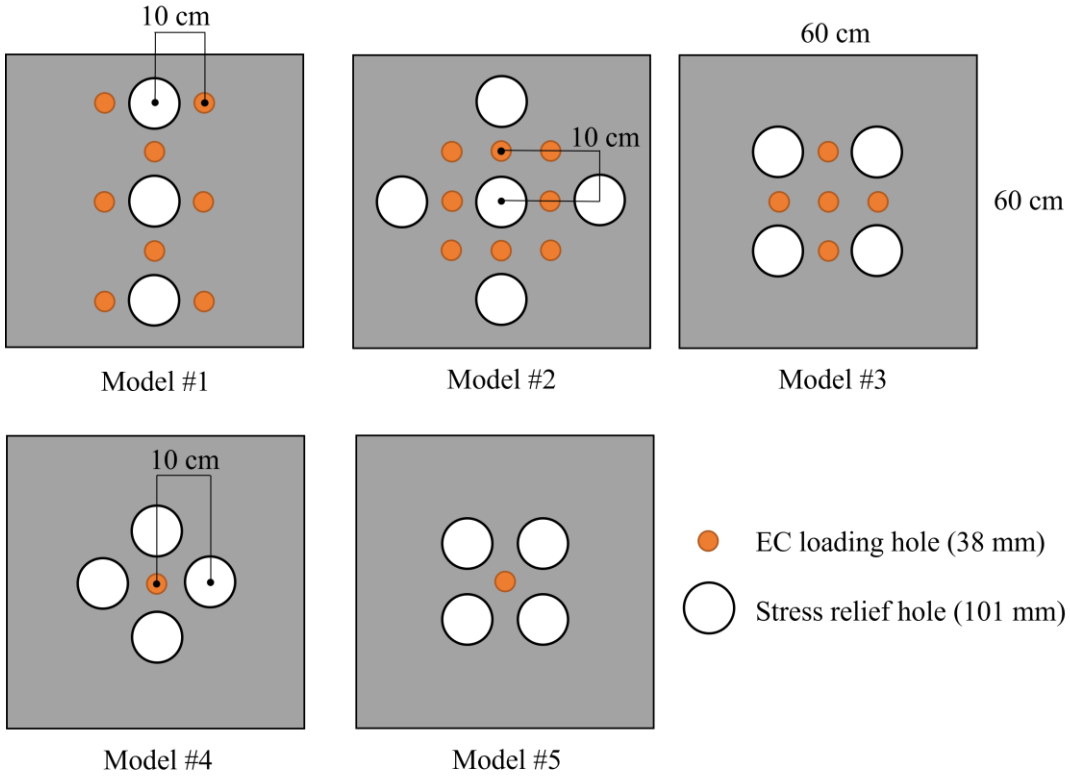

Figure 3.9: Five concrete panels with different EC drill hole patterns.

Prior to loading the EC holes, the biaxial loading conditions are applied to the model boundaries. As shown in Figure 3.10, there are four lines around the model domain that are shown by dotted red lines. The inward motion of the lines is adjusted so that a constant confining pressure is

maintained in the model domain. The applied vertical confinement is 23 MPa and the applied horizontal confinement is 15 MPa. For example, the horizontal stress, vertical stress contours of Model #1 after initial biaxial loading are shown in Figure 3.10.

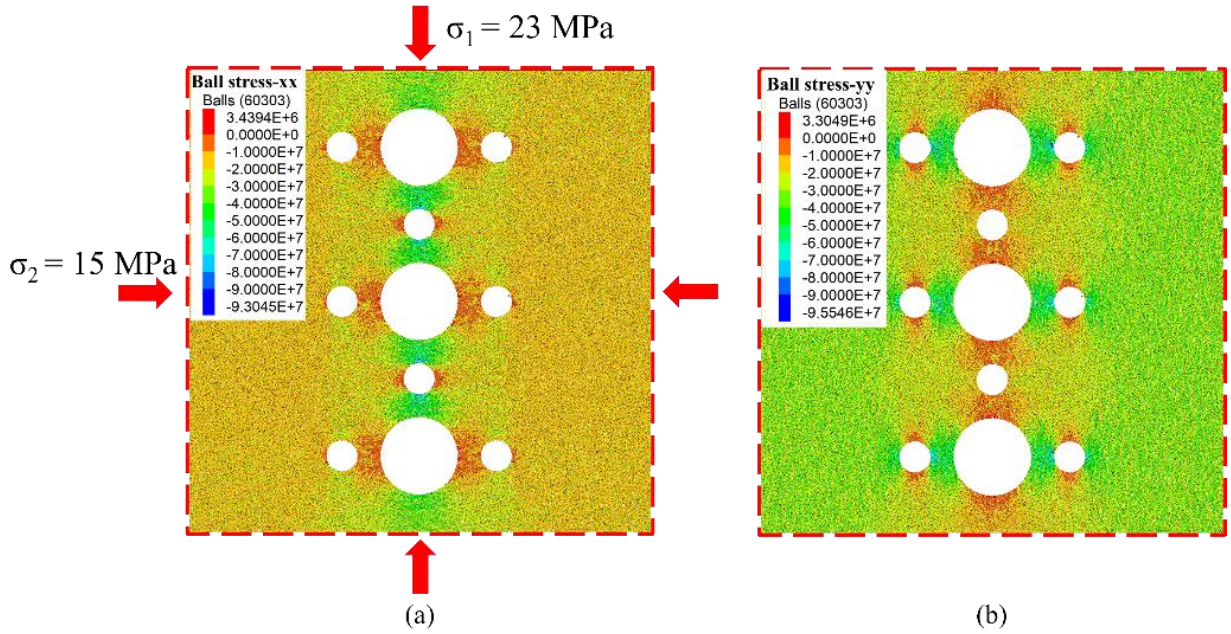

Figure 3.10: Model #1 prior to EC loading. a) Horizontal stress, (b) Vertical stress.

3.3.2 EC pressure simulation

Once the confinement is initialized, the EC pressure needs to be applied. The proposed modelling scheme to simulate pressure generated by EC is illustrated in Figure 3.11. It allows for the gradual increase of the EC pressure p_{EC} from zero to its target peak value p_{Peak}. To do so, the effect of EC is simulated by a rigid ring that is initially placed in the EC hole with no contact with the drill hole, i.e., $p_{EC} = 0$; see Figure 3.11a. The size of the ring is gradually increased until it exceeds that of the EC hole, thus $p_{EC} > 0$ is applied to the drill hole as shown in Figure 3.11b. Finally, the ring will cease to expand when the input value of the EC pressure p_{Peak}. is attained (Figure 3.11c).

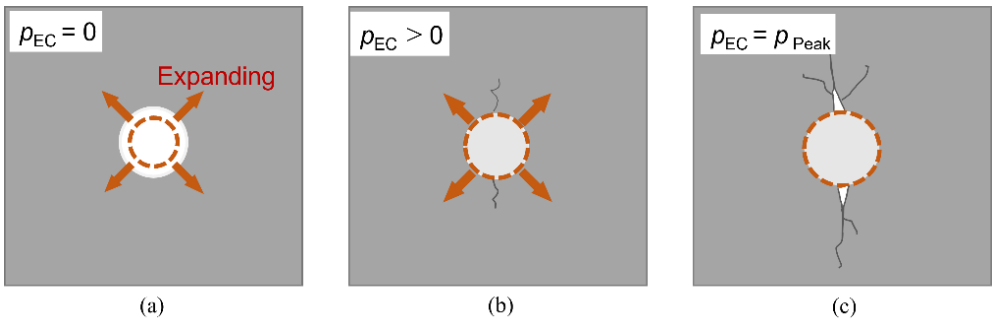

Figure 3.11: Proposed scheme for simulating EC pressure. a) Initial ring placement, b) EC pressure >0, c) EC peak pressure.

3.3.3 Modelling results

In this study, the peak EC pressure generated in high-strength concrete is assumed to be 40 MPa (Habib, 2019). By assuming a constant peak EC pressure, the fracturing results in different panel models can be compared to quantitatively decide which drilling pattern is more efficient for panel fragmentation due to EC.

When the generated EC pressure reaches its peak value, the total number of fractures (broken bonds) is counted for each model. The modelling results are shown in Figure 3.12 and the particle movement directions are annotated by blue arrows. It can be seen from Figure 3.12a, b, c that the drilling patterns in the first three models are not effective. Relatively fewer fractures around the EC holes are observed and the panels remains stable after EC pressure reaches the peak value of 40 MPa. A possible explanation for this might be that the stress relief holes in the first three patterns are only providing uniaxial stress-relief, because each EC hole is subjected to neighboring stress relief in single direction. For example, the top hole in Model #3 (see Figure 3.12c) has adjacent stress-relief holes on two horizontal sides. The particles will be pushed towards two horizontal sides under EC pressure, but they are still subjected to the vertical confinement (green arrows in Figure 3.12c). As a result, the uniaxial stress relief regimes developed in Models #1, #2

and #3 are deemed inefficient. There is also some consistency in the results of the first three models in the sense that Model #3 with the least number of EC boreholes yields less fractures than Models #1 and #2, which have 8 EC holes each. Model #2 has 5 stress-relief holes compared with 3 stress-relief holes in Model #1, thus Model #2 has the greatest number of fractures among the first three models with more EC holes and stress relief holes.

The results of Model #4 and Model #5 are very encouraging. As shown in Figure 3.12d, e, significant fractures are developed around the EC hole and the material between the four stress-relief holes has broken through to form a large cavity at the center of the panel. Interestingly, nearly 4000 fractures are induced from this single EC hole, which is much greater than EC holes in previous models. This shows the importance of arranging boreholes strategically when implementing EC technology under biaxial loading conditions.

Moreover, the significant damage in Model #4 and #5 can be attributed to the biaxal stress-relief regime created around the EC hole, hereby the bonds between particles can be broken easily under EC expansion. We also see that the Model #4 is more recommended compared with Model #5 as the pattern has more fractures caused by EC. This is because the stress relief holes in Model #4 are arranged in the direction of principal stresses, which means the induced stress relief is more efficient and EC is easier to expand and cause fractures.

In summary, these results show that Model #1, #2 and #3 with uniaxial stress relief condition is not efficient and the panels show less damage. From Model #4 and Model #5, it is observed that only one EC hole can lead to much more fractures under biaxial stress relieves condition. In the next step, the modelling results will be tested to validate the PFC modelling results.

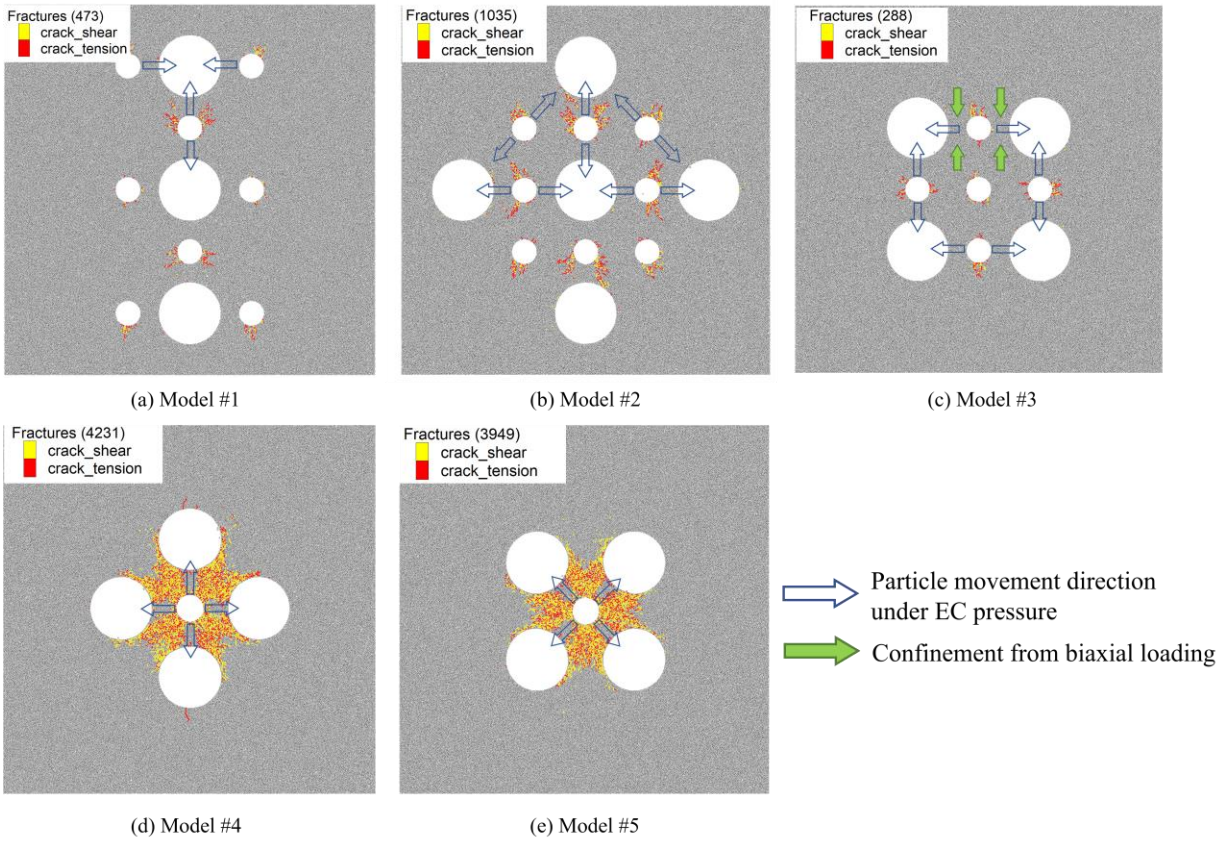

Figure 3.12: Fracturing results for five models.

3.4 Large scale biaxial loading test

3.4.1 Test design

Large-scale biaxial panel breakage tests were conducted at CANMET (Canada Centre for Mineral and Energy Technology) Mining laboratory in Sudbury, Ontario, Canada. The biaxial system used a servo-controlled vertical press having a capacity of 10 MN (Figure 3.13a). A 6 MN lateral self-reaction frame (see Figure 3.13b) was designed and built specifically for this project to be used in conjunction with the vertical press to achieve the desired biaxial loading configuration. Details of the frame design can be found elsewhere (Alvarez De La Garma, 2021). With the available system loading capacity, it was possible to test a panel of 1 m x 1m x 0.25 m, and with only 0.20 of the

thickness subjected to biaxial loading, confinement levels of 23 MPa and 15 MPa were possible to achieve in the vertical and horizontal directions, respectively.

(a) (b)

Figure 3.13: Biaxial loading test apparatus, (a) Vertical press, b) Lateral loading frame.

The large-scale test results will be compared with the numerical modelling results. To verify the model validity and examine EC behaviour under biaxial loading, two concrete panels with dimensions of 1 m × 1 m x 0.25 m were fabricated for testing. The first panel design adopts the idea of uniaxial stress relief in Model #1 which showed more fractures than Model #3. As shown in Figure 3.14, 24 EC holes and 5 stress-relief holes are drilled in the first panel. The diameters of EC holes and stress-relief holes are 31 mm (1.25”) and 101 mm (4”), respectively. All EC holes have the same depth of 158 mm maintain an aspect ratio (drill hole depth-to-diameter) of 5. This would leave a 42 mm thick biaxially stressed zone behind the drill hole toe, in addition to another 50 mm of unloaded skin.

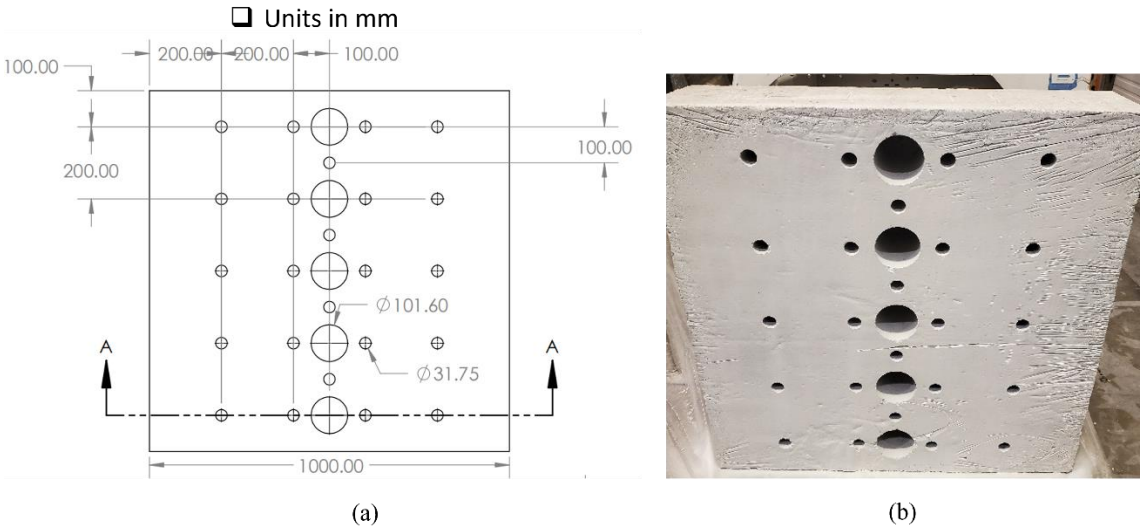

Figure 3.14: Concrete panel # 1. a) Drill hole pattern design, b) Photograph.

Figure 3.15 shows the second panel design which employs biaxial stress-relief regime from Model # 4 that yielded the most fractures amongst all five numerical models. The second panel has 19 EC holes and 10 stress relief holes. As can be seen from Figure 3.15, the diameter of EC drill hole is increased from 31 mm in Panel #1 to 38 mm. As no significant failure was observed in panel #1 test, it was decided to slightly increase the EC drill hole diameter to increase the likelihood of a successful trial. The same drill hole aspect ratio of 5 was employed, resulting in a drill hole depth of 17.78 cm.

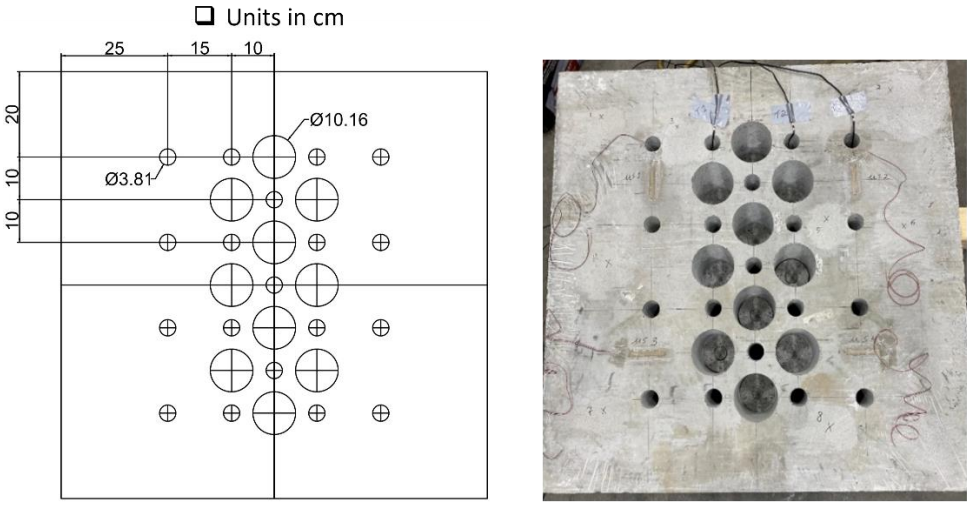

(a) (b)

Figure 3.15: Concrete panel #2 design (a) and picture (b).

3.4.2 Test procedure

The same loading and monitoring procedure is used for both concrete panel tests. For safety reasons, the EC holes were loaded before the panel, placed in the lateral frame, was pushed under the vertical press as shown in Figure 3.16a. The servo-controlled loading was applied both horizontally and vertically. The loads applied on both horizontal and vertical frames were monitored throughout the test to ensure constant load application. Keyence displacement sensors were installed on the loading frames to monitor vertical and horizontal panel deformations. Figure 3.16b illustrates the loading rate for two the loading frames. Horizontal and vertical confinements of 15 MPa and 23 MPa respectively were applied on the panel. A time-lapse camera was set up in front of the panel to monitor and capture the evolution of fracturing. At room temperature (25 °C), cracking time due to EC varied between 6 to 10 hours when the diameter of EC borehole was 31 mm to 38 mm. The experiment was monitored for 24 hours to capture the full effect of EC on the panel. It should be noted that the time provided in Figure18a and Figure20a are the time after load

application is initiated, and not time after EC mixing as the latter took place before final positioning of the panel under the loading frame.

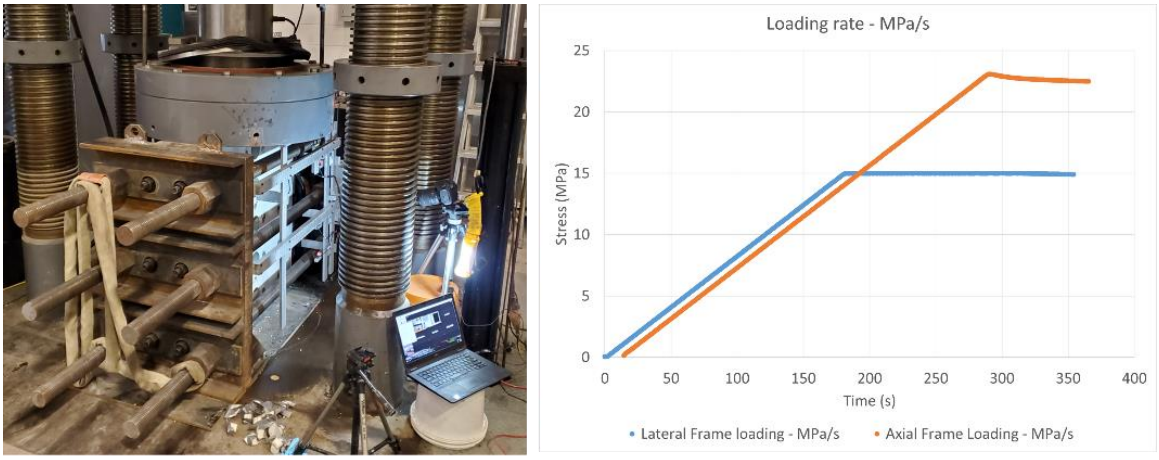

(a) (b)

Figure 3.16: Biaxial load application. a) Lateral frame under the press, b) Applied loading rates.

3.4.3 Test results

3.4.3.1 Concrete panel #1

Figure 3.17 shows the times lapse pictures obtained from panel #1 test. Figure 3.17a shows the panel condition at the beginning of the test. However, after 20 hrs, there is still no failure or significant fractures detected in this test. Only some spalling is observed on the panel surface around the EC hole as shown in the Figure 3.17b.

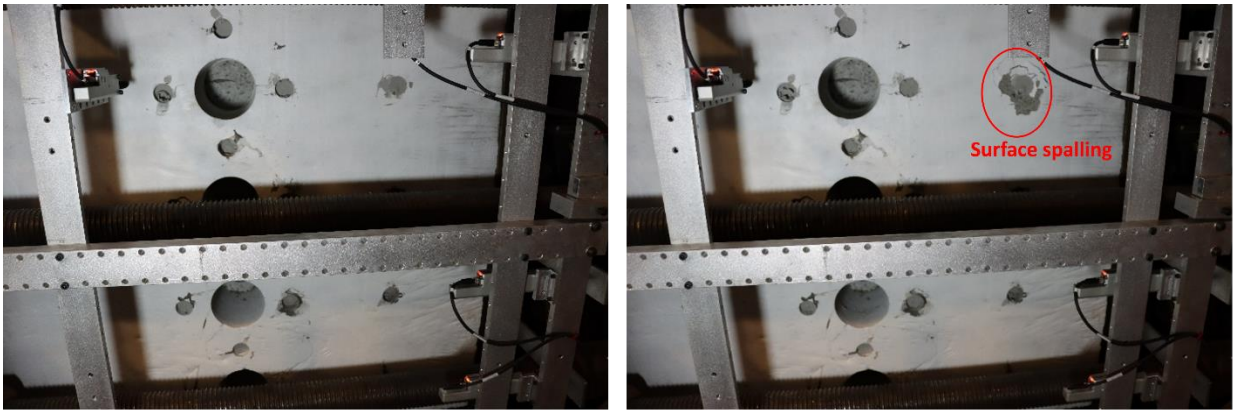

(a) At beginning (b) After 20hrs

Figure 3.17: Pictures of the panel #1 during the test.

Notably, the lateral stress was manually dropped from 15 MPa to 10 MPa before the test was terminated. This was done to see if partial collapse of the panel could occur. However, even with the lateral confinement reduced, the panel was still stable. Therefore, the panel did not break after 20 hours even with 10 MPa lateral confinement. This result is in line with the results of Model #1which reveals that this uniaxial stress-relief pattern is not effective for panel fragmentation.

Figure 3.18a shows the force vs time plot where a steady decay in the vertical load over time is observed. This could be interpreted as slight loss of strength due to EC. The axial frame was set to keep zero displacements at target load. Pressure decay is also observed in the lateral direction over time, albeit much smaller. Given that little pressure decay occurred in the lateral direction, it is concluded that little damage occurred in the panel over the duration of the test.

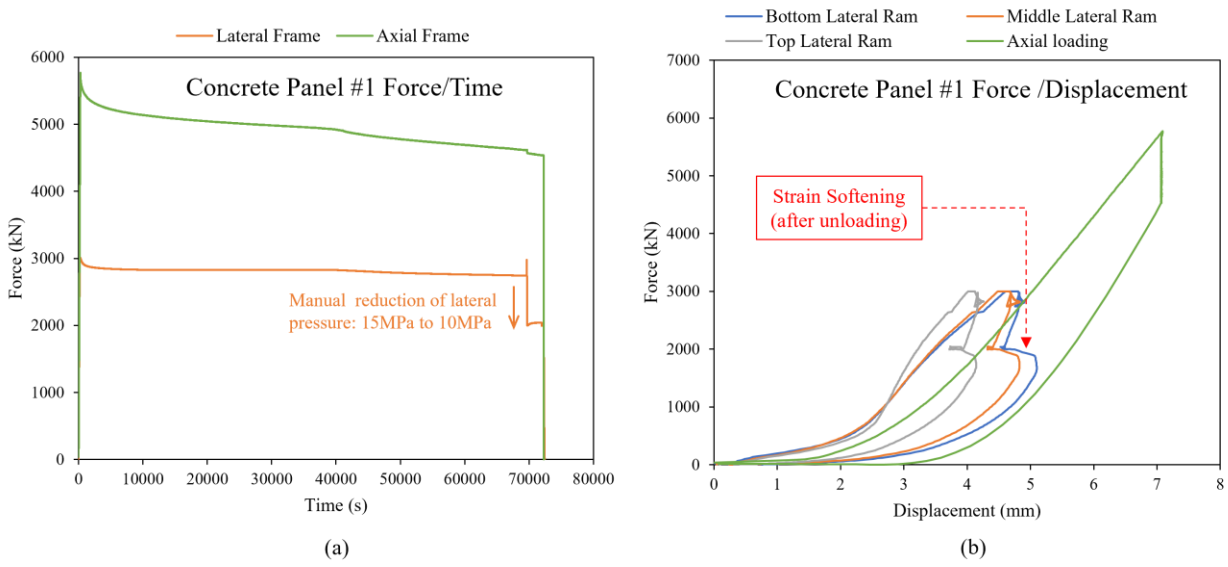

Figure 3.18: Panel #1 test results. a) Force vs time, b) Force vs displacement.

The plot of force vs displacement in Figure 3.18b shows that no ductile strain softening occurred prior to unloading in the lateral direction, indicating that no significant damage occurred in the panel at full load. However, damage did occur when the lateral pressure was reduced from 15 MPa to 10 MPa. This is detected from the ductile deformations of up to 1 mm (e.g., 4 mm to 5 mm total deformation at the bottom lateral ram) that were observed after unloading. However, once the panel was completely unloaded, most deformations recovered, and the panel remained intact albeit with some apparent fracturing.

3.4.3.2 Concrete panel #2

Figure 3.19 presents a series of times lapse pictures obtained from the panel #2 test. Obvious fractures started showing up 5 hrs after the expansive agents are poured in boreholes (see Figure 3.19a). Then, an increasing number of fractures were observed with panel surface spalling and bulging, as shown in Figure 3.19b, c. Interestingly, there are also some bulging mechanisms leading to the panel out-of-plane motion. These out-of-plane fractures can be observed from the

inside of stress-relief holes, as illustrated in Figure 3.19c but could not be simulated using two-dimensional modeling. The panel eventually failed completely at 11 hours 50 minutes after mixing EC when the in-plane shear failures coalesced around the EC holes, as shown in Figure 19d. This is in line with the PFC2D Model #4 that the central EC hole coalesced with the surrounding stress-relief holes and the pattern center was broken through to form a cavity.

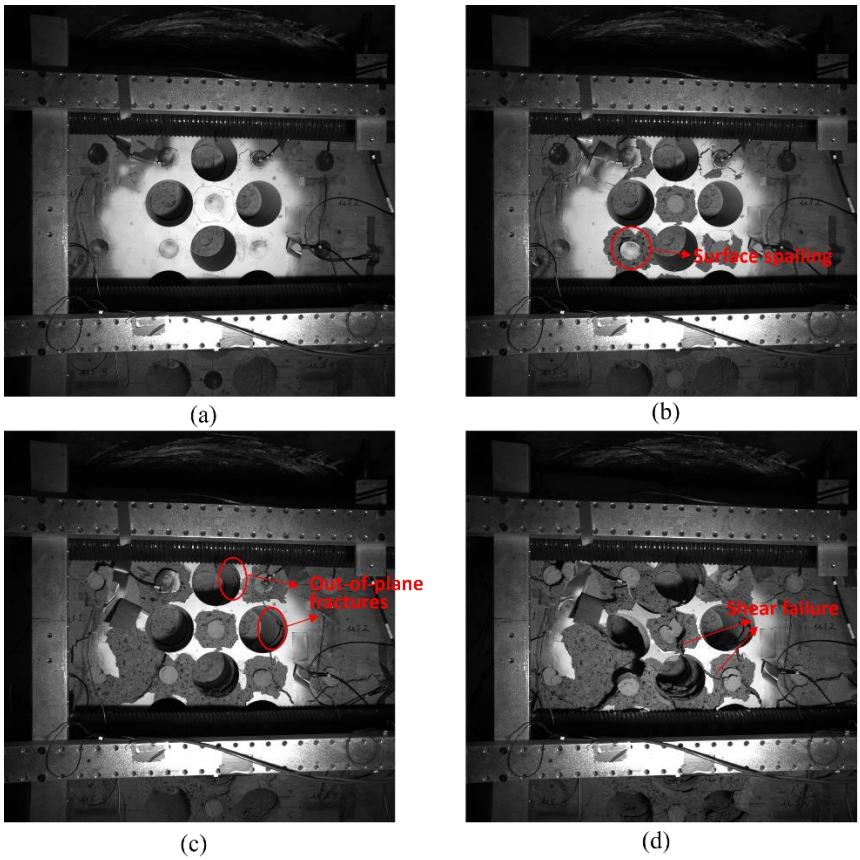

Figure 3.19: Time lapse pictures of panel #2 test. a) At 5 hours, b) At 7 hours, c) At 9 hours, d) At 11 hours 50 mins.

While concrete panel #2 is successfully fractured under biaxial confinement due to EC, out-of-plane failure causing bulging motion of the damaged material could not be simulated with PFC2D. Three-dimensional modelling would be required in future work to help gain better understanding of the out-of-plane panel failure mechanism induced by EC.

The force vs time and force vs displacement for concrete panel #2 are plotted in Figure 3.20a and 3.20b, respectively. Overall, it can be seen that this pattern using biaxial stress-relief regime is more effective for EC to fragment the panel under biaxial loading than the previous pattern of panel #1. In contrast to the steady pressure curve in Figure 3.18a, a gradual pressure decay as of 13000 seconds (3.6 hours) after load application in both directions is observed in Figure 3.20a. This decay started about 6.1 hours after mixing EC and thus it is consistent with the panel fracturing time shown in Figure 3.19, indicating that the EC was continuously damaging the panel during the test once it started expanding. Figure 3.20b shows that the pressure reduction observed in Figure 3.20a corresponds to increase in displacements in all three lateral rams. This can be interpreted as the panel strain-softening after failure. The unloading points for lateral rams are not presented for clarity. Contrary to panel #1 (see Figure 3.19b), strain softening in Figure 3.20b occurred prior to unloading, proving that the EC action has successfully fractured the panel under biaxial confinement. Apparently, more discrete element modelling would help further optimize this pattern in terms of fragmentation density and time to fracturing.

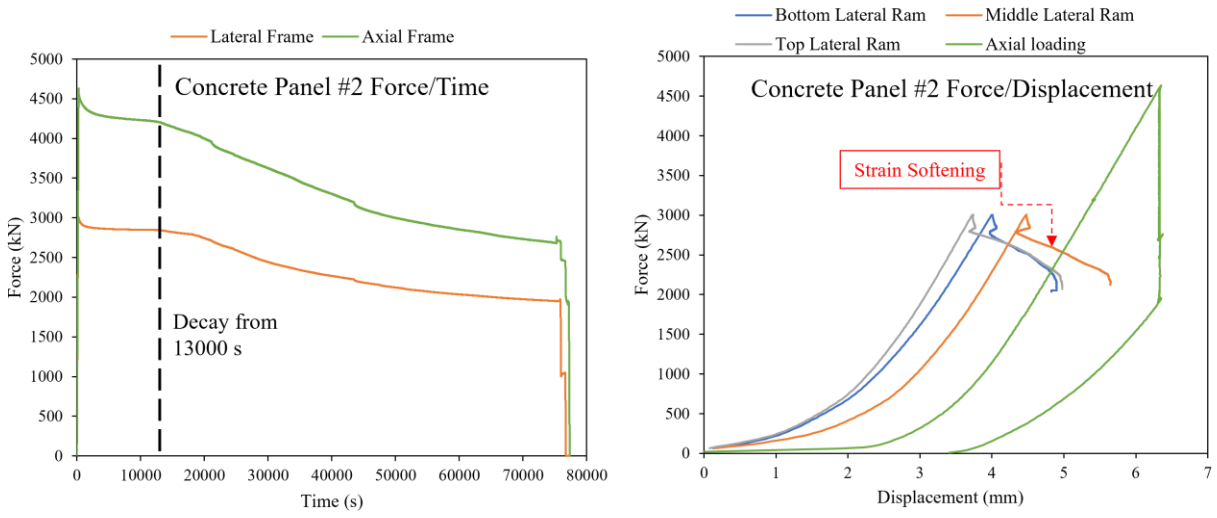

Figure 3.20: Panel #2 test results. a) Force vs time, b) Force vs displacement.

3.5 Conclusion

This work aims to investigate the potential of EC as an alternative to explosives to break hard rock under biaxial confinement. In this study, discrete element modelling with PFC2D code is used to simulate and optimize expansive cement drill hole pattern for fracturing a biaxially loaded panel. Two large-scale panel tests with different EC drill hole patterns, are conducted on high-strength concrete panels, and the results are compared with those from the PFC2D models. The findings of this investigation are summarized below.

- Five PFC2D models are developed to examine the efficiency of EC to fragment a panel under biaxial loading. Based on the numerical modelling results, Models #1 and #4 were selected for large scale testing.
- It is shown that PFC2D modelling results are in line with the experimental results, demonstrating that PFC2D can adequately predict the expansive pressure and fragmentation behaviour due to EC.
- The notion of using stress relief hole to enhance EC fracturing is explored. For a panel under biaxial loading, both modelling and test results indicate that stress relief holes are necessary to break the panel.
- Relief holes in one direction as in Models #1, #2, #3 appear to be less efficient. The simulated panel breaks more fully when relief holes are employed in both loading directions, which is the case for Models #4 and #5.
- Concrete panel #2 is successfully fractured under biaxial confinement due to EC. Apart from in-plane failures as predicted by numerical modelling, there are some out-of-plane failures observed from the large-scale panel test. However, such bulging motion cannot be

simulated with PFC2D. Three-dimensional modelling would be required in future work to help gain better understanding of the out-of-plane panel failure mechanism induced by EC.

- This study sheds light on how EC behaves in rock-like material such as high strength concrete under biaxial confinement. The findings could set the stage for numerous future applications of EC for rock fragmentation of subsurface hard rock excavations such as shafts, tunnels, and mine openings.

References

Alvarez De La Garma, J. (2021). Numerical simulation of rock fracturing due to borehole expansive pressure under biaxial loading condition. Master of Science Thesis. McGill University. Montreal. Canada.

Arjang, B., & Herget, G. (1997). In situ ground stresses in the Canadian hardrock mines: an update. International Journal of Rock Mechanics and Mining Sciences, 34(3-4), 15-e1.

Burman BC. (1971) A numerical approach to the mechanics of discontinua. PhD thesis, James Cook University of North Queensland, Townsville, Australia.

Brady, B. H., & Brown, E. T. (1993). Rock mechanics: for underground mining. Springer science & business media.

Brown, E. T. (1974). Fracture of rock under uniform biaxial compression. In Proc. of the 3th Int. Cong. of Rock Mech (Vol. 2, pp. 111-117).

Cundall PA. (1971) A computer model for simulating progressive, large scale movements in blocky rock systems. Proceedings of the International Symposium Rock Fracture, ISRM, Nancy, Paper No. II-8, vol. 1.

Cundall, P. A., & Strack, O. D. (1979). A discrete numerical model for granular assemblies. geotechnique, 29(1), 47-65.

Chappel BA. (1972). The mechanics of blocky material. PhD thesis, Australia National University, Canberra.

Castro-Filgueira, U., Alejano, L. R., & Ivars, D. M. (2020). Particle flow code simulation of intact and fissured granitic rock samples. Journal of Rock Mechanics and Geotechnical Engineering, 12(5), 960-974.

Cho N, Martin CD, Sego DC (2007) A clumped particle model for rock. Int J Rock Mech Min Sci 44(7):997–1010

Jing, L. (2003). A review of techniques, advances and outstanding issues in numerical modelling for rock mechanics and rock engineering. International Journal of Rock Mechanics and Mining Sciences, 40(3), 283-353.

Haeri, H., Sarfarazi, V., Zhu, Z., & Marji, M. F. (2018). Experimental and numerical simulating of the crack separation on the tensile strength of concrete. Structural Engineering and Mechanics, 66(4), 423-438.

Habib, K-M, (2019) Laboratory investigation into soundless chemical demolition agents for rock breakage in underground mines. Master of Science Thesis. McGill University. Montreal. Canada.

Hoek, E., & Martin, C. D. (2014). Fracture initiation and propagation in intact rock–a review. Journal of Rock Mechanics and Geotechnical Engineering, 6(4), 287-300.

Hanif, M., Mohammed, N. O. O. R., & AL-MAGHRABI, N. H. (2007). Effective use of expansive cement for the deformation and fracturing of granite. Gazi University Journal of Science, 20(1), 1-5.

Itasca (2015) UDEC, Universal distinct element code., 6.0. Itasca Consulting Group. Inc, Minneapolis

Ivars, D. M., Pierce, M. E., Darcel, C., Reyes-Montes, J., Potyondy, D. O., Young, R. P., & Cundall, P. A. (2011). The synthetic rock mass approach for jointed rock mass modelling. International Journal of Rock Mechanics and Mining Sciences, 48(2), 219-244.

Lan, H., Martin, C. D., & Hu, B. (2010). Effect of heterogeneity of brittle rock on micromechanical extensile behavior during compression loading. Journal of Geophysical Research: Solid Earth, 115(B1).

Liu, W., Yuan, W., Yan, Y., & Wang, X. (2019). Analysis of acoustic emission characteristics and damage constitutive model of coal-rock combined body based on particle flow code. Symmetry, 11(8), 1040.

Mitri, H. S., Rispoli, A., & Betournay, M. C. (2005). Strength and behavior of biaxially loaded limestone rock. In Alaska Rocks 2005, The 40th US Symposium on Rock Mechanics (USRMS).

Potyondy, D. O., Cundall, P. A., & Lee, C. A. (1996). Modelling rock using bonded assemblies of circular particles. In 2nd North American rock mechanics symposium. American Rock Mechanics Association.

Potyondy, D. O., & Cundall, P. A. (2004). A bonded-particle model for rock. International journal of rock mechanics and mining sciences, 41(8), 1329-1364.

Shang, J., Hencher, S. R., West, L. J., & Handley, K. (2017). Forensic excavation of rock masses: a technique to investigate discontinuity persistence. Rock Mechanics and Rock Engineering, 50(11), 2911-2928.

Wanne, T. S., & Young, R. P. (2008). Bonded-particle modeling of thermally fractured granite. International Journal of Rock mechanics and mining Sciences, 45(5), 789-799.

Ye, Y., Thoeni, K., Zeng, Y., Buzzi, O., & Giacomini, A. (2019). A novel 3D clumped particle method to simulate the complex mechanical behavior of rock. International Journal of Rock Mechanics and Mining Sciences, 120, 1-16.

Yun, X., Mitri, H.S., Yang, X., and Wang, Y. (2010) Experimental in investigation into biaxial compressive strength of granite. International Journal of Rock Mechanics and Mining Sciences, Volume 47, pp. 334-341.

Bridging text between Chapter 3 and Chapter 4

The previous chapter reports PFC2D modelling and large-scale tests that have been conducted on high-strength concrete panels to optimize SCDA drillhole pattern. The diamond-shaped drillhole pattern successfully fractured the concrete panel. In the following chapter, this drillhole pattern is further examined on Stanstead granite panel test. As the rock material is stronger and stiffer than high-strength concrete, the biaxial confining stress for the granite panel test is increased to 26 MPa and 40 MPa, which corresponds to the pre-mining stress level of 1000 m below surface in Canadian shield. The panel test is well instrumented with time-lapse camera, acoustic emission system, displacement sensors, thermocouples, and confining pressure sensors. The results of the granite panel test are analyzed and compared with the concrete one.

Both concrete and granite panel tests with diamond-shaped drillhole pattern show that SCDA leads to significant out-of-plane fractures in biaxially loaded panels, but this cannot be reflected by the previous PFC2D models. Three-dimensional FLAC3D models is hereby constructed in the following chapter to better understand the fracturing processes and failure mechanisms of the panels. The simulation results of the panel breakage tests are highly consistent with the test observations. Different failure mechanisms of concrete and granite panels are revealed by FLAC3D modelling.

The following chapter is a published paper in the Rock Mechanics and Rock Engineering, 2022, published on May 4, https://doi.org/10.1007/s00603-023-03332-0

Chapter 4: Biaxially confined rock breakage with SCDA: large-scale tests and numerical modelling

Author:

Tuo Chen*, Isaac Vennes, Hani S. Mitri

Affiliation:

Department of Mining and Materials Engineering, McGill University, Montreal, Canada H3A 0E8

Address: 3450 University Street, Montreal, Quebec, Canada H3A 0E8

*Corresponding author. Tel.: +14388662473; E-mail address: tuo.chen@mail.mcgill.ca (T. Chen)

Abstract

Soundless chemical demolition agents (SCDA), also known as expansive cement, represent a potentially viable method for fracturing rock without explosives. Traditionally, expansive cement is used for surface applications like block splitting in dimension stone quarries and demolition of concrete foundations. For deep underground applications, the major challenge with the use of expansive cement in an excavation face has been the presence of high biaxial stress field that would hinder the development of fractures in a mining face. This study aims to explore how expansive cement can be potentially used for rock fragmentation in deep underground environments. To do so, large-scale tests on 1 m × 1 m × 0.25 m concrete and granite panels with a novel drilling pattern are prepared, instrumented, and tested under biaxial confinement conditions. Test results show that the proposed drill pattern for expansive cement boreholes is capable of fracturing both panels under biaxial stresses. A 3D finite-difference modelling code FLAC3D 7.0 was developed and validated with observed panel breakage process and failure mechanisms. Both large-scale tests and numerical modelling show that expansive cement induces significant fracturing parallel to the loading plane. These findings should lay the groundwork and provide guidelines for the future application of expansive cement to underground hard rock excavations.

Keywords: Expansive cements; SCDA drill pattern; Rock fracturing; Large-scale tests; FLAC3D modelling

4.1 Introduction

Soundless chemical demolition agents (SCDA), also known as expansive cement, or static cracking agents, are powdery materials that harden and expand once mixed with water. When an SCDA is poured in a confined borehole, it generates expansive pressure and fractures the surrounding materials during the cement curing process. Since its introduction in the early 1970s, SCDA were mainly used for surface applications in civil engineering field such as rock quarrying and concrete demolition (Cho et al., 2018; Kim et al., 2021). By pouring SCDA slurry into boreholes in boulder or concrete block, the SCDA will expand and produce fracture networks in a controlled manner under no load. SCDA products are environmentally friendly, producing no toxic fumes, which reduces ventilation requirements in underground mines and tunnels. Another important advantage of SCDA is that the rock cracking process is well controlled, eliminating overbreak and decreasing the demand for primary rock supports (Habib et al., 2022a).

Despite the advantages of SCDA, the properties and application guidelines of SCDA have not been widely studied and understood. Some studies have been conducted to examine SCDA physical properties and behaviours in laboratory conditions. SCDA expansion pressure was mostly quantified using thick-walled cylinder method, where the SCDA mixture is poured into a thick-walled metal cylinder with strain gauges installed on the cylinder outer surface. The SCDA pressure is calculated analytically based on the measured tangential strain of the cylinder surface (Hinze & Brown, 1994; Habib et al, 2023; Xu et al., 2021a; Li et al., 2021; Xu et al., 2022). De Silva et al. (2017) investigated the variation of mechanical properties and microstructures of SCDA during the hydration process. Their results showed that SCDA could be more effective to produce higher pressures in fracturing rockmass with high confinement. De Silva et al. (2019) studied the impact of saturation conditions in fracturing performance of SCDA in geological

reservoir rock formations. The results showed that both less pore-water and saline conditions increase the fracture performance of SCDA. Nantanzi et al. (2019) explored the impact of ambient temperature on SCDA chemical changes in steel pipe. It showed the SCDA had higher $Ca(OH)_2$ concentrations and generated greater expansive pressures at 19° ambient temperatures than those at 2°. Wang et al. (2022) loaded small granite rock blocks biaxially with low confinements and two SCDA holes were employed to fracture the sample under different biaxial stress ratios. Their results indicate that the initial stress conditions and injection schemes play important roles in rock fracturing results.

In recent years, there has been a renewed interest in the implementation of SCDA for applications other than concrete and boulder demolition. Natanzi & Laefer (2014) implemented SCDA for rock demolition near historic structures as it does not create vibrations that could damage existing structures. Shang et al. (2017) employed SCDA techniques to explore discontinuity persistence. The SCDA boreholes are drilled along the discontinuity line of rock blocks, whereby the pre-existing persistent area and rock bridge area can be directly observed on the split surface and the discontinuity persistence quantified. De Silva et al. (2018) explored the possible application of SCDA for in-situ leaching through laboratory tests and discrete-element simulations. The results indicates that SCDA could produce controllable fracture network in impervious rocks to for in-situ leaching techniques. Tang et al. (2021) utilized SCDA method to fracture and weaken hard roof in a coal mine successfully. In addition to fracture applications, SCDA has also been successfully used for shale gas reservoir stimulation, ground pressure control and rock support (Guo et al., 2015; Li et al., 2018; Xu et al., 2019; Xu et al., 2021b).

To date, there have been only a few investigations of SCDA application to hard rock underground environments where new challenges exist, mainly high in-situ stress and high rock strength. The

objective of this multi-phase research project is to implement SCDA for the breakage of hard rock under biaxial confinement conditions which are encountered in underground mining or tunnelling faces. In the first section, the paper overviews the design and procedure of the large-scale testing program on concrete and granite panel breakage under biaxial loading. The test results and instrumented data are then discussed in detail. In the second section, the finite difference modelling method is utilized to rebuild the panel breakage process observed. The modelling results are compared to the large-scale test results, validating the breakage mechanism of the panel due to SCDA. The findings should make an important contribution to expand SCDA application to hard rock mining and tunneling, addressing construction and environmental restraints when traditional drilling and blasting method is not applicable for rock breakage underground.

4.2 Test design

4.2.1 Panel preparation

In practice, SCDA is generally used under unconfined or low stress conditions, such as for concrete demolition (Ma et al., 2020; Kim et al., 2021) or tested under uniaxial loading (Musunuri and Mitri, 2009). However, when a rock mass is confined biaxially such as at an underground face, the SCDA could only damage and weaken the rock material around the borehole instead of effectively fragmenting the rock to create a cavity (Tang et al., 2021). This study is part of a multi-phase project, and the previous work has revealed that SCDA drill hole pattern must be designed strategically for the SCDA to produce the desired fracturing effect on a rock face under biaxial confinement. An optimized SCDA hole pattern under biaxial confinement was found using PFC2D modelling (Chen et al., 2022). Thus, a high-strength concrete panel and a Stanstead granite panel were prepared with the same optimized drilling pattern in previous work, as shown in Figure 4.1.

Both panels have the same dimension of 100 cm × 100 cm × 25 cm. Similar to a drilling and blasting face, two types of drill holes are arranged; SCDA is injected in the smaller diameter drill holes, and larger diameter empty holes provide a stress shadow to the SCDA holes relative to the confining pressure. It is also postulated that the empty holes provide space for fragments once cracking and destruction take place, facilitating complete fracturing of the panel.

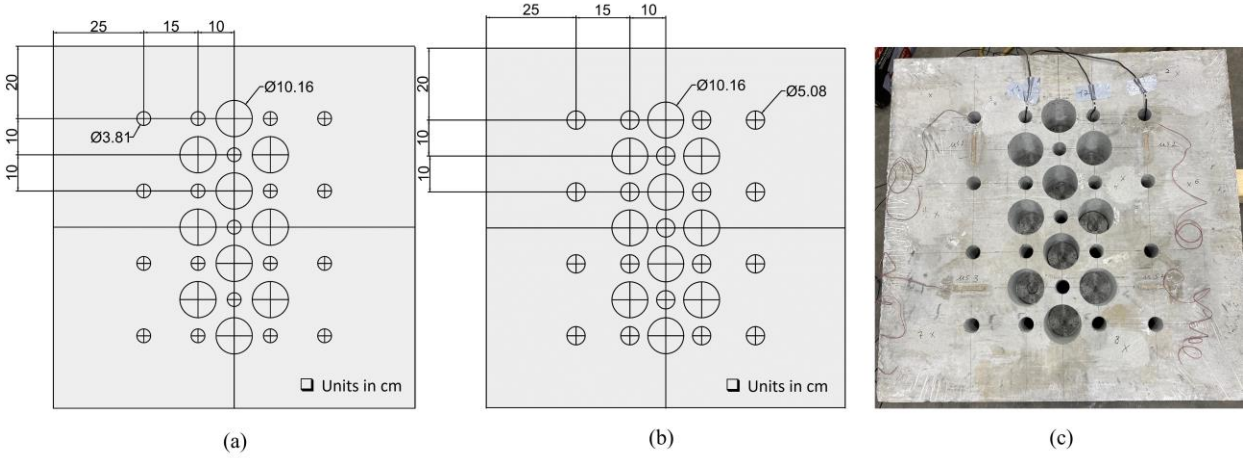

Figure 4.1: Panel drilling design. a) Concrete panel b) Granite panel c) Photograph of the drilled concrete panel.

As shown in Figs. 4.1a and 4.1b, each pattern has 19 SCDA holes and 10 stress relief holes with the borehole depth of 17.78 cm. The distance between centers of stress relief hole and SCDA hole is 10 cm. A photograph of the drilled concrete panel is shown in Figure 1c. The middle part of the pattern aims to fracture the panel and form a vertical fragmented slot with the aid of stress relief holes. Subsequently, two side columns of SCDA holes are utilized to slash the slot to enlarge the cavity. The diameters of SCDA boreholes are different in two panels. The 3.81 cm (1.5 in.) and 5.08 cm (2 in.) SCDA holes are applied in concrete and granite panels, respectively. This is because the granite panel has higher tensile strength than the concrete panel, and the higher expansive

pressure provided by larger-diameter boreholes is required. The loading scheme on the granite panel is also increased proportionally to the tensile strength.

The commercially available SCDA selected for this research is Betonamit Type R. The expansive cement is mechanically mixed with water for 3-4 minutes using a water-to-cement ratio of 0.2. The mixture is then loaded into the borehole at room temperature (25°C). The water temperature is approximately 20°C.

4.2.2 Panel strength properties

The first panel is made of high-strength concrete. The uniaxial, triaxial, and Brazilian tests are conducted on cylindrical specimens that are cored from the concrete block to determine the properties of the high-strength concrete. All tests were conducted by CANMET (the Canada Centre for Mineral and Energy Technology) Mining laboratory in Ottawa. The test results are shown in Table 4.1 and Table 4.2. The tests used an MTS 815 rock mechanical test system with servo control options for load and displacement. Testing was done in accordance with ASTM D4543-19 for sample preparation, ASTM D7012-14 for uniaxial compressive strength, and ASTM D3967-16 for Brazilian tensile strength.

Table 4.1: UCS and triaxial test results for concrete

Specimen ID	Specifications			Strength and elastic properties			
	Diameter (mm)	Length (mm)	Density (g/cm^3)	Peak strength (MPa)	Confinement (MPa)	Young's modulus (GPa)	Poisson's ratio
STAC-C-U1	74.92	169.98	2.32	54.7	0.0	24.6	0.08
STAC-C-U2	74.91	169.98	2.32	51.8	0.0	23.7	0.05
STAC-C-U3	74.92	170.02	2.33	57.4	0.0	24.3	0.07
STAC-C-T1	74.88	170.02	2.34	77.9	5.0	N/A	N/A

STAC-C-T2	74.88	169.99	2.34	102.1	10.0	N/A	N/A
STAC-C-T3	74.78	169.96	2.34	120.2	15.0	N/A	N/A

Table 4.2: Brazilian test results for concrete

Specimen ID	Specifications			Strength	
	Diameter (mm)	Length (mm)	Density (g/cm^3)	Failure load (kN)	Brazilian tensile strength (MPa)
STAC-C-B1	74.82	49.80	2.30	32.20	5.50
STAC-C-B2	74.95	49.78	2.29	14.06	2.40
STAC-C-B3	74.89	49.82	2.29	28.42	4.85
STAC-C-B4	74.63	50.00	2.28	27.35	4.67
STAC-C-B5	74.94	49.98	2.28	29.86	5.08
STAC-C-B6	74.91	49.79	2.30	29.32	5.00

The second panel block is cut from Stanstead granite. Similarly, the UCS, triaxial, and Brazilian tests are carried out on Stanstead granite specimens following the same test procedure to determine the properties of the granite panel. The results are shown in Table 4.3 and Table 4.4. It is found that the strength properties of granite panel are significantly higher than the concrete panel, especially for the compressive strength. The concrete samples have an average UCS of 54.6 MPa, while the granite samples have an average UCS of 117.7 MPa. The average Brazilian tensile strength of concrete and granite samples are 4.5 MPa and 7.2 MPa, respectively.

Table 4.3: UCS and triaxial test results for granite

Specimen ID	Specifications			Strength and elastic properties			
	Diameter (mm)	Length (mm)	Density (g/cm^3)	Peak strength (MPa)	Confinement (MPa)	Young's modulus (GPa)	Poisson's ratio
STAC-SG-U1	44.80	101.00	2.67	117.4	0.0	45.0	0.17
STAC-SG-U2	44.80	101.00	2.67	120.2	0.0	45.9	0.11
STAC-SG-U3	44.80	100.90	2.67	115.4	0.0	45.0	0.13
STAC-SG-T1	44.80	100.90	2.67	169.3	5.0	N/A	N/A
STAC-SG-T2	44.90	100.90	2.67	218.2	10.0	N/A	N/A
STAC-SG-T3	44.90	100.90	2.67	268.1	15.0	N/A	N/A

Table 4.4: Brazilian test results for granite

Specimen ID	Specifications			Strength	
	Diameter (mm)	Length (mm)	Density (g/cm^3)	Failure load (kN)	Brazilian tensile strength (MPa)
STAC-SG-B1	44.83	26.93	2.67	14.69	7.75
STAC-SG-B2	44.85	26.96	2.67	15.25	8.02
STAC-SG-B3	44.85	22.32	2.67	10.53	6.70
STAC-SG-B4	44.81	22.31	2.67	11.45	7.29

STAC-SG-B5	44.86	22.32	2.67	9.52	6.05
STAC-SG-B6	44.85	22.33	2.67	11.87	7.55

4.2.3 Biaxial loading system

The large-scale biaxial panel breakage tests were conducted at CANMET Mining laboratory in Sudbury, Ontario, Canada. The biaxial system uses a servo-controlled vertical press with a load capacity of 10 MN (Fig. 4.2a). A 6 MN lateral self-reaction frame (shown in Fig. 4.2b) was designed and built specifically for this project and is used in conjunction with the vertical press to achieve the desired biaxial loading configuration. Details of the frame design can be found elsewhere (Alvarez De La Garma, 2021). With this loading system, it is possible to test a large panel of 1 m x 1m x 0.25 m. 20 cm of the panel thickness is subjected to biaxial loading and the panel back of 5 cm remains unloaded. A maximum confinement of 40 MPa and 26 MPa in the vertical and horizontal directions, respectively, can be achieved with this test configuration. Such high level of confinement approximates a virgin far-field stress condition of approximately 1000 m below ground surface in the Canadian shield (Arjang and Herget, 1997), whereby the overburden stress (26 MPa) is vertical, and the major stress (40 MPa) is horizontal.

(a) (b)

Figure 4.2: Biaxial loading test apparatus, (a) Vertical press, b) Lateral loading frame.

The 40 MPa and 26 MPa confining pressure was applied on the granite panel in vertical and lateral directions. Given that high-strength concrete panel has relatively lower strength properties, a reduced confinement of 23 MPa and 15 MPa was applied to the concrete panel. For safety reasons, the SCDA holes were loaded with expansive cement prior to confinement load application. The time between loading the holes and the placement of the panel in the lateral frame was within 15 minutes. Next, the entire lateral frame was pushed under the vertical press as shown in Figure 4.3. The servo-controlled loading was then applied both horizontally and vertically, with the same loading rate (0.08 MPa/s) in both directions until target confinement was achieved.

Once the target vertical load is reached, a vertical displacement lock is applied. The lateral frame is equipped with three 200-ton hydraulic cylinders, as shown in Fig. 3c. It is not a servo-control system. However, to ensure uniform horizontal pressure application on the panel, all three cylinders are connected to the same pump and the pressure in each line is monitored. Once the target lateral load is attained, shutoff valves were used to maintain the load. It is noteworthy that such load control arrangement permits both horizontal and vertical pressures to be maintained, albeit with slight variation in response to panel fracturing over the duration of the test.

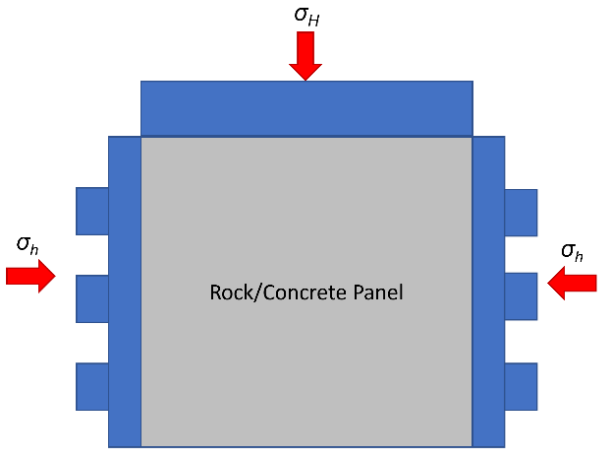

(a) Schematic diagram.

(b) Biaxial loading system.

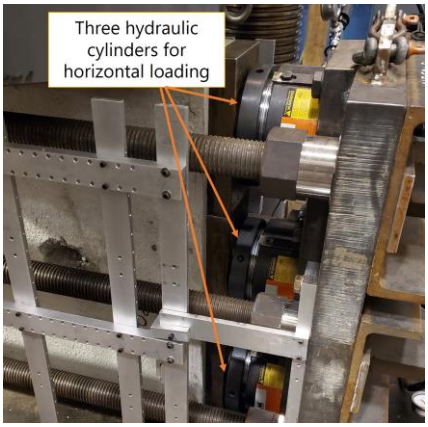

(c) Hydraulic lateral press.

Figure 4.3: Biaxial load application.

4.2.4 Instrumentation

Different monitoring methods were utilized to continuously monitor SCDA reaction and panel fracturing, including acoustic emission (AE) system, Keyence sensors, thermocouple, and a high-resolution timelapse camera. A 16-channel Micro-II Express AE system made by Physical Acoustics is utilized for the AE detection. Sixteen microphones with resonant frequency of 150 kHz were arranged on the front and back of the panel to locate micro-fracturing and damages over the entire duration of the test. The AE system was calibrated before the biaxial loading to ensure AE events occur at anywhere of the panel can be detected precisely by optimizing sensor locations. The detailed layout of the AE sensors mounted on the panel is shown in Figure 4.4. Keyence sensors were mounted to measure panel deformation during tests in different directions. Eight Keyence sensors were installed for this test; two sensors for monitoring out-of-plane displacements at panel front face and back, three sensors for monitoring panel vertical displacement and three sensors for lateral displacement at top, middle and bottom sections of the panel. The locations and purposes of some Keyence sensors are illustrated in Figure 4.5.

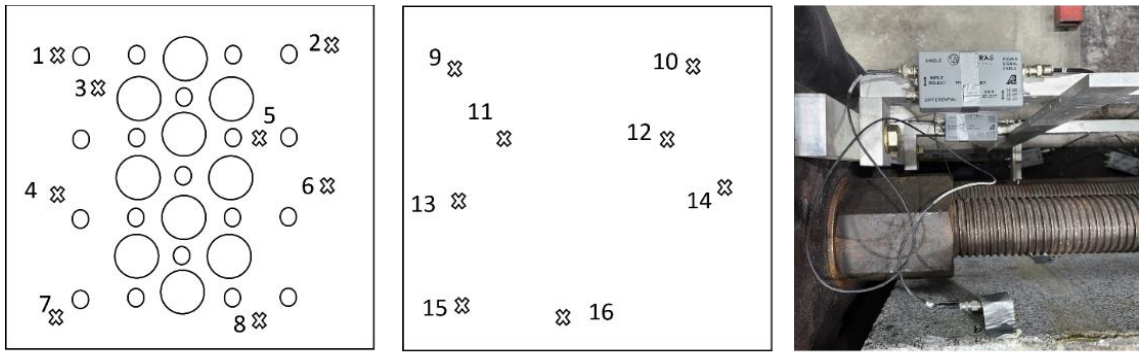

Figure 4.4: AE sensor layout a) Front b) Back c) Photograph of AE sensors on panel back.

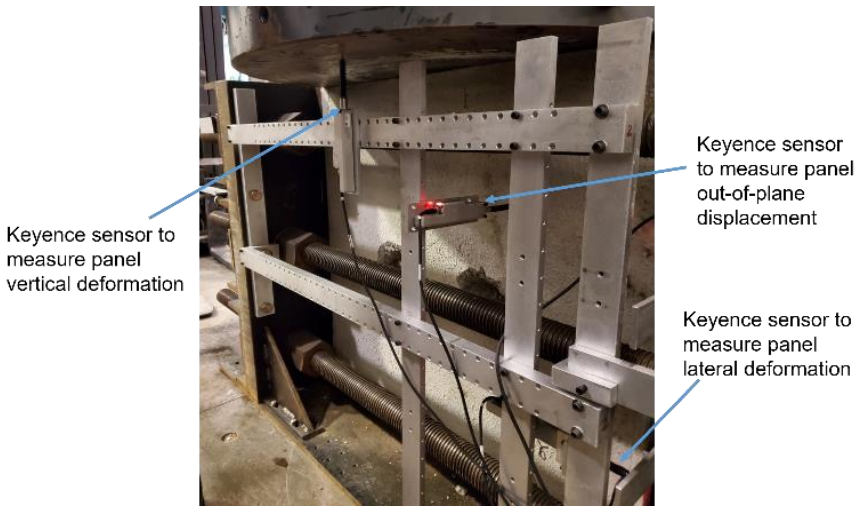

Figure 4.5: The location of purpose of Keyence sensors.

Additionally, thermocouple sensors were embedded inside few SCDA boreholes during the granite test to monitor temperature changes of SCDA material. The hydration reaction of SCDA mixture is an exothermic reaction which increases temperature, and the rate of cement expansive development is related to the heating process (De Silva et al., 2016). Thus, the starting time of the SCDA reaction and expansion can be identified by monitoring temperature variation of the material. A high-resolution timelapse camera was also set up in front of the panel to monitor and capture the evolution of fracturing, taking one picture per minute. Based on previous laboratory measurements, SCDA pressure peaks within 12 hours (Habib et al., 2023). Thus, all monitoring systems and loads were kept online for 24 hours to capture the full effect of SCDA on the panel. If the panel maintains stability for 24 hours, the test will be ceased, and the trial will be deemed unsatisfactory.

4.3 Test results

4.3.1 Concrete test

4.3.1.1 Testing procedure

Figure 4.6 shows the instrumented concrete panel under lateral loading frame. The SCDA boreholes have been filled with expansive cement before biaxal loading application. During the test, a confinement of 23 MPa and 15 MPa was applied on the concrete panel. Figure 4.7 presents a series of times lapse pictures obtained from this test. Apparent cracking around the SCDA borehole started 5 hours after the expansive agents were poured in boreholes (see Fig. 4.7a). Then, an increasing number of fractures were observed with panel surface spalling and bulging, as shown in Figure 4.7b and 4.7c. Interestingly, those bulging mechanisms eventually lead to exponential increase of out-of-plane displacement. Out-of-plane fractures can also be observed from the inside of stress-relief holes, as illustrated in Fig. 4.7c. These out-of-plane tensile fractures persisted across the entire panel. Combined with in-plane shearing cracks radiating from the SCDA holes (see Fig. 4.7d), the central part of concrete panel broke through completely at 11 hours 50 minutes after pouring SCDA. At that point, visible in-plane shear failures coalesced in the center of the panel, but a large amount of confining pressure still existed until remanent pressure is manually released at 24 hours when the test finished.

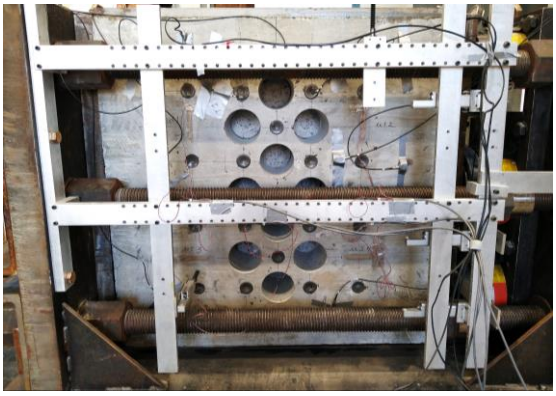

Figure 4.6: Concrete panel prior to load application.

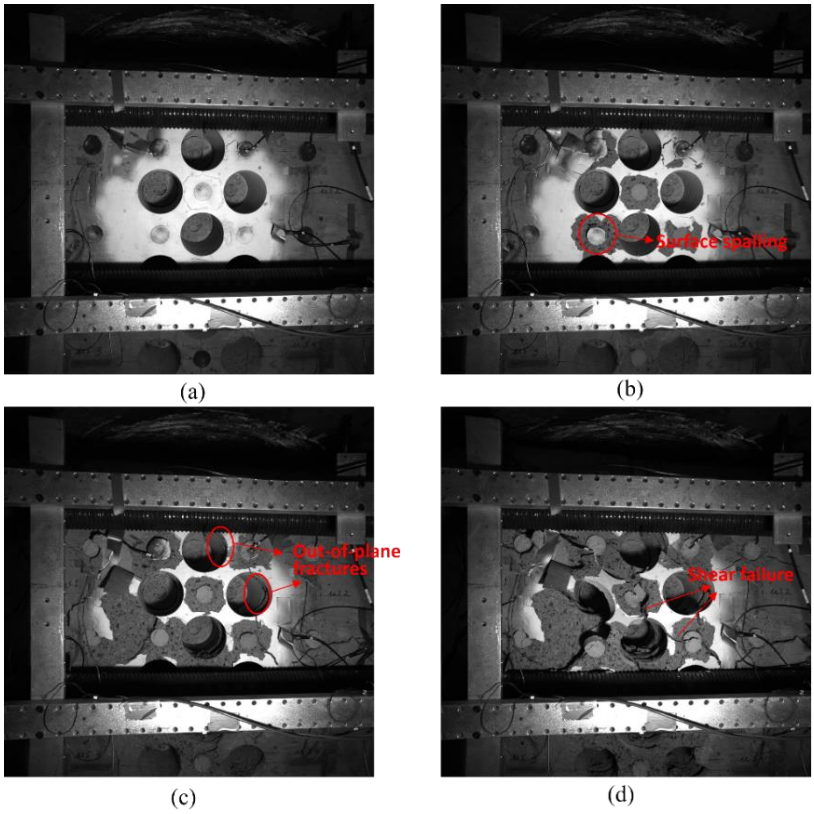

Figure 4.7: Time lapse pictures of concrete panel test. a) At 5 hours, b) At 7 hours, c) At 9 hours, d) At 11 hours 50 mins.

The state of the panel after the test is shown in Figure 4.8. Fig. 4.8a shows the remanent depth of a borehole. The borehole was 17.78 cm deep and only around 2.54 cm (1 in.) depth was left after

the test, showing SCDA effectively demolishing the panel. After the central crater was formed using the dense SCDA pattern and stress relief holes, free faces are created to enable the side SCDA columns to split, pushing surrounding material inward and enlarging the cavity. A fracture coalescing between side SCDA holes is shown in Fig. 4.8b. In Figure 4.8d, the location of the center pattern has been circled by yellow dashed lines. It can be seen the side SCDA holes successfully slashed and enlarged the previously formed crater, as delineated by red dashed lines. Figure 4.8c shows a crack separating the front and the back of the panel when hoisting the panel out of loading frame. This could be attributed to the partial loading of the panel sides (5 cm back of the panel was not loaded during the test to increase the lateral and vertical stresses); as the panel center is damaged by the SCDA, the stiff and intact back is progressively sheared off the panel. Figure 4.8e shows the panel after it was taken out of the loading frame. The panel back was completely detached from the rest of the panel, and the SCDA formed a crater in the center of the panel.

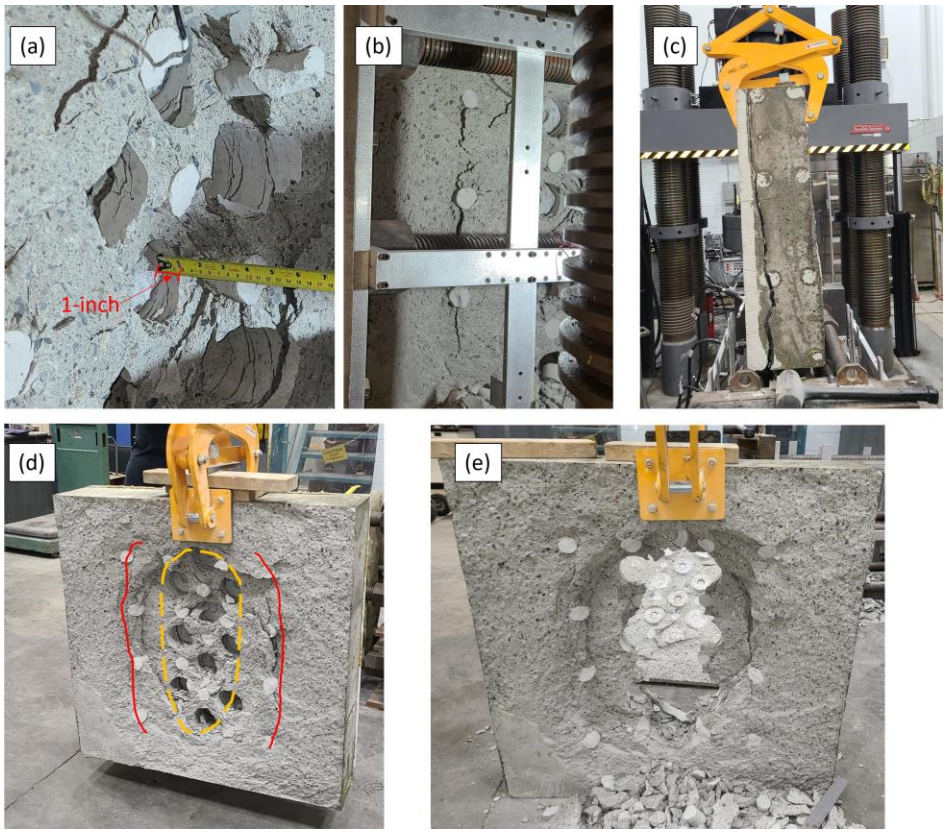

Figure 4.8: Concrete panel condition after test. a) Remanent borehole depth, b) Fracture coalescence, c) Side fracture, d) Crater expansion d) Final crater.

4.3.1.2 Force and displacement data

The force vs time and force vs displacement for the concrete panel are plotted in Figs. 4.9a and 4.9b, respectively. 4600 kN and 3000 kN are applied in the vertical and horizontal directions of the panel, respectively, corresponding to the confinement level of 23 MPa and 15 MPa. An apparent pressure decay starting about 6 hours after mixing SCDA in both directions is observed in Fig. 4.9a. The pressure decay time corresponds with the panel fracturing time shown in Fig. 4.7, indicating that the SCDA was continuously damaging the panel during the test. High stress was sustained on the panel for the entire duration of the test. After the central crater was formed at 11

hours 50 mins, the surrounding concrete materials continued to support the panel, displaced, and released the confining stress gradually.

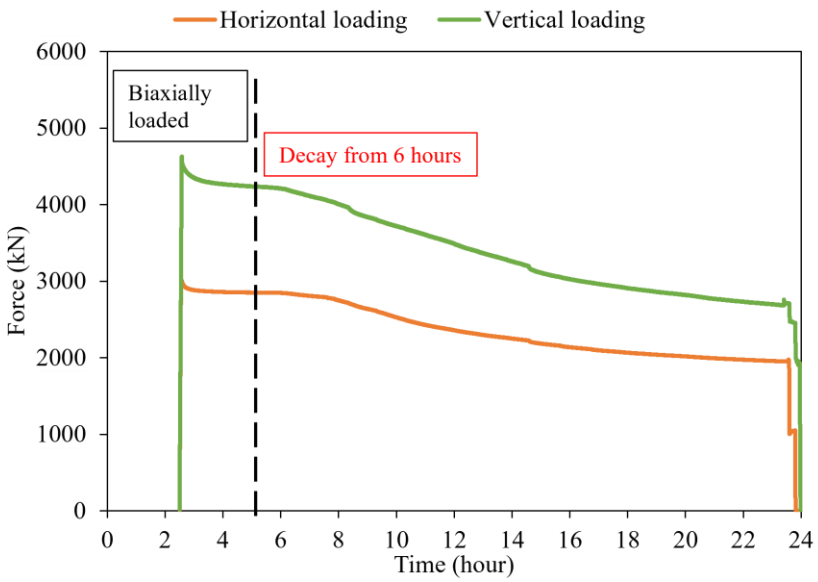

(a) Appied biaixal load variation with time.

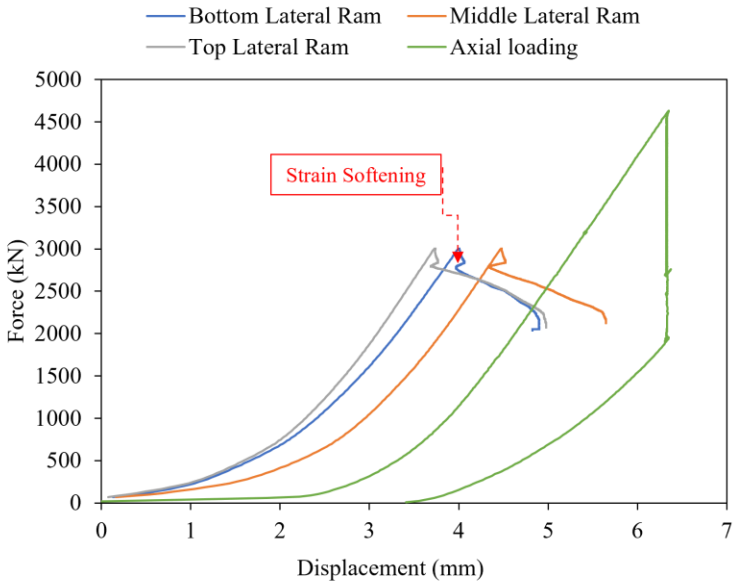

(b) Panel axial load vs. lateral displacements.

Figure 4.9: Concrete panel test instrumentation results.

Fig. 4.9b shows that the confining pressure reduction corresponds to the increase in displacements for all three lateral rams. The panel strain-softening after failure can be identified from the curve, proving that the expansive cement has yielded the panel under biaxial confinement. Fig. 4.10a shows the out-of-plane displacements monitored on the panel front and the back. Significant out-of-plane displacements up to 40 mm are measured with the displacement sensor pointing perpendicular to the panel front face, as shown in Fig. 4.10b. On the other hand, approximately 7 mm of displacement was measured with the sensor in contact with the back of the panel. The severe tensile cracks and gaps associated with theses displacements are visible in Fig. 4.10b.

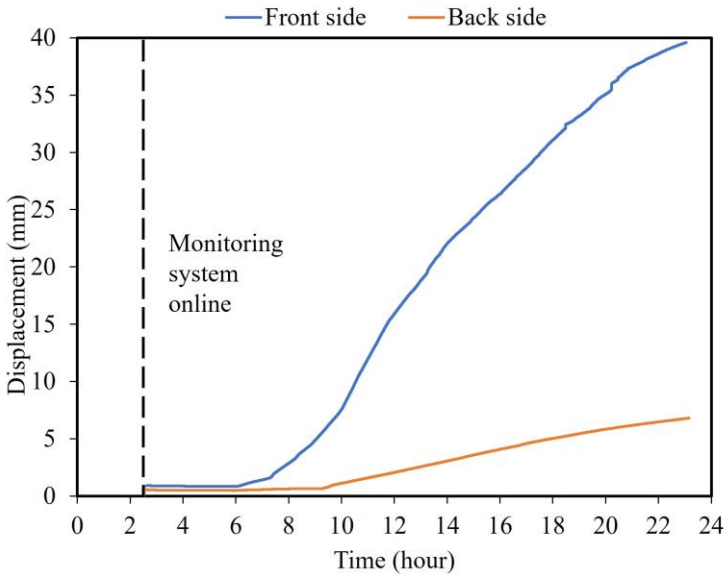

(a) Panel out-of-plane displacement over time.

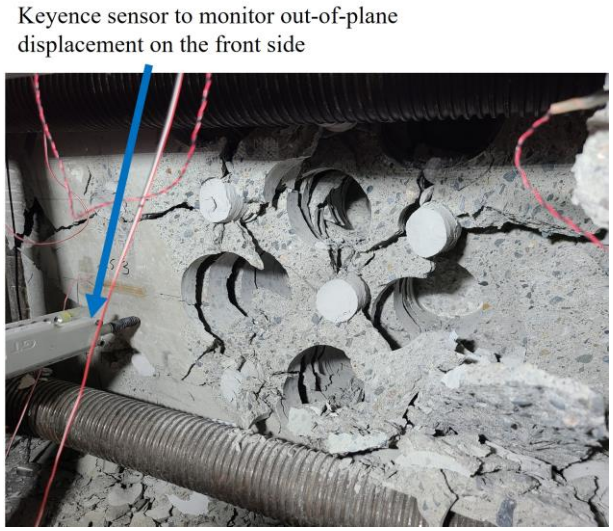

(b) Panel bulging fractures.

Figure 4.10: Panel out-of-plane displacement.

4.3.1.3 AE data

Acoustic emissions were monitored for the entire duration of the test to determine the time and location of micro-fractures that could potentially occur before any visible fracturing takes place on the slab surface. Fig. 4.11a shows the detected AE energy projected onto the front surface of the panel. Both X position and Y position axes range from 0 to 1000 mm, representing the width and the height of the panel, respectively. The third dimension of the figure is the accumulated AE energy recorded during the test. It can be observed that the highest AE energy occurs at the center of the panel. This AE trend is consistent with the panel fracturing pattern, where the middle of the panel was subjected to the most damage, forming a crater. Fig. 4.11b shows AE event count and cumulative AE energy over time for the entire panel. There is a burst of AE events at the beginning of the chart during panel loading. However, cumulative energy of these events is relatively low compared to the energy subsequently released by SCDA induced damage. This indicates that the panel was not damaged during loading application. A quiet period then follows, corresponding to

the SCDA mixture curing and building up the expansive pressure, until micro-fractures started showing up about 4.5 hours after SCDA mixing. This is about 1.5 hours before fractures can be distinguished from other monitoring measures such as time-lapse pictures and force and displacement monitoring. From both the cumulative AE energy and event counts curves, SCDA-induced panel fracturing occurred between 4.5 hours to 11 hours after mixing, lasting around 6.5 hours. Although some small spikes of AE activity can be observed after 11 hours, the cumulative energy curve plateaued.

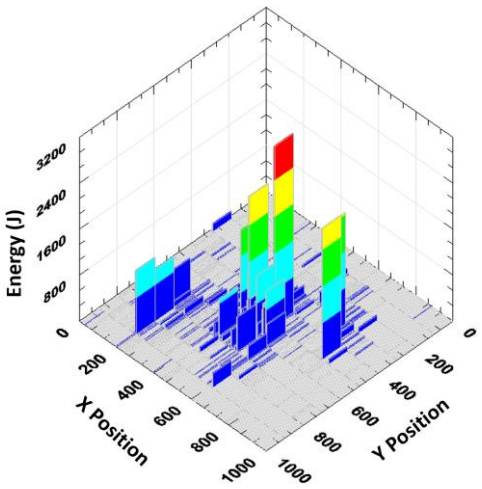

(a) AE energy spatial distribution

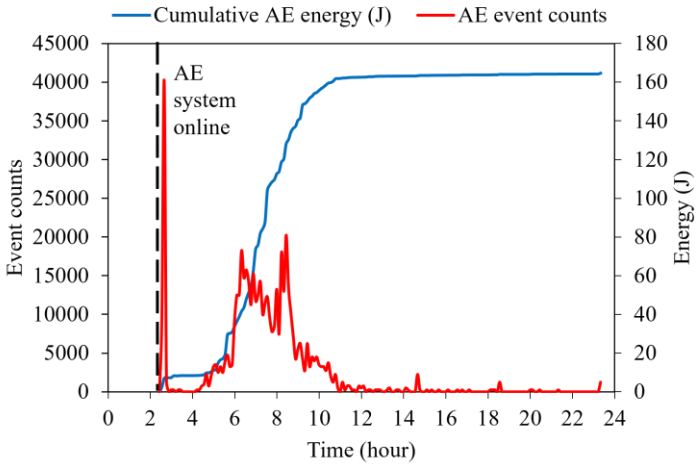

(b) Event counts and cumulated energy

Figure 4.11: AE data for concrete test.

4.3.2 Granite panel test

4.3.2.1 Test process

The loading and monitoring procedure described previously is repeated for the granite panel. However, the biaxial confinement stress is increased to 40 MPa and 26 MPa in the vertical and lateral directions, respectively, to mimic a virgin stress condition at around 1000 m below surface in the Canadian shield. Timelapse pictures in Figure 4.12 show the granite panel fracturing during the test. Figure 4.12a shows the undamaged panel 2 hours 20 mins after SCDA mixing. Figure 4.12b shows the first visible cracking on the panel front surface 3 hours 12 minutes after mixing. The cracks first appeared on the right side of the pattern. Only one minute after, a spalling failure occurred at the same location, ejecting a large piece of rock which fell and got stuck between the panel and the horizontal thread bar, as shown in Figure 4.12c. A very short time passed between the appearance of superficial cracking and the spalling failure, indicating the failure of granite panel is more brittle when compared to the preceding concrete panel test. As the fracturing progressed due to SCDA expansion, a large cavity formed 3 hours 31 minutes in the top right corner of the dense drill pattern, as shown in Figure 4.12d. This was followed by visual fracture coalescence between the left column of SCDA holes 6 hours 7 minutes after mixing, as shown in Figure 4.12e, which further expanded the cavity in the middle. After 7 hours 18 minutes, the entire panel failed in a brittle manner (see Figure 4.12f) and almost all confining stresses were instantaneously released.

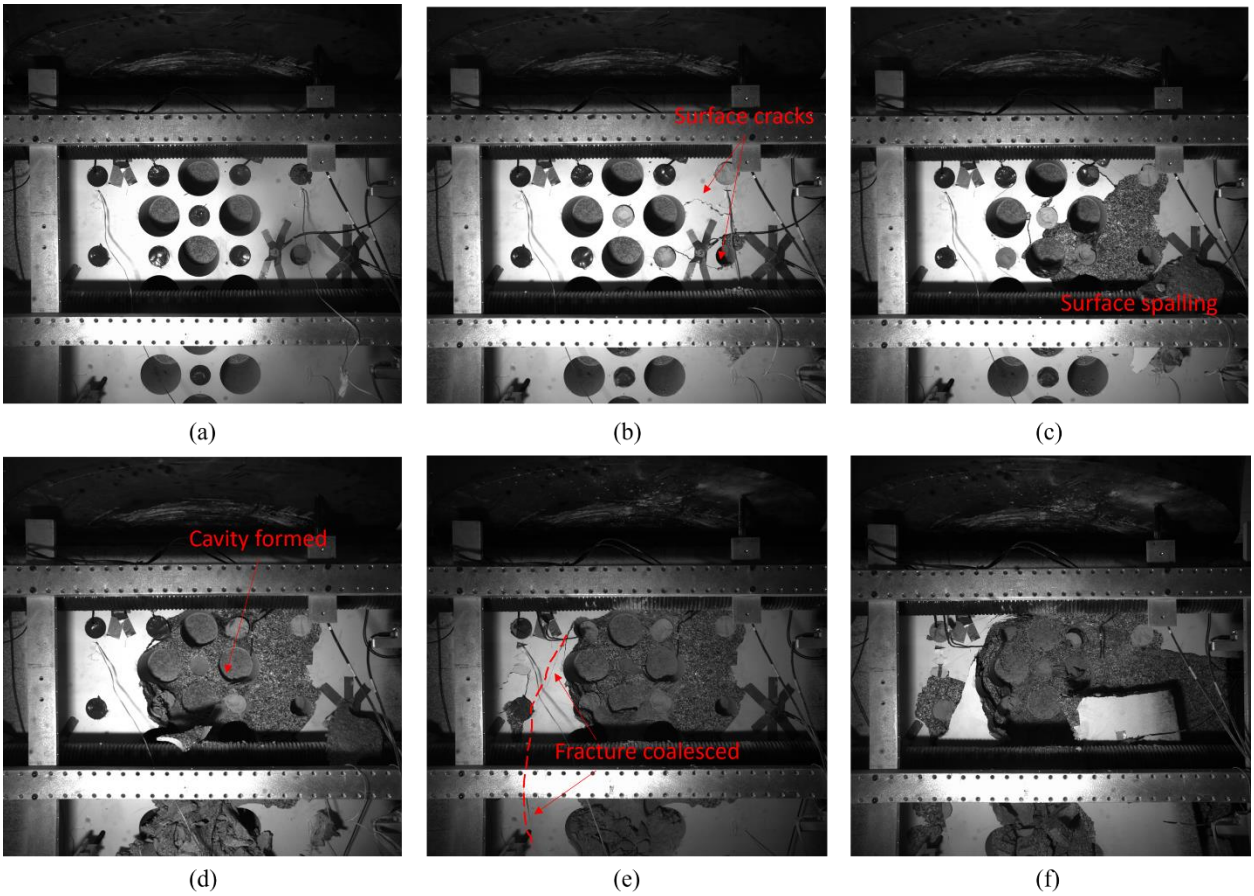

Figure 4.12: Time lapse pictures of granite panel test. a) At 2 hours 20 mins b) At 3 hours 12 mins, c) At 3 hours 13 mins, d) At 3 hours 31 mins, e) At 6 hours 7 mins f) At 7 hours 18 mins.

Figure 4.13 provides a series of photographs of the destroyed granite panel. Figure 4.13a shows the panel after it was removed from biaxial loading. Figure 4.13b shows the fracturing from the top of the panel and Figure 4.13d shows the out-of-plane fractures inside a stress-relief hole. These two figures reveal that the out-of-plane failure mechanism that was previously found in concrete test also exists in granite panel. By comparing Figure 4.13d and Figure 4.8a, it can be concluded that the out-of-plane tensile cracks due to SCDA axial expansion are denser in the concrete panel than that in granite panel, which can be explained by the tensile strength and brittleness difference between two materials. A typical piece of spalled rock was measured to have a length of about 61 cm (24 in.) and a thickness of 7 cm (2.7 in.), as shown in Fig. 4.13c and 4.13e. Figure 4.13f shows

how the entire panel had been fractured and only the unloaded back was left intact after mucking the granite fragments.

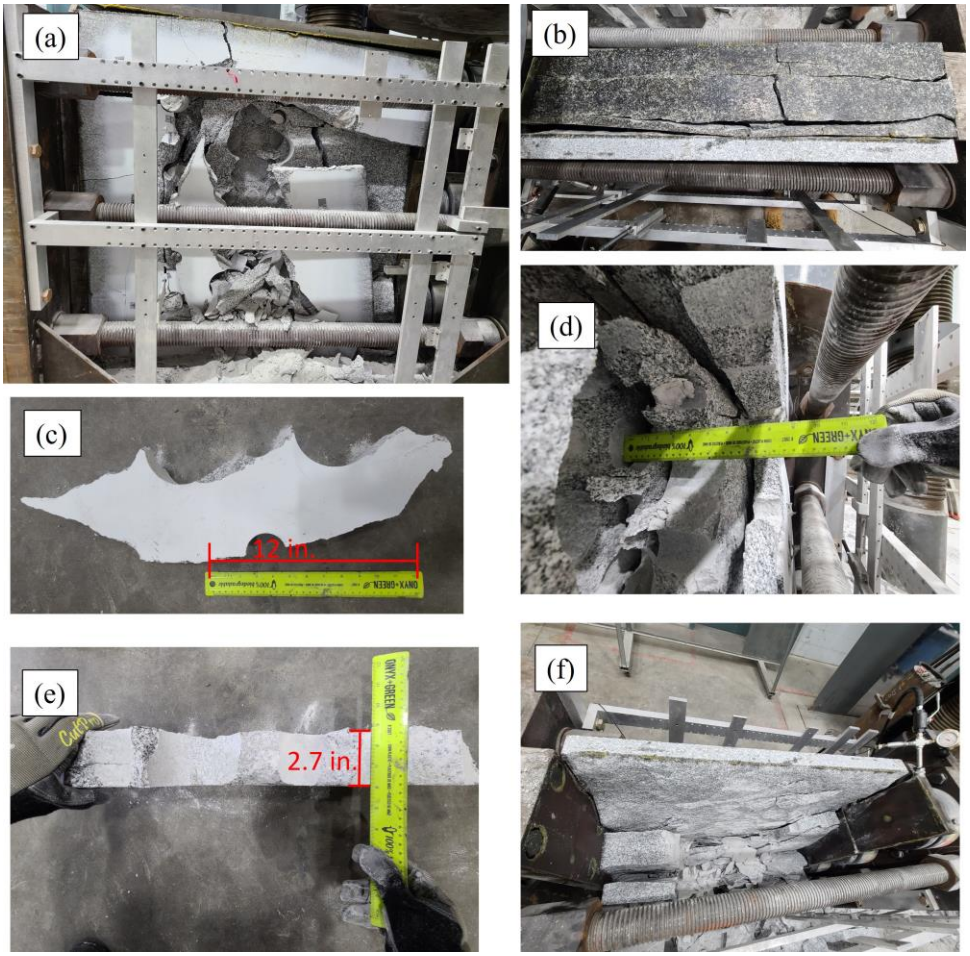

Figure 4.13: Granite panel pictures. a) Collapsed panel after test, b) Fractures on panel top, c) Length of a fragmented piece, d) Remaining borehole depth, e) Thickness of a fragmented piece, f) Panel condition after fragment removal.

4.3.2.2 Force and displacement data

The force vs time and force vs displacement plots for the granite panel are provided in Fig. 4.14, respectively. 8000 kN and 5200 kN forces were applied in the vertical and horizontal directions, respectively, corresponding to an applied stress of 40 MPa and 26 MPa on the loaded faces of the

panel. 3.2 hours after mixing SCDA, pressure decay was observed with both loading frames, as shown in Figure 4.14a. This occurred concurrently with observed surface spalling as shown in Figure 4.12b. Interestingly, compared with concrete test whose confining pressure dropped gradually until the end of the test, the pressures on granite panel only slightly decreased with the occurrence of major cracking events. Most of the pressure maintained until the panel suddenly failed and released all stresses at 7.2 hours. This corresponds to the brittle failure of the panel captured in Figure 4.12f. Figure 4.14b shows that the pressure reduction corresponds to an increase in displacements measured from all three lateral rams. Much shorter strain-softening curves can be observed compared with ones found in concrete test (Figure 4.9a), revealing the granite panel failure was substantially more brittle than the concrete one.

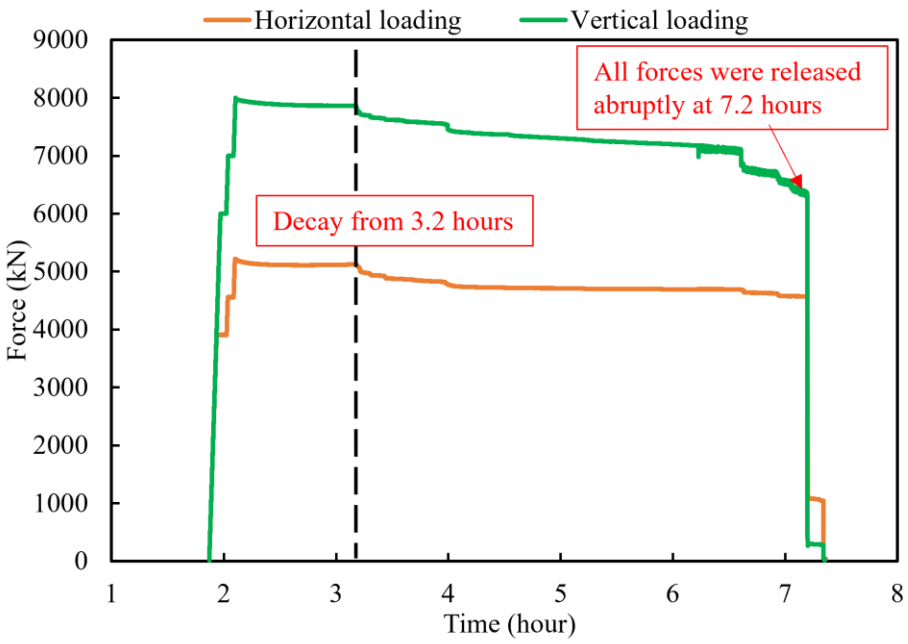

(a) Appied biaixal load variation with time.

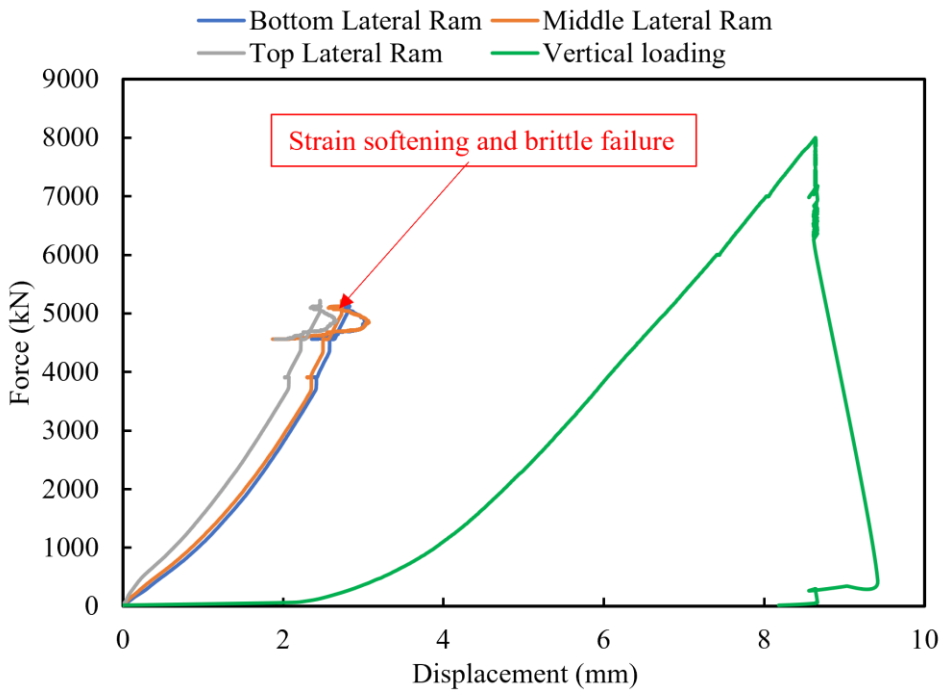

(b) Panel axial load vs. lateral displacements

Figure 4.14: Granite panel test instrumentation results.

Figure 4.15 shows the out-of-plane displacements monitored by the out-of-plane displacement sensors. The out-of-plane displacements of 1.5 mm and 5.5 mm are measured at the front face and the back face, respectively. Although the out-of-plane cracks and deformations are similar to those occurring in concrete panel, the concrete panel showed significantly more out-of-plane displacements (up to 40 mm) and cracks. This can be attributed to the difference in brittleness between concrete and granite.

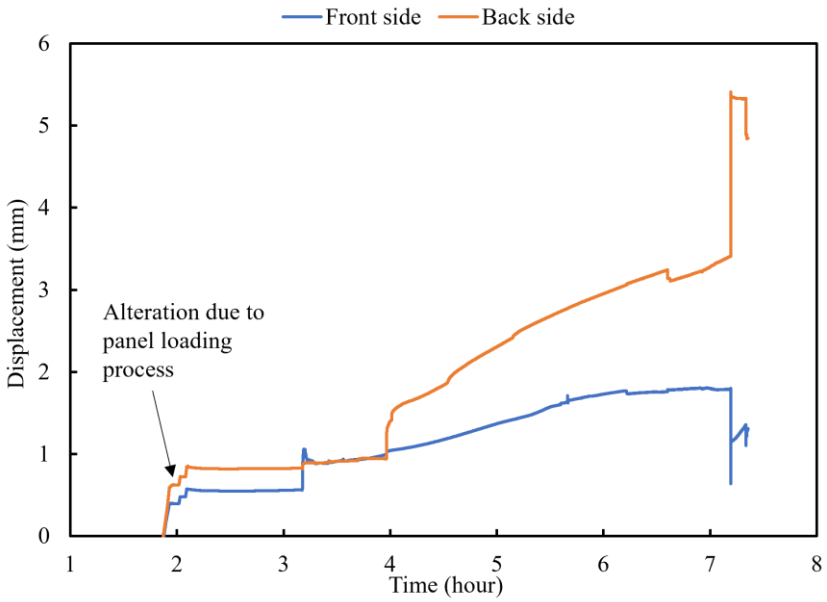

Figure 4.15 Panel out-of-plane displacement on the face and back sides over time.

4.3.2.3 AE data

Fig. 4.16a shows the distribution of accumulated AE energy emission projected onto the front surface of the panel. As can be seen, the highest AE energy occurs at the center of the panel, which is consistent with the centered SCDA pattern in the panel. Fig. 4.16b shows the cumulative AE energy of all events recorded over time. The AE energy starts to increase exponentially at 3.18 hours which is in line with the surface cracking that was firstly observed. Interestingly, the growth of the cumulative acoustic emission energy curve shows a brittle behaviour. Instead of gradually increasing as observed in the concrete test (see Fig. 4.11b), the AE energy increases abruptly several times during the granite test and the AE energy was relatively steady between each rise. The eventual accumulated AE energy in granite test is around 32000 J, which is approximately 8 times the cumulative AE energy when fracturing concrete panel.

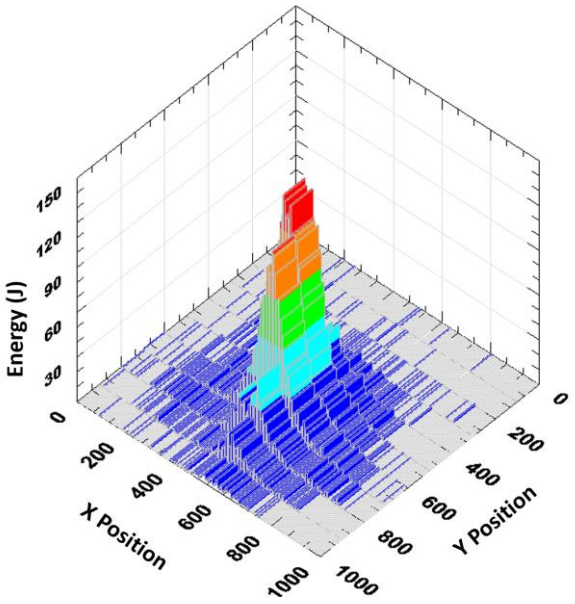

(a) AE energy spatial distribution.

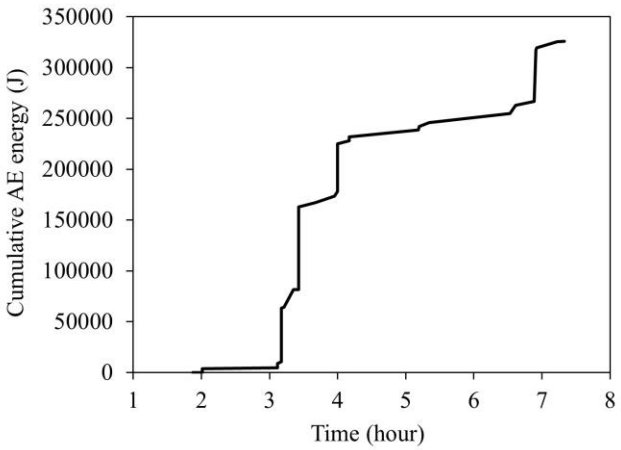

(b) Cumulative AE energy over time.

Figure 4.16: AE data for granite test.

4.3.2.4 SCDA Temperature

Two thermocouple sensors were embedded into two SCDA boreholes at the top of the pattern during the granite test. The temperature variation of SCDA reflects the expansion rate of SCDA directly as the hydration reaction of SCDA is exothermic. It can be observed from Fig. 4.17 that

the temperature steadily increased from the start of monitoring and indicates SCDA curing. The temperatures in two boreholes rose exponentially after 3.2 hours and reached their peak at 3.44 and 3.74 hours, respectively. The period between 3.2 hours and 4 hours when high SCDA temperature experienced is consistent with the time of significant AE energy increase as showed in Fig. 4.16b. This indicates high SCDA temperatures are pertinent with high rock fracturing rates, which can be interpreted as the SCDA undergoing rapid expansion and therefore pressure increasing in pressure. Notably, immediately after reaching peak temperatures, both curves showed sudden drops back to room temperature. This is because the thermocouple sensors fell out of the panel after panel surface spalling.

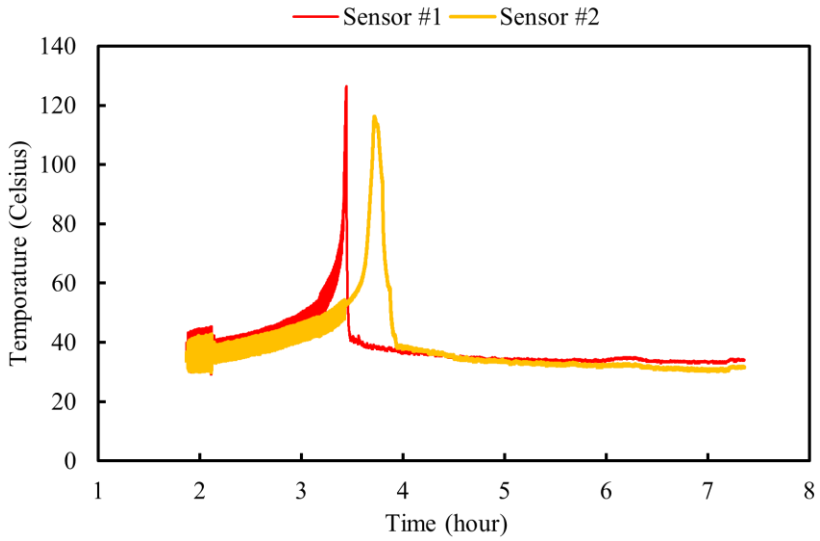

Figure 4.17: SCDA temperature change during the test.

4.4 Numerical modelling

4.4.1 Model setup

Recent work using PFC2D code simulated 2D material fracturing on a panel face with SCDA (Chen et al., 2022). However, the laboratory test results showed significant out-of-plane fracturing and displacement on both concrete and granite panels, which can not be reflected using 2D modelling code. Hereby, the finite-difference modelling code FLAC3D 7.0 is utilized to simulate panel breakage with SCDA and confirm the panel out-of-plane mechanism. The geometry and mesh of the numerical models are shown in Fig. 4.18. Each model has a grid point density of 8 mm, yielding about 480000 grid points.

To simulate the biaxial loading conditions, 23 MPa and 15 MPa are applied to four side boundaries of the concrete model and 40 MPa and 26 MPa are applied to the side boundaries of the granite model. After the model reaches equilibrium in the initial loading step, the boundary pressure is removed and the positions of boundary grid points are fixed, mimicking the zero-displacement setting of the biaxial frame during the test. The SCDA materials are filled in the SCDA holes and hydrostatic pressure is initialized in the SCDA to force the elastic material to expand axially and radially against borehole. The initialized stress in the SCDA material is then increased in subsequent steps until the panel is fully fractured.

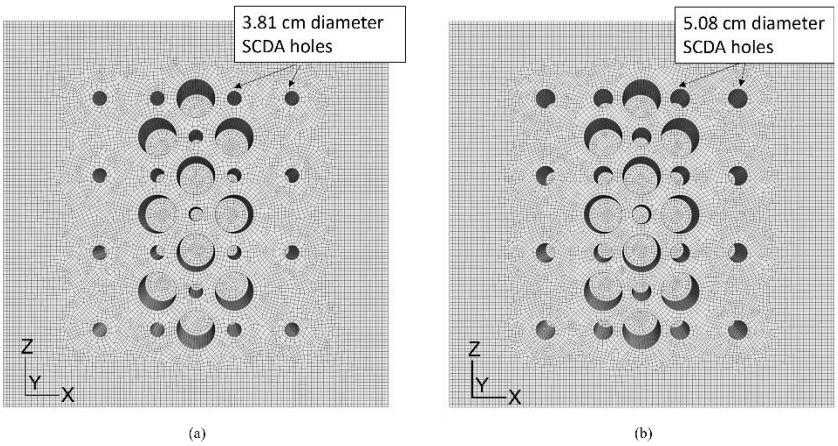

Figure 4.18: FLAC3D model setup. a) Concrete model b) Granite model.

4.4.2 Material properties

Mohr-Coulomb model is employed for modelling the behaviour of the panel materials. The concrete and granite model parameters are obtained from the testing program discussed in Section 4.2.2, and the input material parameters in FLAC3D are shown in Table 4.5. The SCDA material is modelled as a linear elastic material to simulate the relation between hydrostatic pressure generated by SCDA hydration process and SCDA material deformation. The density and elastic modulus of SCDA in a confined borehole are obtained from laboratory measurement (Habib et al., 2023). Some literature showed a high Poisson's ratio of SCDA between 0.2 ~ 0.4 during SCDA curing process (De Silva et al., 2017; Xu et al., 2021), but those values were obtained in a uniaxial test and might not be directly used for SCDA expansion modelling. The impact of different Poison's ratios on panel fracturing condition is shown in the modelling results section. Based on the model calibration with the field observation, the Poisson's ratio of 0.15 is selected in the modelling.

Table 4.5: Material parameters in FLAC3D

Material	Model	Density	Young's modulus (GPa)	Poisson's ratio	Friction (°)	Cohesion (MPa)	Tension (MPa)
Concrete	Mohr-Coulomb	2320	24	0.07	38.9	13.3	5.6
Granite	Mohr-Coulomb	2670	45	0.13	57.0	24.6	7.2
SCDA	Linear elastic	2000	8	0.15	N/A	N/A	N/A

4.4.3 Modelling results

Fig. 4.19 shows the stress state on the face of concrete panel after applying the boundary stresses. It shows that the designed stress-relief holes effectively shield the SCDA holes from compressive stresses due to the stress shadow effect. The applied vertical and lateral confinements from the model boundary are 23 MPa and 15 MPa, respectively, while the vertical and horizontal stresses in the shadowed area around SCDA holes are both about 8 MPa.

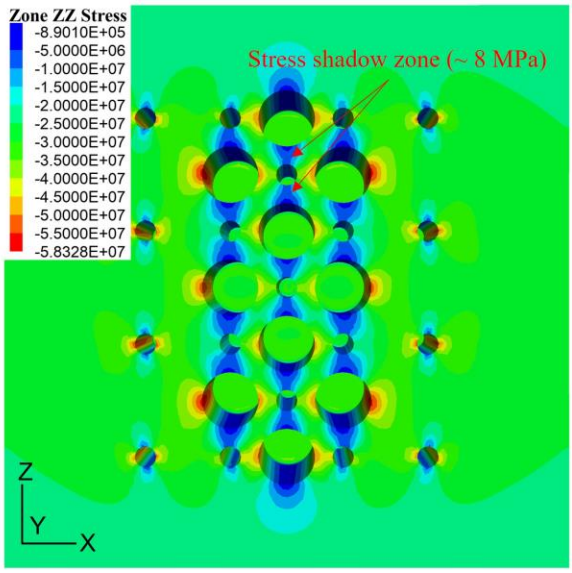

(a) Vertical stress

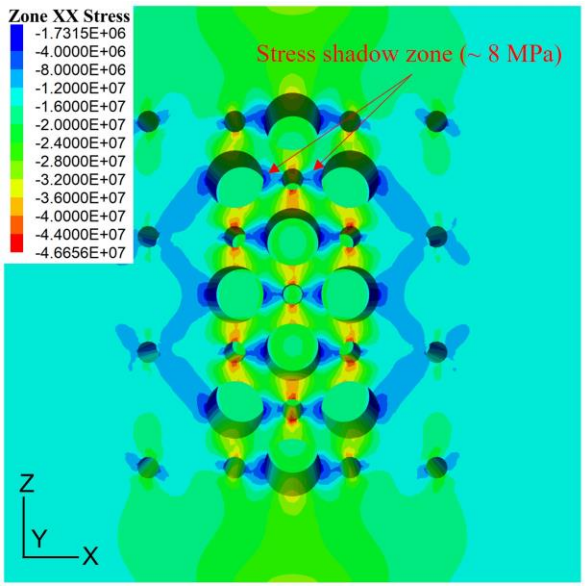

(b) Horizontal stress

Figure 4.19: Stress contours for concrete panel after confinement application.

The effect of Poisson's ratio on the SCDA expansive pressure in the concrete panel is examined in FLAC3D modelling when 30 MPa hydrostatic pressure of SCDA is applied. Fig. 4.20 shows that when Poisson ratio is 0.1, the panel center has almost completely yielded, and dense tensile fractures are observed to radiate from the relief holes. The tensile fractures imply the panel out-of-

plane motion and bulging failure mechanism as observed in the large-scale test (Fig. 7c and Fig. 8a). When the Poisson's ratio is increased to 0.2, the out-of-plane fractures still exist but are less dense. If the Poisson's ratio of SCDA is 0.3 or 0.4, the out-of-plane fractures disappear inside the relief holes and much less yielding is generated by SCDA pressure. This could be explained by the interplay of axial and radial strains with high Poisson's ratio. Based on the comparison of modelling results with field observations, a Poisson's ratio of 0.15 is used for subsequent models.

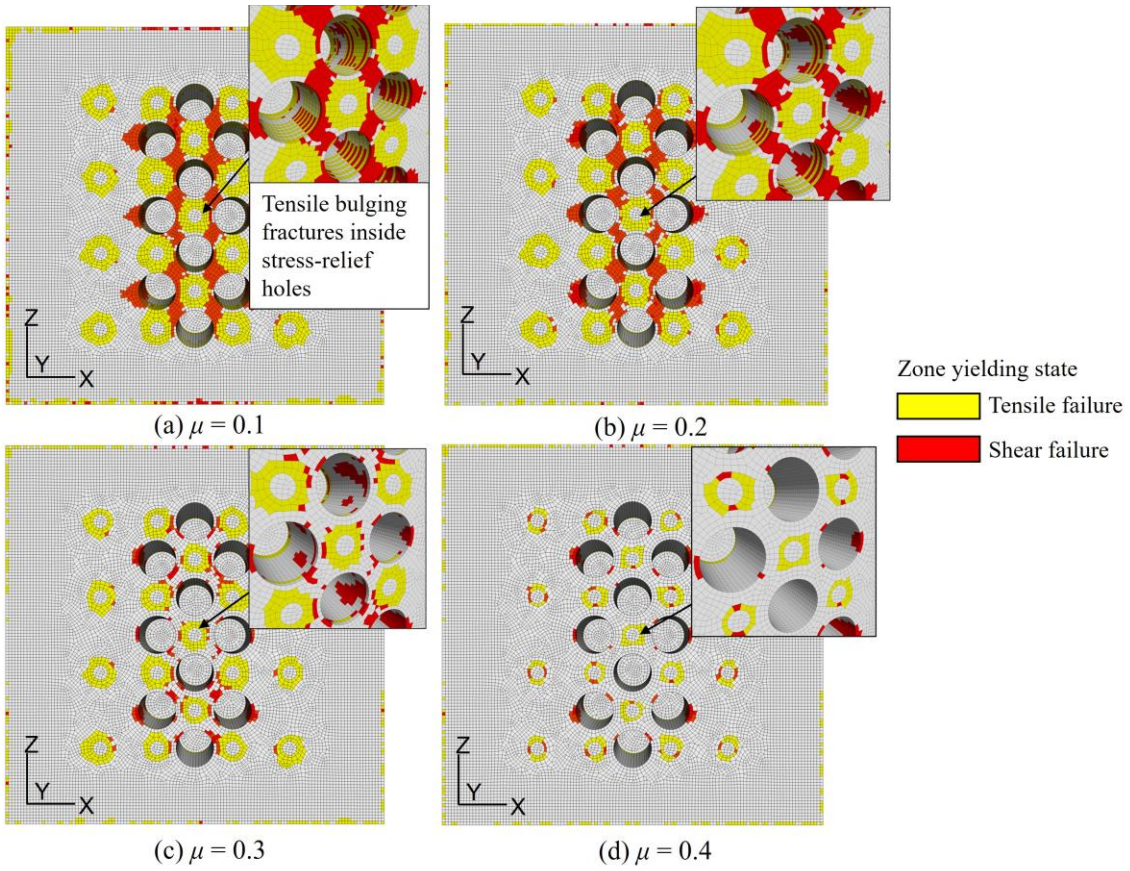

Figure 4.20: The impact of Poisson's ratio values on concrete panel fracturing with 30 MPa SCDA pressure.

Fig. 4.21 shows the modelled panel fracturing conditions in both concrete and granite panels. Fig. 4.21a shows the concrete panel yield zone with an initialized SCDA pressure of 20 MPa. Tensile failure can be observed around the SCDA holes, which are in line with the surface spalling which

first occurred in the concrete test. The modelled concrete panel completely failed with an initialized SCDA pressure of 30 MPa, with the bridges around SCDA holes being sheared and forming a cavity in the panel center, as shown in Fig. 4.21b. This failure mechanism is highly consisting with the field observation. For the granite panel failure, a different failure mechanism can be observed in modelling. On the one hand, the tensile yielding is dominant without apparent shear failures when panel failed at 25 MPa SCDA pressure in Fig. 4.21d. This difference can be attributed to the much higher friction angle of granite than that of concrete, meaning the global shear resistance of the granite panel is much higher. The large-scale test results also show there was no obvious shear failure of the granite panel; the central cavity was formed by the cascade of tensile spalling (see Fig. 4.12c and 4.12d). On the other, the required SCDA pressure for fully fragmenting granite pattern is less than that for concrete one (30 MPa). This can be attributed to the larger SCDA holes, providing a higher area on which the SCDA pressure is applied, as well as reducing the amount of material between the SCDA hole and relief holes.

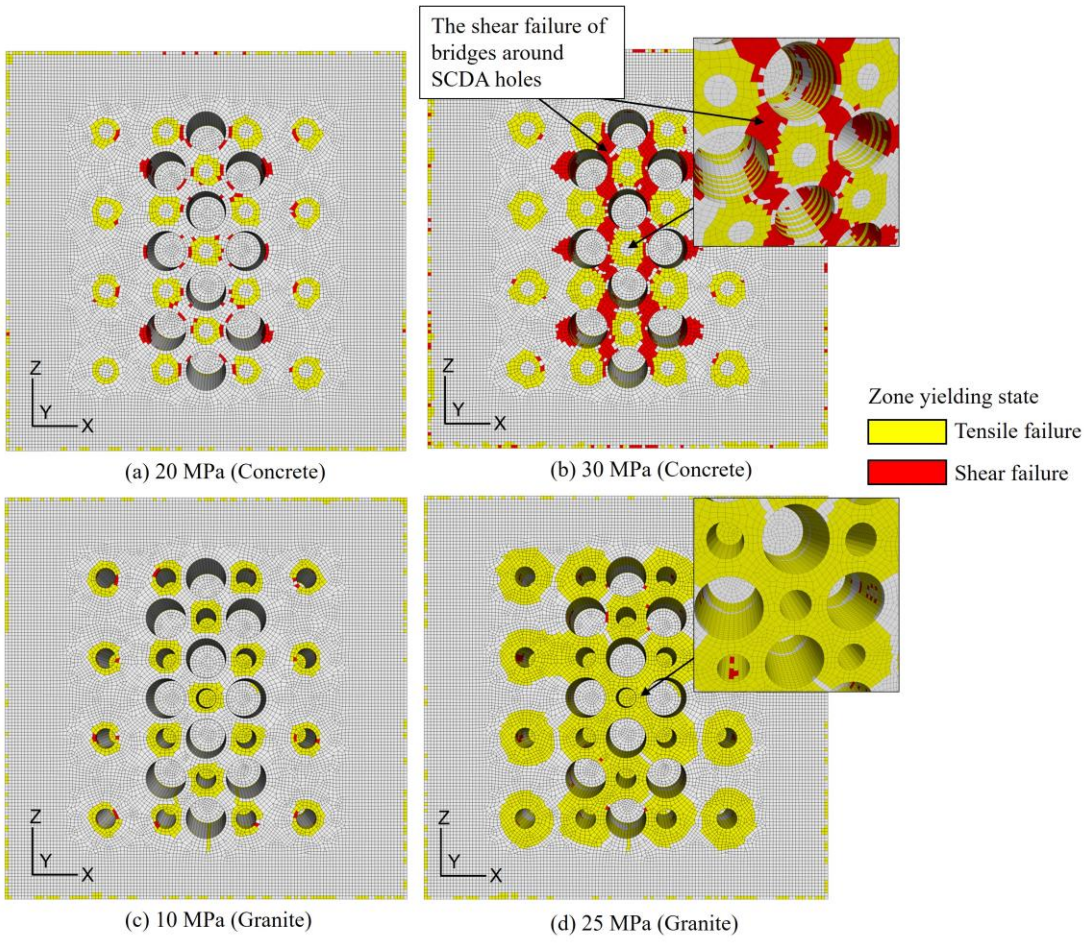

Figure 4.21: Simulated fracturing conditions of concrete and granite panels.

4.5 Discussion

Both AE and displacement data show that the granite panel started fracturing 3.2 hours after mixing, while and concrete panel began showing obvious fractures 6 hours after mixing. The granite panel completely failed at 7 hours 18 minutes, which is about 4.5 hours ahead of the collapse of the concrete panel. This should be due to the 5.08 cm (2 in.) SCDA boreholes in granite panel is larger than the 3.81 cm (1.5 in.) borehole in concrete panel, leading to faster and larger expansive pressure development.

SCDA-induced fracturing in unconstrained and uniaxially loaded granite prismatic blocks with a central SCDA borehole has been recently investigated by Habib et a. (2022b). It is observed that fractures are of type I and are generally oriented radially from the borehole when the host rock is under no constraint. While the fracture orientation may be random, it may be influenced by the block geometry whereby the fractures propagate first in the direction of least resistance. When the rock block is uniaxially loaded, the fracture orientation is dictated by the the loading direction. This is due to the the state of stress generated around the borehole due to uniaxial loading. In the current work, the biaxial state of stress effectively inhibits crack initiation in both directions when no shield holes are employed. The introduction of shield holes essentially serves to create a low stress regime around the SCDA hole thus allowing the SCDA pressure to eventually initiate cracking in both loading directions towards the surrounding shield holes.

The results show denser and more obvious out-of-plane fractures in concrete panel than that in granite panel, which could be attributed to the granite material being more brittle than concrete. This brittleness difference can be identified during the fracturing process of the two panels. The concrete panel showed continuous out-of-plane creeping, confining pressure loss and gradual AE energy increase, while the granite panel had less out-of-plane displacements and showed a staircase curve of cumulative AE energy release.

The concrete panel test and modelling showed a combination of tensile and shear failure mechanisms; dense bulging fractures and out-of-plane movement occurred initially, and the central cavity was eventually created by the bridge shear failure around SCDA holes. In contrast, the granite panel showed dominant tensile failures. The difference in failure mechanism can be attributed to the high friction angle of the granite, which makes the shear failure more difficult to initiate in the granite panel.

4.6 Conclusion

This work aims to explore the use of SCDA for the breakage of hard rock under high biaxial confinement. It could shed light on the potential usage of SCDA as an alternative to fragmentation with explosives in underground excavations. In this paper, large-scale test setup for panel breakage under biaxial loading is introduced. The test results and instrumentation data show that two panels under high confinement were fractured to demolition with SCDA, notwithstanding that distinctly different failure behaviour and mechanisms were observed. Also, the finite-difference modelling code FLAC3D 7.0 is utilized to simulate panel breakage process to explore the failure mechanism of two panels. The modelling results are found to be comparable to experimental observations. This research should set the stage for future implementations of SCDA to underground hard rock excavation. The main findings of the research are summarized below.

- Both large-scale tests and numerical modelling show that SCDA induces significant out-of-plane fractures in biaxially loaded panels. As existing studies mainly focused on the fracturing associated with radial expansion induced by SCDA, this new finding extended our knowledge of how SCDA work under biaxial confinement and has significant implications for the future applications in such circumstances.
- Distinct failure mechanisms are observed during the breakage of the two panels. The concrete panel showed a combination of ductile tensile failures and eventual bridge shear failures, while the granite panel with higher shear strength showed dominant brittle tensile failures.
- Both AE and displacement data show an accelerated onset of granite panel fracturing than that of concrete (3 hours vs. 6 hours), which led to the granite panel failure 4.5 hours earlier

than the concrete panel. This can be explained by the larger SCDA boreholes in granite panel leading to faster and larger expansive pressure development.

- A lower Poisson's ratio of SCDA than the laboratory measurements was used in the modelling to simulate the panel bulging failure observed in the tests. The FLAC3D modelling show that the applied drilling pattern with relief holes effectively shadowed the high confining pressures around SCDA holes, which facilitates the expansion of SCDA under high confinements.

References

Alvarez De La Garma, J. (2021). Numerical simulation of rock fracturing due to borehole expansive pressure under biaxial loading condition. Master of Science Thesis. McGill University. Montreal. Canada.

Arjang, B., & Herget, G. (1997). In situ ground stresses in the Canadian hardrock mines: an update. International Journal of Rock Mechanics and Mining Sciences, 34(3-4), 15-e1.

Cho, H., Nam, Y., Kim, K., Lee, J., & Sohn, D. (2018). Numerical simulations of crack path control using soundless chemical demolition agents and estimation of required pressure for plain concrete demolition. Materials and Structures, 51(6), 1-13.

De Silva, R. V., Pathegama Gamage, R., & Anne Perera, M. S. (2016). An alternative to conventional rock fragmentation methods using SCDA: a review. Energies, 9(11), 958.

De Silva, V. R. S., Ranjith, P. G., Perera, M. S. A., Wu, B., & Rathnaweera, T. D. (2017). Investigation of the mechanical, microstructural and mineralogical morphology of soundless cracking demolition agents during the hydration process. Materials Characterization, 130, 9-24.

De Silva, V. R. S., Ranjith, P. G., Perera, M. S. A., Wu, B., & Wanniarachchi, W. A. M. (2018). A low energy rock fragmentation technique for in-situ leaching. Journal of Cleaner Production, 204, 586-606.

De Silva, V. R. S., Ranjith, P. G., Perera, M. S. A., & Wu, B. (2019). The effect of saturation conditions on fracture performance of different soundless cracking demolition agents (SCDAs) in geological reservoir rock formations. Journal of Natural Gas Science and Engineering, 62, 157-170.

Guo, T., Zhang, S., Ge, H., & Qu, Z. (2015). A Novel" Soundless Cracking Agent Fracturing" for Shale Gas Reservoir Stimulation. International Journal of Environmental Science and Development, 6(9), 681.

Habib, K. M, Shnorhokian S, Mitri H. S (2022a) Evaluating the Application of Rock Breakage without Explosives in Underground Construction—A Critical Review of Chemical Demolition Agents. Minerals.12(2):220.

Habib, K., Vennes, I., Mitri, H.S. (2022b) Laboratory investigation into the use of soundless chemical demolitions agents for the breakage of hard rock. International Journal of Coal Science and Technology, 9(1), 70,1-10

Habib, K. M., Vennes, I., & Mitri, H. S. (2023). Methodology for the estimation of expansive cement borehole pressure. International Journal of Mining Science and Technology, 33(1), 73-81.

Hinze, J., & Brown, J. (1994). Properties of soundless chemical demolition agents. Journal of construction engineering and management, 120(4), 816-827.

Kim, K., Cho, H., Sohn, D., & Lee, J. (2021). The use of expansive chemical agents for concrete demolition: Example of practical design and application. Construction and Building Materials, 272, 121849.

Li, Y., Li, K., Feng, X., & Cai, M. (2018). Development and evaluation of artificial expandable pillars for hard rock mining. International Journal of Rock Mechanics and Mining Sciences, 110, 68-75.

Li, R., Yan, Y., Jiang, Z., Zheng, W., & Li, G. (2021). Impact of hole parameters and surrounding constraint on the expansive pressure distribution and development in soundless chemical demolition agents. Construction and Building Materials, 307, 124992.

Ma, J., Du, F., & Zhang, S. (2020). Acoustic Emission Characteristics of Normal and Layered Concrete Blocks during Dilating/Static Fracture. Advances in Materials Science and Engineering, 2020.

Musunuri, A., & Mitri, H. (2009). Laboratory investigation into rock fracturing with expansive cement. International Journal of Mining and Mineral Engineering, 1(4), 327-345.

Natanzi, A. S., Laefer, D. F., Kakali, G., & Iman Zolanvari, S. M. (2019). Temperature-Induced Chemical Changes in Soundless Chemical Demolition Agents. Journal of Materials in Civil Engineering, 31(7), 04019098.

Natanzi, A. S., & Laefer, D. F. (2014). Using chemicals as demolition agents near historic structures. In 9th International Conference on Structural Analysis of Historical Constructions, Mexico City, Mexico, 14-17 October, 2014.

Shang, J., Hencher, S. R., West, L. J., & Handley, K. (2017). Forensic excavation of rock masses: a technique to investigate discontinuity persistence. Rock Mechanics and Rock Engineering, 50(11), 2911-2928.

Tang, W., Zhai, C., Xu, J., Sun, Y., Cong, Y., & Zheng, Y. (2021). The influence of borehole arrangement of soundless cracking demolition agents (SCDAs) on weakening the hard rock. International Journal of Mining Science and Technology, 31(2), 197-207.

Chen, T., Vennes, I., & Mitri, H. S. (2022). Investigation into Rock Breakage with Expansive Cement Under Biaxial Confinement. Rock Mechanics and Rock Engineering, 1-15.

Wang, L., Duan, K., Zhang, Q., Li, X., & Jiang, R. (2022). Study of the Dynamic Fracturing Process and Stress Shadowing Effect in Granite Sample with Two Holes Based on SCDA Fracturing Method. Rock Mechanics and Rock Engineering, 1-17.

Xu, S., Hou, P., Cai, M., & Li, Y. (2019). An experiment study on a novel self-swelling anchorage bolt. Rock Mechanics and Rock Engineering, 52, 4855-4862.

Xu, S., Hou, P., Li, R., & Cai, M. (2021a). An experimental study on the mechanical properties and expansion characteristics of a novel self-swelling cartridge for rock breakage. Rock Mechanics and Rock Engineering, 54(2), 819-832.

Xu, S., Yang, Z., Cai, M., & Hou, P. (2021b). An experimental study on the anchoring characteristics of an innovative self-swelling Split-set. Tunnelling and Underground Space Technology, 112, 103919.

Xu, S., Hou, P., Li, R., & Suorineni, F. T. (2022). An improved outer pipe method for expansive pressure measurement of static cracking agents. International Journal of Mining Science and Technology, 32(1), 27-39.

Bridging text between Chapter 4 and Chapter 5

In the previous chapter, the SCDA diamond-shaped drillhole pattern selected based on PFC2D modelling is found effective for promoting hard rock fracturing when the panel is subjected to high confinement. Another SCDA drillhole pattern namely the V-cut is proposed in the following chapter. V-cut drillhole design has been used in conventional drilling and blasting method. Compared to the diamond-shaped pattern introduced in Chapter 4, the V-cut offers several advantages. It requires fewer boreholes and less drilling accuracy compared to long parallel boreholes, making it an efficient and practical choice. The V-cut also allows the easy rock casting towards the free face. Thus, it is deemed suitable for small-scale rock excavation projects such as narrow vein mining.

A novel V-cut drill hole pattern employing two sets of three SCDA holes angled at 45º from the face is proposed for the rock face breakage application of SCDA. The V-cut is examined on two Standstead granite panels of 1 m x 1 m x 0.25 m subjected to 40 MPa and 26 MPa. Panels are well instrumented with time-lapse camera, acoustic emission system, displacement sensors, thermocouples, and confining pressure sensors. Two panels are successfully demolished with the proposed V-cut drilling patten using SCDA. FLAC3D modelling is employed to analyze the V-cut panel failure process. Based on numerical modelling, the SCDA pressure required to initiate panel cracking is obtained and the rock demolition mechanism of the novel V-cut with SCDA is verified.

The following Chapter is a paper submitted to International Journal of Rock Mechanics and Mining Sciences. It is currently under review.

Chapter 5: Explosive-free rock breakage under biaxial loading condition using V-cut drill hole pattern

Author:

Tuo Chen*, Isaac Vennes, Hani S. Mitri

Affiliation:

Department of Mining and Materials Engineering, McGill University, Montreal, Canada H3A 0E8

Address: 3450 University Street, Montreal, Quebec, Canada H3A 0E8

*Corresponding author. Tel.: +14388662473; E-mail address: tuo.chen@mail.mcgill.ca (T. Chen)

Abstract

Interest in soundless chemical demolition agents (SCDA) as a potentially viable alternative to explosives for rock fragmentation has been growing in recent years. In this paper, a novel SCDA method for underground rock face breakage is proposed and examined using a large-scale testing system. The work investigates the SCDA performance for rock panel demolish under high biaxial confinements of 26 MPa and 40 MPa. A novel V-cut drillhole pattern employing two sets of three SCDA holes angled at 45º from the face, is designed, tested, and analyzed in laboratory. Standstead granite panels of 1 m x 1 m x 0.25 m are loaded biaxially corresponding to an in-situ stress state of 1000 m depth in the Canadian shield. Two panels were successfully demolished with the V-cut. Acoustic emission data shows that the panel test undergoes three phases: SCDA pressure buildup, steady micro-fracture development, and unstable fracture development. FLAC3D modelling is used to analyze the panel failure mechanisms, which helps validate the experimental observations. Through V-cut drillhole design, this study demonstrates that the proposed SCDA method can effectively demolish hard rock panels subjected to high biaxial confinements, which mimic the condition of an underground rock face.

Keywords: Explosive-free rock breakage; rock fragmentation; soundless chemical demolition agents; expansive cement; V-cut drilling; biaxial loading;

5.1 Introduction

Drilling and blasting methods are widely used for underground excavation activities such as tunnelling and mining. While popular, these methods are known to be accompanied with drawbacks such as strong ground vibrations, noise, toxic fumes, and damage to surrounding buildings (Nateghi, 2012; Ozcelik, 2018). Thus, with the increase of safety and environmental constraints in recent years, there has been a growing interest in developing non-explosive rock fragmentation methods that could render the construction process more environmentally friendly. Soundless chemical demolition agent (SCDA), also known as expansive cement, is an environmentally friendly and safer alternative to explosives for hard rock fracturing (Habib et al., 2022a). When SCDA is mixed with water and poured in a blind borehole, high expansive pressure develops during the cement curing process causing the surrounding material to fracture. Since its introduction in the early 1970s, SCDA has been mainly used for surface applications such as block splitting in dimension stone quarrying and the demolition of concrete foundations (Cho et al., 2018; Kim et al., 2021). The development of such method has great potential and could be beneficial for field applications. The use of SCDA does not produce toxic fumes and thus would not require the same ventilation as blasting with explosive energy in mines and tunnels. Rock fracturing with SCDA is docile due to the static and gradual nature of the curing process. Hence, issues such as fly rocks, overbreak, dust, and noise are avoided. In this paper, a novel explosive-free method for underground rock face breakage is proposed and examined using indoor large-scale testing and 3D numerical modelling.

Many studies have been conducted to examine SCDA properties and performance in laboratory. The peak SCDA expansive pressure is traditionally measured using the thick-walled cylinder experiment, which involves pouring the SCDA mixture into a thick-walled metal cylinder with

circumferential strain gauges mounted on the outer surface of the cylinder. SCDA pressure is calculated analytically based on the measured tangential strain on the cylinder surface (Hinze & Brown, 1994; Xu et al., 2021; Li et al., 2021). Habib et al. (2023) found that the measured peak expansive pressure is consistently higher than the estimated pressure from the thick-walled cylinder method. A correction factor α of 1.31 was derived to correct the estimated SCDA stress from the analytical solution. Shang et al. (2017) employed SCDA to explore discontinuity persistence. The SCDA boreholes are drilled along the discontinuity line of rock blocks, whereby the pre-existing persistent area and rock bridge area can be directly observed on the split surface and the discontinuity persistence quantified. De Silva et al. (2018) explored possible application of SCDA for in-situ leaching through laboratory tests and discrete-element simulation. The results indicate that SCDA could produce controllable fracture network in impervious rocks to enhance in-situ leaching. De Silva et al. (2019) investigated the influence of saturation conditions on the fracturing results due to SCDA in reservoir rock formations. Natanzi et al. (2019) investigated the influence of ambient temperature on SCDA chemical alterations in steel pipes. It was shown that the SCDA produces higher $Ca(OH)_2$ concentrations and greater expansive pressures at higher temperature. Maneenoi et al. (2022) investigated the impact of chemical admixtures on SCDA performance. $MgCl_2$ and $CaCl_2$ were found to accelerate the SCDA process.

As shown in Figure 1, there are three different categories of cuts for drift development. They are burn cut, V-cut, and fan cut (Darling, 2011). Burn cuts (Figure 5.1a) belong to the category of parallel hole cuts. They are the most widely used in mining operations having hydraulic-electric equipment like jumbo drills, which come with automatic parallelism (Jimeno et al. 2006). A burn cut consists of a series of charged holes accommodated in a systematic pattern around one or several uncharged holes of larger diameter (Nobel, 2010). The uncharged holes, shown in light

gray in Fig 1a, are commonly known as relief holes, and they are usually drilled first. Subsequently, the relief holes are surrounded by smaller diameter holes (dark gray), which are charged with explosives. The other two types of cuts, V-cut in Fig. 5.1b and fan cut in Fig. 5.1c, use angled holes to create a relief space or a crater. V-cuts and fan cuts, on the other hand, use only small diameter holes and require lesser drilling accuracy than long parallel holes used in burn cuts. This makes them easy to use in tunneling and drifting projects (Wang et al., 2019; Yang et al., 2020; Cheng et al., 2021; Yu and Mitri, 2012).

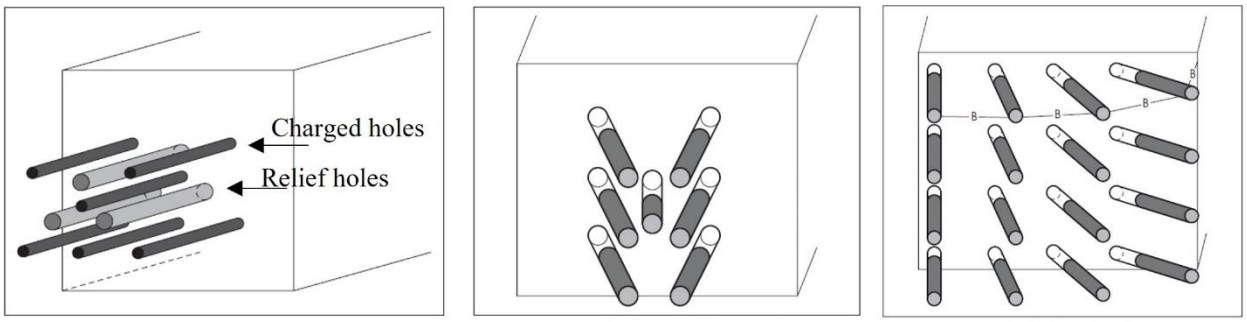

(a) (b) (c)

Figure 5.1: Different cut categories: a) burn cut; b) V-cut with a center “buster hole”; c) fan cut showing swing of holes (Darling, 2011).

To date, there have been barely any investigations on SCDA application to rock face breakage underground where challenges such as high stress confinement and rock stiffness exist. The objective of this research is to examine a novel SCDA method for hard rock face breakage under biaxial stress condition using V-cut drill holes. Such method can be applicable to underground mining or tunnelling where biaxial stresses exist at the excavation face. Firstly, the design of the V-cut pattern with SCDA method is first examined. The large-scale testing program for granite panel loaded with high biaxial stresses is then presented. The test results and instrumentation data are discussed in detail. FLAC3D modelling is employed to confirm the test results and analyze the

panel failure mechanism. The findings should make an important contribution to expand application of SCDA to hard rock mining and tunneling by providing an alternative rock face breakage method without the use of explosives.

5.2 V-cut test design under biaxial loading

5.2.1 V-cut drill hole pattern design

In practice, SCDA is generally used under unconfined or low-stress conditions, such as in concrete demolition (Ma et al., 2020; Kim et al., 2021) or applied under uniaxial loading (Musunuri and Mitri, 2009; Habib et al., 2022b). When rock mass is confined biaxially such as the case of an underground rock face, the SCDA could only damage and weaken the surrounding rock medium (Tang et al., 2021), instead of creating a cavity. This is because the biaxial confinement suppresses the expansion of SCDA, and such constraint prevents the rock medium from casting. This study is part of a multi-phase project whereby previous work has proposed an effective diamond-shaped drillhole pattern and revealed that the arrangement of empty holes around SCDA boreholes enables the generation of a rock cavity under biaxial confinement (Chen et al., 2022). In this paper, a V-cut drillhole pattern for SCDA application is proposed, which requires fewer drillholes and allows for easy rock casting toward the free face.

Two Stanstead granite panels were prepared with the same V-cut pattern. The panels have dimensions of 100 cm × 100 cm × 25 cm as shown in Fig. 5.2a. The pattern has 10 stress-shield (empty) holes of which four are inclined to be parallel to the V-cut as shown in Fig. 5.2a. The shield holes are 10.16 cm in diameter (4 in.) and the 6 SCDA holes that are 5.08 cm (2 in.) in diameter and 22.7 cm deep. The SCDA holes are inclined at an angle of 45° in a V-shape to provide an expansive force for rock fragments to cast outwards from the panel face and form a wedge-

shaped crater. The stress-shield holes serve the purpose of shadowing the applied confining stress around the SCDA holes. The distance between two SCDA holes forming of a V-cut is 34 cm, and the spacing between the V rings is 20 cm. Six stress shield-holes are 10 cm from the V-cut holes and are perpendicular to the face as shown in Fig. 5.2b and 5.2c.

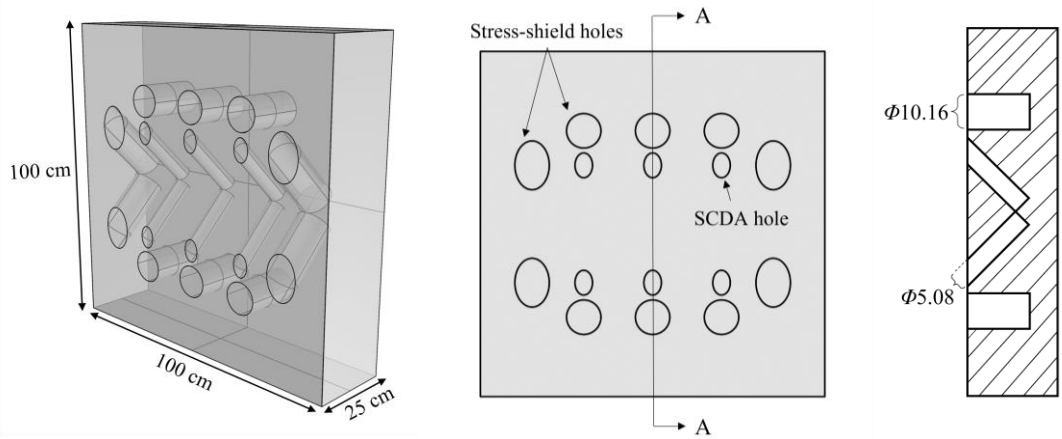

(a) Isometric view (b) Front view (c) Sectional view

Figure 5.2: Proposed SCDA borehole pattern.

5.2.2 Panel strength properties

Uniaxial, triaxial, and Brazilian tests are conducted on cylindrical specimens that are cored from the Stanstead granite panel to determine its physical properties. The test results are shown in Table 5.1 and Table 5.2. The uniaxial compressive strength (UCS) and triaxial tests are completed using axial displacement control at 0.0009 mm/s and the Brazilian tests are completed using axial load control at 0.10 kN/s. It is found that the granite samples have an average UCS of 117.7 MPa and an average Brazilian tensile strength of 7.2 MPa.

Table 5.1: UCS and triaxial test results for granite.

Specimen ID	Specifications			Strength and elastic properties			
	Diameter (mm)	Length (mm)	Density (g/cm^3)	Peak strength (MPa)	Confinement (MPa)	Young's modulus (GPa)	Poisson's ratio
STAC-SG-U1	44.80	101.00	2.67	117.4	0.0	45.0	0.17
STAC-SG-U2	44.80	101.00	2.67	120.2	0.0	45.9	0.11
STAC-SG-U3	44.80	100.90	2.67	115.4	0.0	45.0	0.13
STAC-SG-T1	44.80	100.90	2.67	169.3	5.0	50.4	0.21
STAC-SG-T2	44.90	100.90	2.67	218.2	10.0	54.7	0.19
STAC-SG-T3	44.90	100.90	2.67	268.1	15.0	58.3	0.25

Table 5.2: Brazilian test results for granite.

Specimen ID	Specifications			Strength	
	Diameter (mm)	Length (mm)	Density (g/cm^3)	Failure load (kN)	Brazilian tensile strength (MPa)
STAC-SG-B1	44.83	26.93	2.67	14.69	7.75
STAC-SG-B2	44.85	26.96	2.67	15.25	8.02
STAC-SG-B3	44.85	22.32	2.67	10.53	6.70
STAC-SG-B4	44.81	22.31	2.67	11.45	7.29
STAC-SG-B5	44.86	22.32	2.67	9.52	6.05
STAC-SG-B6	44.85	22.33	2.67	11.87	7.55

5.2.3 Biaxial loading system

The large-scale biaxial panel breakage tests were conducted at CANMET Mining laboratory in Sudbury, Ontario, Canada. The biaxial system uses a servo-controlled vertical press with a load capacity of 10 MN (Fig. 5.3a). A 6 MN lateral self-reaction frame (shown in Fig. 5.3b) was designed and built specifically for this project and is used in conjunction with the vertical press to

achieve the desired biaxial loading configuration. Details of the frame design can be found elsewhere (Alvarez De La Garma, 2021). With this loading system, it is possible to test a panel of 1 m x 1m x 0.25 m.

(a) (b)

Figure 5.3: Biaxial loading system, a) Vertical press, b) Lateral loading frame (Chen et al., 2022).

In the test, 20 cm of the panel thickness is subjected to biaxial loading and the panel back of 5 cm remains unloaded. This setup safely allows for maximum confining pressures of 40 MPa and 26 MPa to be applied to the granite panel in vertical and lateral directions. Such high level of confinement approximates an in-situ stress condition of approximately 1000 m below ground surface in the Canadian shield (Arjang and Herget, 1997), whereby the overburden stress (26 MPa) is vertical, and the major stress (40 MPa) is horizontal.

5.3 Test procedure

5.3.1 SCDA preparation

Betonamit Type R, a commercially available SCDA, was used for this experiment. The cement is mixed with water at room temperature (25°C) until it becomes consistent for 3 minutes, as shown in Fig. 5.4a. The water-to-cement ratio is 0.2 and the water temperature is around 20°C. For safety

reasons, the SCDA holes were loaded with expansive cement while the panel is lying flat as shown in Fig. 5.4b. The time between loading the holes and the placement of the panel in the loading frame was within one hour.

(a) Mixing SCDA powder with water

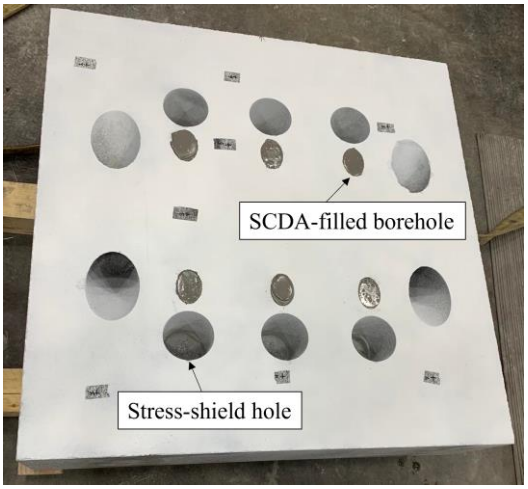

(b) Loading SCDA slurry

Figure 5.4: SCDA preparation and loading.

5.3.2 Loading granite panel

The lateral frame was pushed under the vertical press after SCDA hole charging was completed, as shown in Figure 5.5a. The servo-controlled loading was then applied both horizontally and vertically, with the same loading rate (0.08 MPa/s) in both directions until the target confinement was reached. The biaxial confinement stresses are 40 MPa and 26 MPa in the vertical and lateral directions, respectively. Such level of confinement was selected to mimic a virgin stress condition at around 1000 m below surface in the Canadian shield, all without exceeding the safe limit of the loading equipment. Vertical displacement was locked in position after the target load was attained. Likewise in the horizontal direction, a hydraulic oil lock was applied to the lateral frame using shutoff valve (Fig. 5.5b). With this arrangement, pressure variation was allowed to take place in response to panel fracturing.

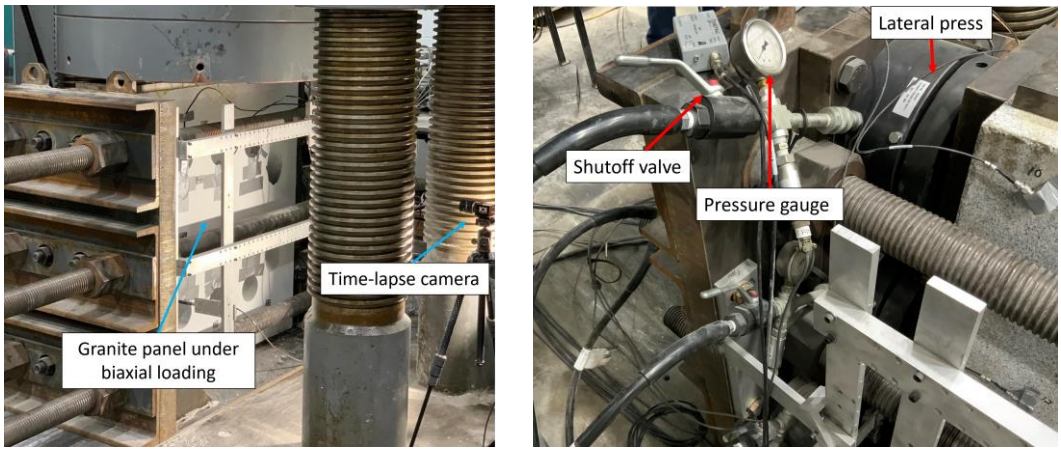

(a) Overall setup (b) Hydraulic lateral press

Figure 5.5: Application of biaxial loading on granite panel.

5.3.3 Instrumentation

The panel was not fully instrumented for the trial Test #1. After the first test had succeeded, it was repeated with complete instrumentation. Both test results and findings are presented in this paper. The monitoring systems employed in Test #2 include acoustic emission (AE) system, Keyence displacement sensors, thermocouples, and a high-resolution timelapse camera. A 16-channel Micro-II Express AE system made by Physical Acoustics is utilized for AE monitoring. Sixteen microphones with resonant frequency of 150 kHz were glued and taped around the panel and connected with AE preamplifiers, as shown in Fig. 5.6a. Thus, micro-damages in the panel are detected consistently during the test. High-precision Keyence displacement sensors were mounted on the loading frame to measure panel deformation during tests, as shown in Fig. 5.6b. Eight Keyence sensors are installed for this test; 2 sensors for monitoring out-of-plane displacements at panel front face and back, 3 sensors for monitoring panel vertical displacement and 3 sensors for lateral displacement at top, middle and bottom sections of the panel. Additionally, thermocouple

sensors were inserted in three top SCDA boreholes to monitor SCDA temperature. The hydration reaction of SCDA mixture is an exothermic reaction causes temperature increase, and the rate of expansive pressure development is related to the heating process (De Silva et al., 2016). Thus, the starting time of SCDA reaction and expansion can be identified by monitoring the SCDA temperature. A high-resolution timelapse camera was set up in front of the panel to capture the evolution of fracturing, taking one picture per minute, as shown in Fig. 5.5a. All monitoring systems and loads were kept online for 24 hours to capture the full effect of SCDA on the panel.

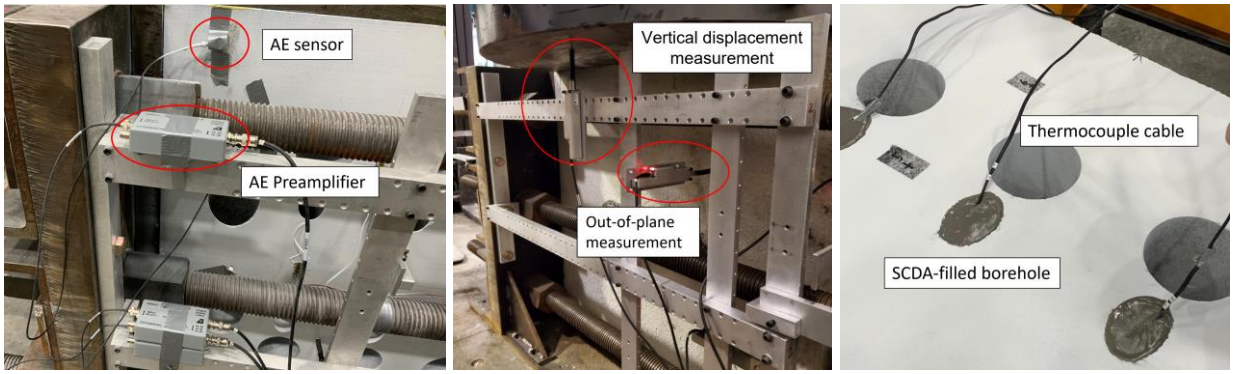

(a) AE system (b) Keyence sensors (c) Thermocouples

Figure 5.6: Arrangement of monitoring systems.

5.4 Experiments

5.4.1 Test #1

Timelapse pictures in Figure 5.7 show the first granite panel fracturing using the proposed explosive-free rock breakage method. Fig. 5.7a presents the initial condition of the panel without damage. Four hours and 20 minutes after mixing SCDA, visible minor cracks showed up on the front face around SCDA holes, as shown in Fig. 5.7b. Three hours later, significant spalling was observed around the SCDA holes, accompanied by visible extrusion of SCDA due to its axial

expansion, as shown in Fig. 5.7c. Major factures occurred on the front face 9 hours and 50 minutes after mixing SCDA. Several fractures were observed connecting from SCDA holes to adjacent shield holes, as annotated in Fig. 5.7d. About half an hour later, a horizontal fracture coalesced through the top three SCDA holes. A subvertical fracture also extended from upper middle hole to the lower left hole. After 11 hours 53 minutes, the entire panel collapsed in a brittle manner (see Fig. 5.7f) and the test ended.

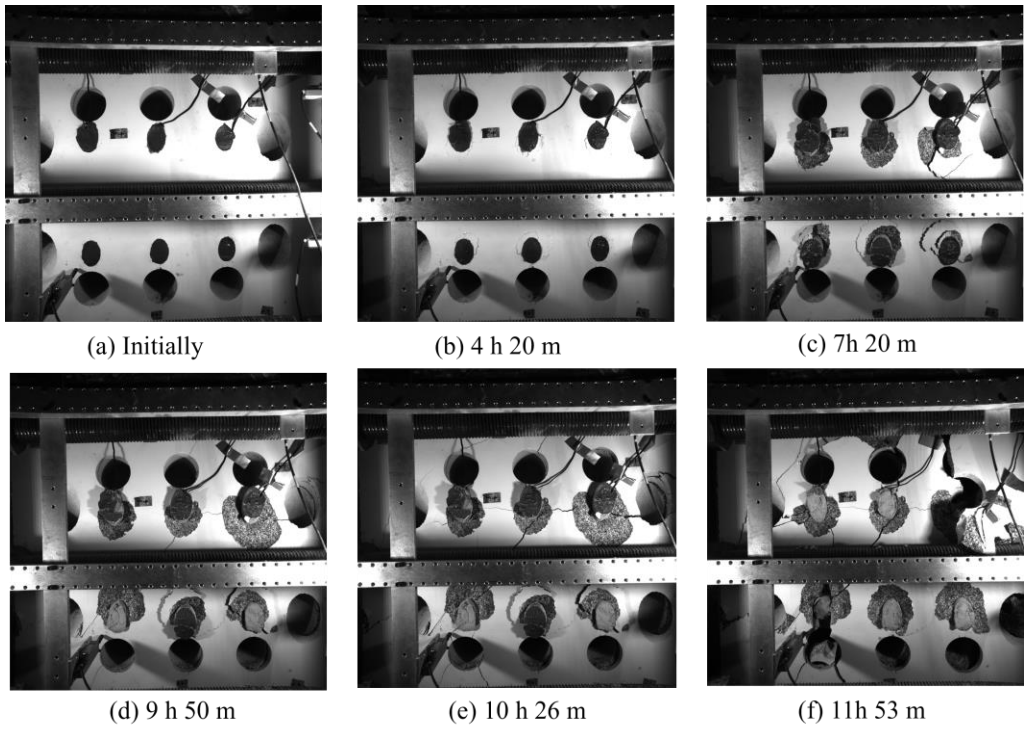

Figure 5.7: Time-lapse photos of panel fracturing due to SCDA.

The proposed method is designed to cast rock with V-shaped SCDA holes. Figure 5.8a presents the panel out-of-plane displacement and bulging during the test. It can be seen the face side had experienced significant bulging up to 42 mm after the panel failed. Such behaviour corroborates the feasibility of applying SCDA for non-explosive rock face breakage under high biaxial confinement. The out-of-plane deformation increase began at 5.5 hours and became exponential

at 9.8 hours (see Fig. 5.8a). The exponential increase of panel bulging was accompanied by surface fracturing as shown in Figure 5.7d. Basically, the trend of measured displacement is inline with the visual observations in Figure 5.7. The back of the panel also experienced some displacements, however less than 5 mm, until the end of the test.

Biaxial force variation of the two loading frames is illustrated in Fig. 5.8b. The changes indicate damage to the panel and the final loads could represent the residual strength of the panel during the test. Initially, 8000 kN and 5200 kN were applied in the vertical press and horizontal frame, respectively. At 5.3 hours after mixing SCDA, slight load decay was observed on both loading frames, as shown in Fig. 5.8b. This occurred concurrently with initial panel face bulging detected in Fig. 5.8a. Applied pressure was maintained until 9.7 hours when major fractures began to form on the panel face (see Fig. 5.7d). At 11.9 hours, the remaining forces dropped abruptly in a brittle manner. This is consistent with the final panel failure captured in Fig. 5.7f.

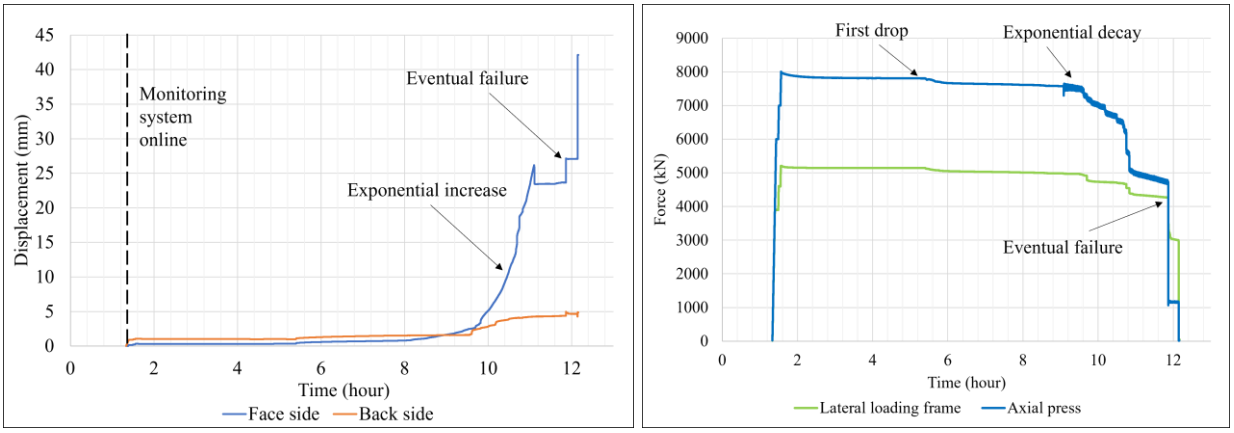

(a) Out-of-plane displacement (b) Biaxial load variation

Figure 5.8: Load and displacement data during Test #1.

5.4.2 Test #2

Figure 5.9 presents a series of timelapse pictures of the instrumented Test #2. Fig. 5.9a presents the initial condition of the panel. Minor cracks appeared around SCDA holes 4 hours and 20 minutes after mixing SCDA, as shown in Fig. 5.9b. At 5 hours 41 minutes, the panel experienced surface spalling around SCDA holes, as shown in Fig. 5.9c. The fractured granite fragments started to delaminate from the face. At 6 hours 44 minutes, some tensile cracks can be observed from bottom two stress shield holes (see annotation in Fig. 5.9d). After 7 hours 28 minutes, the entire panel face abruptly bulged out, as shown in Fig. 5.9e. One minute later, the panel back failed in a brittle manner (Fig. 5.9f), and nearly all the confining stresses were released.

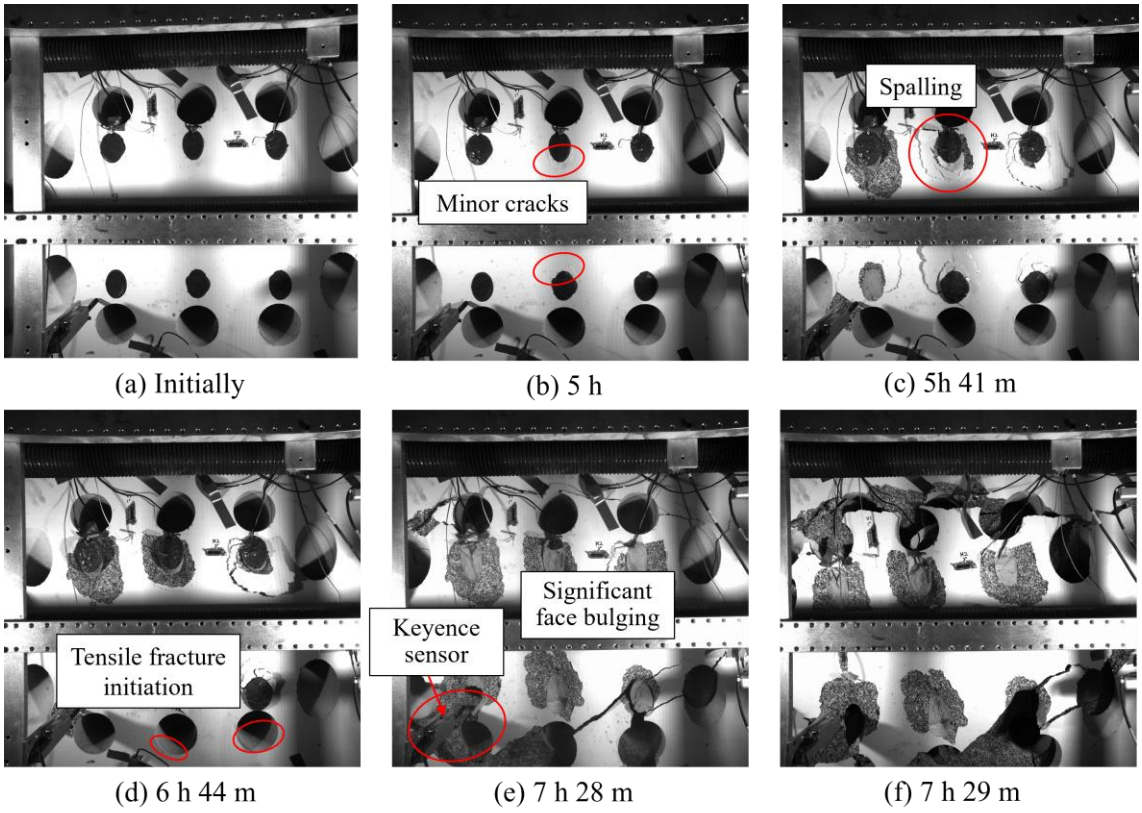

Figure 5.9: Time-lapse photos of panel fracturing due to SCDA.

The out-of-plane displacements towards front and back sides of the panel are plotted in Fig. 5.10a. It is shown that out-of-plane displacements on the front side begin to increase at 5 hours. This occurred simultaneously with the appearance of small cracks surrounding SCDA holes (see Fig. 5.9b). The displacements on the face side then accelerated until it struck a trough at 6.2 hours. This may be the result of local damage to the rock surface that the Keyence sensor was placed against, as can be seen in Fig. 5.9e. Consequently, the peak bulging displacement detected was only around 10 mm, which is much less than the highest displacement reported in the previous test, which was 42 mm (see Fig. 5.8a). Besides, both curves show displacement ramp up from 6.8 hours, which coincided with the onset of tensile fracture initiation observed in Fig. 5.9d.

Biaxial force variation in Fig. 5.10b reveals a similar rock damage trend. Initial pressure decay was observed after 5 hours. Loads were then maintained until around 1000 KN pressure suddenly delayed at 6.8 hours, coinciding with the observed panel tensile fracturing initiation from timelapse recording (Fig. 5.9d). Most of the loads, particularly on the lateral frame, was maintained and abruptly released with the ultimate failure of the panel at 7.5 hours. This also indicates the high brittleness characteristic of the Stanstead granite material.

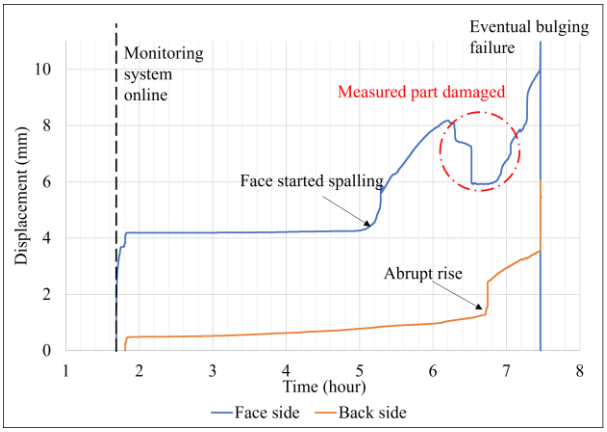

(a) Out-of-plane displacement

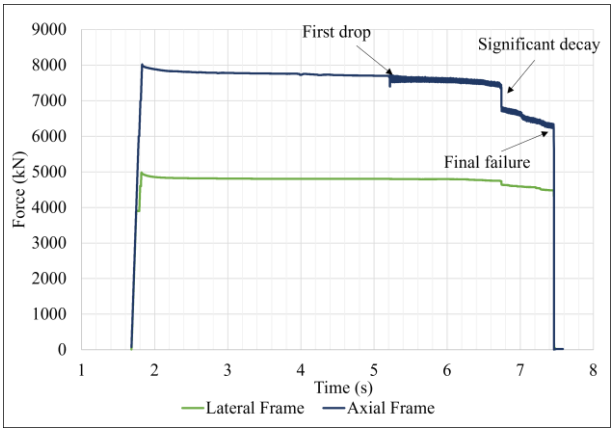

(b) Biaxial load variation

Figure 5.10: Load and displacement changes during test #2.

Acoustic emissions were monitored throughout Test #2 to capture micro-fractures that may occur before any visual cracking shows up on the slab face. Figure 5.11 shows a similar increase between AE event count and cumulative AE energy over time. A quiet period in the first 3.5 hours corresponds to SCDA curing and evolution of expansive pressure. A gradual increase of both AE energy and AE hit count between 3.5 hours and 5.8 hours, indicating stable development of micro-fractures in the panel. The initial cracking detected by AE is about 1.5 hours earlier than minor fracturing distinguished on time-lapse pictures (Fig. 5.9b). The rate of AE activity grew exponentially from 5.8 hours, and eventually, the AE energy and hit count peaked at 7.5 hours when panel demolished recording 3×10^7 J and 7.5×10^5 J, respectively.

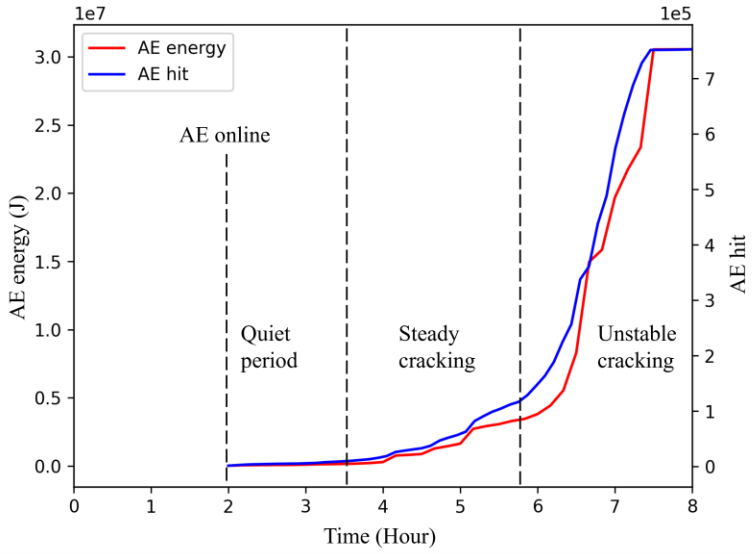

Figure 5.11: AE data of test #2.

Three thermocouple sensors were embedded into top three SCDA boreholes during the test. Because the hydraulic reaction process of SCDA is exothermic, the change in SCDA temperature directly reflects its expansion rate. It can be observed from Fig. 5.12 that all sensors indicate rapid

temperature rise from the beginning. The rate of temperature increasing is highest in the first 4 hours reaching 35 ℃. What is interesting about the temperature data is that it decreases steadily from 3.9 hours until the end of the test; nevertheless, the AE monitoring indicates that the panel incurred the greatest damage after 4 hours (see Fig. 5.11). This result exposes the hysteresis behaviour of rock fracture using SCDA, i.e., the rock had the most damage after the peak expansive reaction of SCDA.

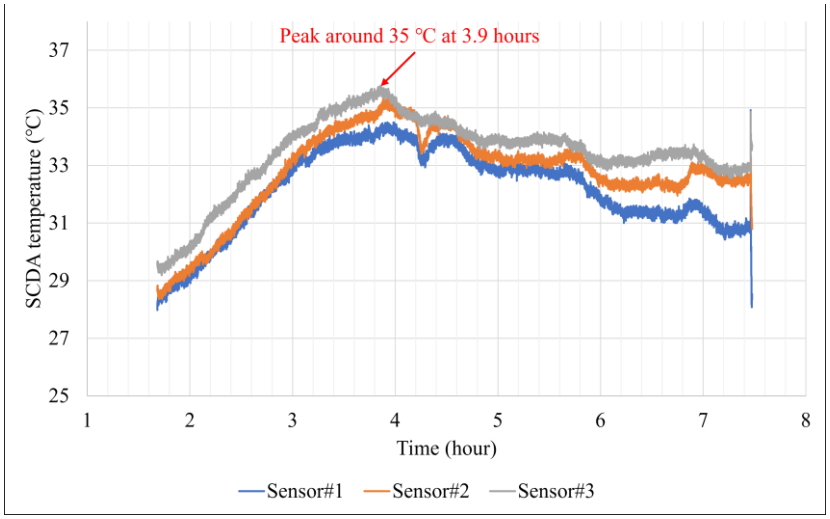

Figure 5.12: Thermocouple data of Test #2.

5.4.3 Discussion of results

Although the two panel tests with SCDA were identical, the second panel was demolished about 4.5 hours earlier than the first one. It can also be observed from Figure 5.8a and 5.10a that significant out-of-plane displacement appeared in Test #2 approximately 4.5 hours earlier than that that of Test #1. This striking difference can be explained by two possible reasons. First, there could be slight inconsistency during the mixing operation of SCDA cement, resulting in SCDA overheating and accelerating in Test #2, or the SCDA was not mixed adequately in Test #1 which caused the delay of demolition. Secondly, there could be some discrepancies between the two

material properties of the Stanstead granite panels. For instance, the first panel experienced much larger out-of-plane displacements and more frequent confining pressure loss during the test than in Test #2, indicating its higher ductility and higher tensile strength than that of the second panel.

5.5 Numerical modelling

5.5.1 Modelling approach

To further explain the experimental results and panel failure mechanism, the finite-difference modelling software FLAC3D 7.0 of Itasca Ltd is employed to simulate the V-cut test. The finite-difference method can solve complex nonlinear rock behaviour by solving the partial differential equations in model domain, so that the stress distributions and material failure state based on yielding criterion can be obtained. However, as this is a continuum method, i.e., it requires domain continuity between neighbouring elements, it cannot explicitly reflect the separation due to cracking. In this study, although FLAC3D model should not be relied on to anticipate the peak SCDA pressure that leads to panel eventual failure, it can be utilized to demonstrate the deformation trend and yielding process of the panel with increasing SCDA pressure using elastic-plastic panel material. The main modelling objectives are to (i) obtain the SCDA pressure that causes panel crack initiation, (ii) demonstrate panel bulging deformation behaviour, and (iii) confirm the panel failure mechanism due to the V-cut pattern.

5.5.2 Model geometry and boundary conditions

The model geometry is identical to the tested granite panel, as shown in Figure 5.13. The minimum mesh size is 1 cm, and the model has a total of 258,164 grid points and 35,4552 zones.

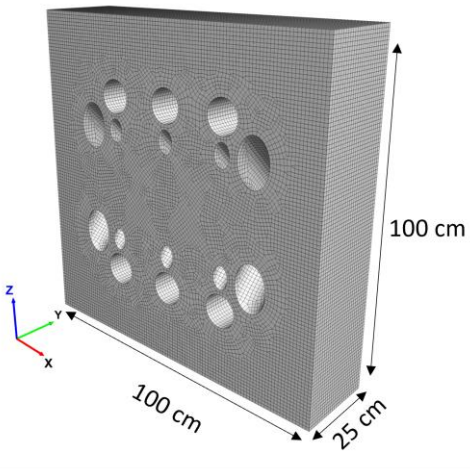

Figure 5.13: FLAC3D model geometry.

To simulate the biaxial loading conditions, 40 MPa and 26 MPa are applied to 20 cm of the panel thickness in the vertical and horizontal sides of the model, respectively. After the model reaches equilibrium in the biaxial loading phase, the 6 SCDA holes of the V-cut are filled with solid, elastic material, and a hydrostatic pressure representing the expansive SCDAS pressure, is applied as initial stress. This modelling technique proved to be superior to the traditional method of applying uniform boundary pressure along the SCDA hole perimeter (Habib et al., 2023). The applied SCDA pressure in the form of initial stress will force the elastic SCDA material to expand and pressurize the borehole wall. The initialized SCDA pressure is increased until the panel cracking is detected (objective #1). It is then further increased until the panel has completely yielded.

5.5.3 Material properties

Mohr-Coulomb model is employed for modelling the behaviour of the rock material. The granite model parameters are obtained from the testing program discussed in Section 5.2.2, and the input material parameters in FLAC3D are shown in Table 5.3. The SCDA material is modelled as a linear elastic to simulate the relation between hydrostatic pressure generated by SCDA hydration process and SCDA material deformation. The density and elastic modulus of SCDA in a confined

borehole are measured based on laboratory tests (Habib et al., 2023). Poisson's ratio of 0.15 is used for SCDA according to the model calibration with the test observation.

Table 5.3: Material parameters in FLAC3D.

Material	Model	Density (Kg/m^3)	Young's modulus (GPa)	Poisson's ratio	Friction (°)	Cohesion (Mpa)	Tension (Mpa)
Stanstead Granite	Mohr-Coulomb	2670	45	0.13	57.0	24.6	7.2
SCDA	Linear elastic	2000	8	0.15	N/A	N/A	N/A

5.5.4 Modelling results

The simulated granite panel V-cut results are presented in Fig. 5.14. The orange and pink colors represent tensile and shear failure respectively based on Mohr-Coulomb criterion. Fig. 5.14a shows the panel yielding results after biaxial loading. It shows that the panel is not damaged under the high biaxial confinement. Next, SCDA material is simulated and 10 MPa pressure is initialized. As can be seen from Fig. 5.14b, rings of shear and tensile failure appear at the periphery of all six SCDA holes. It can be discerned that the SCDA pressure required to initiate panel cracking is 10 MPa. This initial yielding patten is in line with the fracturing first occurred in the laboratory tests (Figs. 5.7b and 5.9b). When SCDA pressure is increased to 30 MPa, the tensile yielding ring zones further expand around the SCDA holes, as shown in Fig. 5.14c. This is consistent with the spalling failure that occurred during the experiments (Figs. 5.7c and 5.9c). When SCDA pressure reaches 50 MPa, yielding extends to the relief holes. Such result corresponds to the last phase in two tests (Figs. 5.7e and 5.9e), leading to final panel failure.

Panel bulging deformation due to V-cut is also examined with FLAC3D model. Figure 5.15 shows the out-of-plane displacement (in model Y-direction) when the SCDA pressure is 50 MPa in plan and sectional views. As shown in Fig. 5.15a, the panel undergoes out-of-plane deformation in the center where SCDA pressure is initialized. However, the panel has greater displacement at two side columns of SCDA holes than the one in the center. The maximum displacement on the side is approximately 1.5 times that of the center. This could be attributed to the benefits of the stress-shield holes arranged near the side SCDA holes, which promotes the panel displacement by shielding high biaxial confining stress from the boundary. Fig. 5.15b demonstrates the out-of-plane displacement in a section view. The rock casting behaviour on the face side due to V-cut hole pattern can be clearly observed. Furthermore, the bulging displacement of the panel back is 3×10^{-5}, which is one-quarter of the deformation of the front face. This difference is almost consistent with the test monitoring results in Fig. 5.10a, although the panel displacement magnitude cannot be directly corelated to the test results due to the limitation of the continuum modelling method.

In summary, FLAC3D modelling has helped validate the behaviour of the V-cut experiments in terms of observed panel out-of-plane deformation and tensile failure progressive failure mechanisms. The proposed modeling method can be used to further optimize the SCDA pattern or estimate V-cut field performance in mine-wide models.

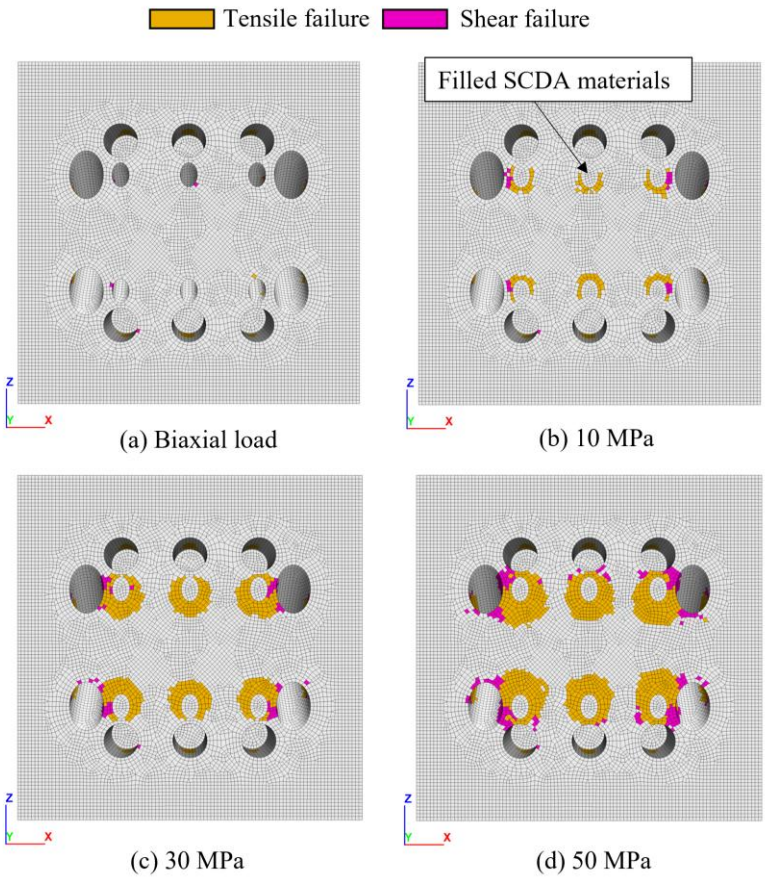

Figure 5.14: Granite panel V-cut modelling results.

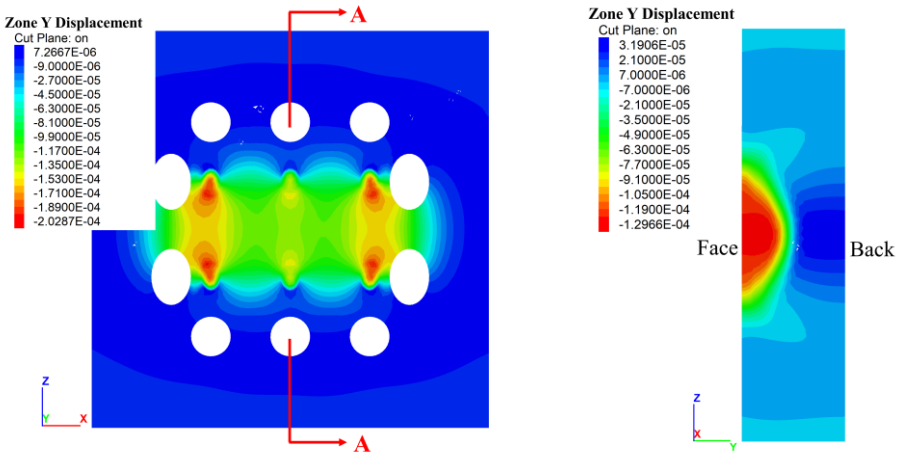

(a) Plan view (b) Sectional view A-A

Figure 5.15: Panel displacement results with 50 MPa SCDA pressure (unit: meter).

5.6 Conclusion

This work aims to investigate the application of SCDA for explosive-free rock breakage under high biaxial confinement using V-cut drillhole design. Large-scale test setup for V-cut tests is introduced, including drillhole pattern design and biaxial loading system. High biaxial confinement of 40 MPa and 26 MPa is applied in the vertical and lateral directions, respectively, corresponding to a virgin stress condition of 1000 m below surface in the Canadian shield. Two Stanstead granite panels were tested under biaxial confinement, monitored, and successfully demolished after 11 hours 53 minutes and 7 hours 29 minutes using SCDA with the proposed V-cut drilling patten. Panel instrumentation included the monitoring of SCDA temperature, vertical and out-of-plane displacements, confinement pressure, and AE energy and hit count, and a time-lapse camera was used to capture visual crack development to collapse. The results confirm the success of the proposed V-cut design for the demolition of a rock face under biaxial stress condition.

A finite-difference model was developed with FLAC3D to validate the observed panel fracturing process and failure mechanisms. The modelling results are found to be comparable to experimental observations. This research demonstrates the feasibility of SCDA method for hard rock breakage using V-cut drillhole pattern. Future work will explore field implementation of this method.

References

Alvarez De La Garma, J. (2021). Numerical simulation of rock fracturing due to borehole expansive pressure under biaxial loading condition. Master of Science Thesis. McGill University. Montreal. Canada.

Arjang, B., & Herget, G. (1997). In situ ground stresses in the Canadian hardrock mines: an update. International Journal of Rock Mechanics and Mining Sciences, 34(3-4), 15-e1.

Cho, H., Nam, Y., Kim, K., Lee, J., & Sohn, D. (2018). Numerical simulations of crack path control using soundless chemical demolition agents and estimation of required pressure for plain concrete demolition. Materials and Structures, 51(6), 1-13.

Chen, T., Vennes, I., & Mitri, H. S. (2022). Investigation into Rock Breakage with Expansive Cement Under Biaxial Confinement. Rock Mechanics and Rock Engineering, 55(10), 6263-6277.

Cheng, B., Wang, H., Zong, Q., Xu, Y., Wang, M., & Zheng, Q. (2021). Study of the double wedge cut technique in medium-depth hole blasting of rock roadways. Arabian Journal for Science and Engineering, 46(5), 4895-4909.

Darling, P. (Ed.). (2011). SME mining engineering handbook (Vol. 1). SME.

De Silva, R. V., Pathegama Gamage, R., & Anne Perera, M. S. (2016). An alternative to conventional rock fragmentation methods using SCDA: a review. Energies, 9(11), 958.

De Silva, Vms. R. S., Ranjith, P. G., Perera, M. S. A., Wu, B., & Wanniarachchi, W. A. M. (2018). A low energy rock fragmentation technique for in-situ leaching. Journal of Cleaner Production, 204, 586-606.

De Silva, V. R. S., Ranjith, P. G., Perera, M. S. A., & Wu, B. (2019). The effect of saturation conditions on fracture performance of different soundless cracking demolition agents (SCDAs) in geological reservoir rock formations. Journal of Natural Gas Science and Engineering, 62, 157-170.

Habib, K. M., Shnorhokian, S., & Mitri, H. (2022a). Evaluating the Application of Rock Breakage without Explosives in Underground Construction—A Critical Review of Chemical Demolition Agents. Minerals, 12(2), 220.

Habib, K. M., Vennes, I., & Mitri, H. (2022b). Laboratory investigation into the use of soundless chemical demolitions agents for the breakage of hard rock. International Journal of Coal Science & Technology, 9(1), 1-10.

Habib, K. M., Vennes, I., & Mitri, H. S. (2023). Methodology for the estimation of expansive cement borehole pressure. International Journal of Mining Science and Technology. Volume 33, Issue 1, January 2023, Pages 73-81.

Hinze, J., & Brown, J. (1994). Properties of soundless chemical demolition agents. Journal of construction engineering and management, 120(4), 816-827.

Jimeno, C. L., Jimeno, E. L., and Javier, A. C. (2006). Drilling and blasting of rocks. London: Taylor & Francis.

Kim, K., Cho, H., Sohn, D., & Lee, J. (2021). The use of expansive chemical agents for concrete demolition: Example of practical design and application. Construction and Building Materials, *272*, 121849.

Li, R., Yan, Y., Jiang, Z., Zheng, W., & Li, G. (2021). Impact of hole parameters and surrounding constraint on the expansive pressure distribution and development in soundless chemical demolition agents. Construction and Building Materials, 307, 124992.

Ma, J., Du, F., & Zhang, S. (2020). Acoustic Emission Characteristics of Normal and Layered Concrete Blocks during Dilating/Static Fracture. Advances in Materials Science and Engineering, 2020.

Maneenoi, N., Bissen, R., & Chawchai, S. (2022). Influence of admixtures on the performance of soundless chemical demolition agents and implications for their utilization. Journal of Sustainable Mining, 21(2), 93-111.

Musunuri, A., & Mitri, H. (2009). Laboratory investigation into rock fracturing with expansive cement. International Journal of Mining and Mineral Engineering, 1(4), 327-345.

Natanzi, A. S., Laefer, D. F., Kakali, G., & Iman Zolanvari, S. M. (2019). Temperature-Induced Chemical Changes in Soundless Chemical Demolition Agents. Journal of Materials in Civil Engineering, 31(7), 04019098.

Nateghi, R. (2012). Evaluation of blast induced ground vibration for minimizing negative effects on surrounding structures. Soil Dynamics and Earthquake Engineering, 43, 133-138.

Nobel, D. (2010). Blasting and explosives quick reference guide. Dyno Nobel Asia Pacific Pty Limited, Kalgoorlie.

Ozcelik, M. (2018). Back analysis of ground vibrations which cause cracks in buildings in residential areas Karakuyu (Dinar, Afyonkarahisar, Turkey). Natural hazards, 92(1), 497-509.

Shang, J., Hencher, S. R., West, L. J., & Handley, K. (2017). Forensic excavation of rock masses: a technique to investigate discontinuity persistence. Rock Mechanics and Rock Engineering, 50(11), 2911-2928.

Tang, W., Zhai, C., Xu, J., Sun, Y., Cong, Y., & Zheng, Y. (2021). The influence of borehole arrangement of soundless cracking demolition agents (SCDAs) on weakening the hard rock. International Journal of Mining Science and Technology, 31(2), 197-207.

Wang, Z., Gu, X., Zhang, W., Xie, Q., Xu, X., & Wang, Q. (2019). Analysis of the cavity formation mechanism of wedge cut blasting in hard rock. Shock and Vibration, 2019.

Xu, S., Hou, P., Li, R., & Cai, M. (2021). An experimental study on the mechanical properties and expansion characteristics of a novel self-swelling cartridge for rock breakage. Rock Mechanics and Rock Engineering, 54(2), 819-832.

Yang, D., Wang, X., Wang, Y., An, H., & Lei, Z. (2020). Experiment and analysis of wedge cutting angle on cutting effect. Advances in Civil Engineering, 2020.

Yu, Y. Q., & Mitri, H. S. (2012). Physical scale modelling of roadway advance with wedge cut blasting for South Wing Rail at Tunliu Mine.

Bridging text between Chapter 5 and Chapter 6

The previous chapters investigate the feasibility and performance of using SCDA for hard rock breakage in underground mining environment through large-scale indoor experiments. In the laboratory tests, the SCDA slurry is poured into the drill holes while the panel was laid flat on the floor. To date, there is no established method for SCDA slurry charging in non down holes. The present SCDA applications typically work by pouring the slurry into borehole by gravity. Therefore, to implement SCDA method in underground mines, the problem of charging SCDA slurry into horizontal, uptilted, or wet drill holes must be solved. There could also be applications whereby the drill hole is open at both ends, i.e., not a blind hole. In the following chapter, a novel cartridge loading method of SCDA is developed to address the abovementioned conditions. Various cartridge prototypes are designed and fabricated from low-cost plastics using 3D printers. The performance of each cartridge material is investigated in unconfined rock slab tests to determine the best host material for SCDA. The results show that the optimum SCDA cartridge not only suits various application requirements, but also significantly improves the rock fracturing efficiency with SCDA. A field test is also carried out to demonstrate the advantage of the novel cartridge method for potentially expanded SCDA applications in underground mines.

The following chapter is a paper that describes in detail the abovementioned research. The paper was submitted to CIM journal and is currently under review.

Chapter 6: Development of a novel cartridge for expansive cement application to hard rock breakage

Author:

Tuo Chen*, Kelly-Meriam Habib, Yizhuo Li, Hani S. Mitri

Affiliation:

Department of Mining and Materials Engineering, McGill University, Montreal, Canada H3A 0E8

Address: 3450 University Street, Montreal, Quebec, Canada H3A 0E8

*Corresponding author. E-mail address: tuo.chen@mail.mcgill.ca (T. Chen)

Abstract

Expansive cement (EC), aka soundless chemical demolition agents, is generally of liquid nature and poured into vertical holes for surface rock breakage applications. In this paper, a novel cartridge is developed for expanding EC applications in horizontal, uptilted, or wet boreholes. Various cartridge prototypes are made with low-cost and available plastics using 3D printers. The performances of the cartridges are investigated in unconfined rock slab tests, and polylactic acid (PLA) cartridge is found to be superior to others. Through partial heat containment, the PLA cartridge can expedite the EC hydraulic reaction and advance the onset of rock destruction by 30%. Finally, an extended rock breakage application of EC is achieved in an underground mine using PLA cartridges. The novel cartridge for EC can not only suit various application requirements beyond the scope of present EC surface applications with vertical holes, but significantly improve the rock fracturing efficiency with EC.

Keywords: Expansive cement; field applications; Soundless chemical demolition agents; Non-explosive rock breakage; Laboratory tests;

6.1 Introduction

Expansive cement (EC), aka soundless chemical demolition agents, refers to chemically based powdery compound that is a potential alternative to rock fracturing without explosives. It was first marketed in the early 1970s, but it did not draw widespread attention until 40 years later, when the patent has expired, and more EC manufactures are available on the market (Huynh & Laefer, 2009). Over the last decade, EC has been applied for surface engineering projects as dimension rock quarrying and explosive-free concrete demolition (Cho et al., 2018; Kim et al., 2021; Jiang et al., 2021). ECs are mostly powdery materials consisting of Portland cement and expansive additives

(see Fig. 6.1a) and turn into liquid nature after mixing with water. After EC slurry is poured into a confined borehole, it expands and creates a fracture network in surrounding material, as shown in Fig. 6.1b. The EC expansive pressure stems primarily from the hydraulic reaction of CaO, which generates Portlandite ($Ca(OH_2)$) during mixture curing. This crystallization process leads to progressive increase in radial pressure in a confined borehole in rock or concrete, as illustrated in Fig. 6.2 (Manatunga et al., 2021). The environmentally friendly EC method offers certain advantages over blasting for rock fracturing applications, such as no toxic fume generation, elimination of noise and vibration, as well as the reduction of ventilation requirements in underground spaces (Habib et al., 2022). Due to increasing environmental and political restrictions on the use of explosives, it is important to develop EC as an alternative to the conventional explosive method for rock fracturing projects in both civil and mining fields.

(a) EC powder before mixing (b) Concrete demolition with EC

Figure 6.1: Concrete demolition using EC (Kim et al., 2021).

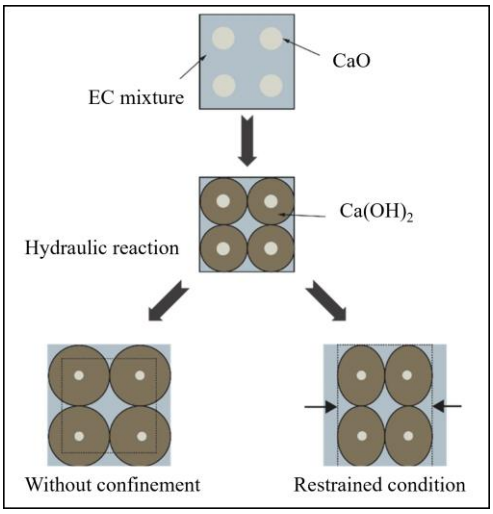

Figure 6.2: Expansion model of EC (modified from (Manatunga et al., 2021)).

The physical properties and mechanical behaviour of EC have been studied in laboratory conditions. Its expansive pressure is commonly quantified using thick-walled cylinder method, where the EC slurry is poured into a thick-walled metal cylinder with strain gauges installed on cylinder outer surface. The EC pressure is calculated analytically based on measured tangential strain on the outer cylinder surface (Hinze & Brown, 1994, Laefer et al., 2018; Li et al., 2021). Habib et al. (2023) developed a direct measurement method for EC pressure using a high-capacity pressure sensor, and a correction factor between measured EC pressure and estimated pressure using thick-walled cylinder method. De. Silva et al. (2019) investigated the impact of saturation condition on EC fracturing performance in reservoir rock formations. They found that performance of EC is maximized with less pore-water and saline conditions. Yutong et al. (2023) examined the usage of a self-propagating heating tube to heat up and speed up the reaction of EC. It was found the heating could accelerate EC hydration process, leading to a sudden rise of the expansive pressure. Calvo et al. (2022) analyzed the microstructural mechanisms involved in the expansion

process of EC. It was shown that the air pores due to air-entraining admixture increase the expansive rate of EC.

Currently, the engineering application of EC is mainly for rock quarrying and the removal of concrete foundations. Some attempts have been found in literature to expand the scope of EC applications. Akgün & Daemen (2000) examined the method of EC grout for borehole plugs using welded tuff cylinders. The test results indicated that the plug strength measures decrease with increasing plug radius. Natanzi & Laefer (2014) adopted EC for rock demolition close to historic buildings to prevent blasting vibrations from adjacent structures. EC methods were used by Shang et al. (2017) to investigate discontinuity persistence. The pre-existing persistent region and rock bridge area can be directly measured on the split surface, allowing the discontinuity persistence to be assessed. Through laboratory experiments and discrete-element modelling, De Silva et al. (2018) investigated the potential use of EC for in-situ leaching. EC might create a controlled fracture network in impermeable rocks to boost in-situ leaching efficiency. Chen et al. (2022) studied rock breakage with EC under biaxial confinement. High-strength concrete panels were successfully fractured under using an optimized drill hole pattern. This suggests that EC could be implemented in underground hard rock excavations, such as tunnels or underground mine openings.

Although the abovementioned studies indicate that the EC could have a broader scope of applications, there is still a lack of established approaches for loading EC in non-vertical holes in the field. The present EC applications typically work by pouring the slurry downhole to fill the holes by gravity. To expand EC applications, slurry loading into horizontal, uptilt, or wet boreholes must be addressed. This is often the case in subsurface conditions such as tunnels and mines. Xu et al. (2021) proposed a self-swelling EC cartridge made of sponge, kraft paper, and thread rod to solve the EC loading problem; see in Fig. 6.3a. However, it was shown that a large cartridge

thickness will greatly impede the expansive performance of EC. Also, this method preloads modified EC powder into the cartridge (Fig. 6.3b) that is immersed in water for a certain period before it is loaded into the borehole. Therefore, this research seeks to develop a more practical and cost-effective cartridge method for hosting EC slurry, without modifying it, to expand EC applications when non-vertical loading is needed.

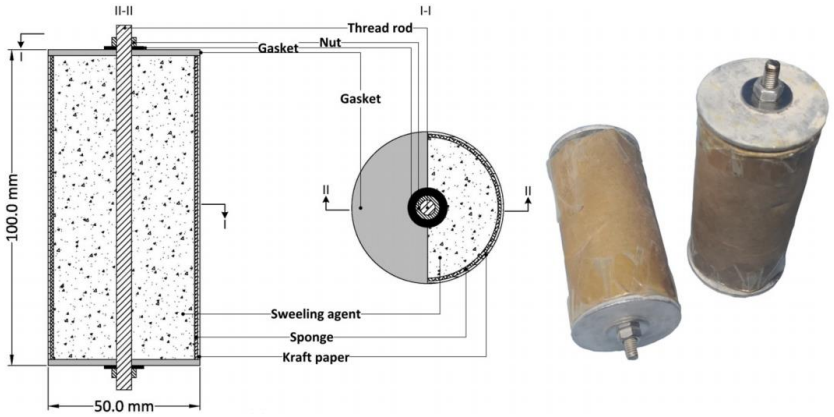

(a) Cartridge structure (b) Examples

Figure 6.3: Self-swelling EC cartridge (Xu et al., 2021).

6.2 Challenges of the study

There are several difficulties associated with loading conventional EC slurry into non-vertical holes. First, EC slurry cannot be pumped into boreholes as it may risk spilling out of the hole. EC exothermic reaction and expansion may also cause damage to the pump components if it is not washed clean almost immediately after each use. This is the reason that the cartridge method is preferred and tested for loading EC in this work.

The main challenge for developing cartridge method is to search for a proper host material for EC. The host material must not hinder the performance of EC in terms of reaction time and generated

expansive pressure. Besides, the host material should be cost effective and commercially available for field applications. Most importantly, the host material must have proper thermal conductivity to avoid the spout-out of EC. Spout-out phenomenon often occurs when cement mixture temperature exceeds a certain threshold so that high vapor pressure risen inside boreholes would cause explosive spalling of the concrete due to high temperature (Lu et al., 2022). Betonamit Type R EC (the EC product used in this study) manufactured by KUBATEC has an application temperature range between 5°C and 35°C. If the selected host material has a low thermal conductivity, the heat generated from the EC may not dissipate enough resulting in high temperature exceeding the application limit. This may lead to abrupt spout-out of EC from the hole, and hence no demolition effect is obtained due to material loss. For example, pilot tests of this study employed thin Kraft paper tubes as EC cartridge as shown in Figure 6.4a. Such low cost, commercially available material is sufficiently strong and impermeable to prevent leakage of slurry from the cartridge. However, it was observed that the 1.5 mm thick Kraft paper has poor thermal conductivity in rock slab demolition test (see Figure 6.4b), which caused EC mixture to overheat to 123.8 °C and abruptly blow out of a 50.8 mm (2 inches) diameter borehole.

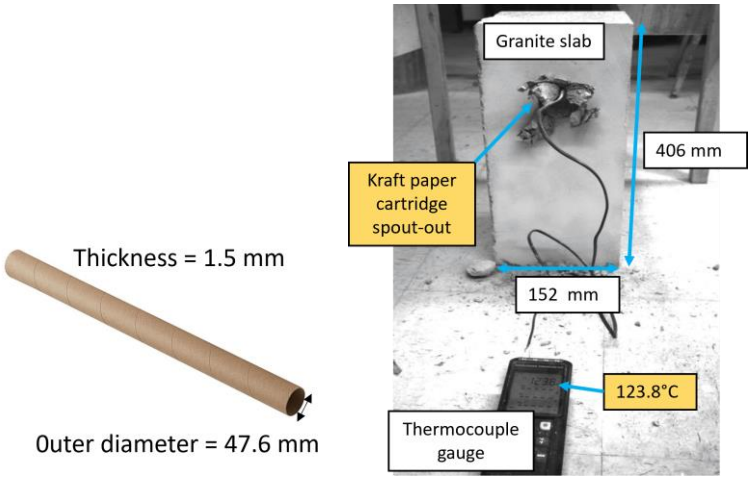

(a) Kraft paper cartidge (b) EC spout-out

Figure 6.4: Pilot test of EC cartridge made from Kraft paper.

To tackle the abovementioned issues and provide a feasible method for loading EC in horizontal and uptilt boreholes where gravity pouring is not possible, several types of cartridges are designed and manufactured using 3D printing technology in this study. To select the proper host material, the performance of different EC-filled cartridges is compared with that of EC loading by gravity in rock slab fragmentation tests. The EC temperature during the tests is monitored to reveal the heat conductivities of the host materials relating to spout-out risks. At the end, a field trial is conducted in an underground mine to validate the designed cartridge to load EC for subsurface application.

6.3 EC cartridge design

6.3.1 Fused Deposition Modeling (FDM)

Fused Deposition Modeling (FDM) is the most widely used 3D printing technology as it provides accurate and well-detailed products in an easy and budget-friendly manner. The way of building an object using FDM is by depositing melted material layer by layer. In this work, a high-quality desktop printer Ultimaker S3 is employed to fabricate EC cartridge prototypes, as shown in Figure 6.5. The Ultimaker S3 has dual extrusion, allowing printing single object with multiple materials at once. This printer consumes material in filaments made from plastic. It can produce large objects up to 230 mm × 190 mm × 200 mm. The deposition is carried out in a specific manner controlled by a slicing program called Ultimaker Cura.

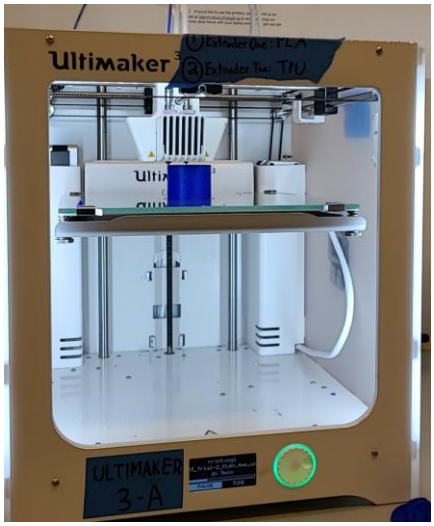

Figure 6.5: Ultimaker S3 3D printer.

6.3.2 Select cartridge materials

Four different plastic materials are selected for EC cartridge prototypes in this research. They are thermoplastic polyurethane (TPU), polylactic acid (PLA), polyethylene terephthalate glycol (PETG), and acrylonitrile butadiene styrene (ABS). They are selected based on their market availability and low cost, which makes the production of cartridges feasible for potential field applications. In this study, the cartridge material as host for the EC is subjected to EC expansive pressure during the test. Therefore, some key physical properties of the material such as tensile strength and elongation threshold are important; see Table 6.1 below. As can be seen, PLA has the highest tensile modulus of 2852 MPa and the lowest elongation at break of 2.8%, hence it is considered the most brittle. TPU has the lowest tensile modulus of 26 MPa and the highest elongation at break of 588%, hence it is considered the most ductile.

Table 6.1: Physical properties of the 3D printing materials.

Material type	TPU	PLA	PETG	ABS

Tensile modulus	26 Mpa	2852 Mpa	1939 Mpa	1962 Mpa
Tensile stress at yield	8.6 Mpa	38.1 Mpa	46.2 Mpa	38.2Mpa
Tensile stress at break	39 Mpa	36.3 Mpa	38.5 Mpa	35.7Mpa
Elongation at yield	55%	2.1%	5.9%	4.1%
Elongation at break	588%	2.8%	7.6%	4.6%
Shore Hardness	95	-	70	76

6.3.3 Cartridge preparation

In this study, EC cartridges are printed in Ultimaker S3 printer (shown in Fig. 6.5) using the abovementioned materials. Xu et al. (2021) showed that the insertion gap between borehole and cartridge outer surface has a great impact on EC performance after testing 1 mm to 6 mm insertion gaps. A larger insertion gap dramatically lowers the effective EC expansive pressure as the filling degree of EC borehole is lowered. One significant advantage using 3D printing technology is that precise cartridge diameter can be achieved for different sizes of boreholes to eliminate the insertion gap. More importantly, a minimal cartridge thickness can be achieved to further increase the EC filling degree using 3D printing. As the planned borehole size for the test is 44.45 mm (1.75″), cartridges are printed with a diameter of 44.35 mm (1.746″) and a length of 177.8 mm (7″), as shown in Figure 6. A minimal 0.2 mm cartridge wall thickness is achieved.

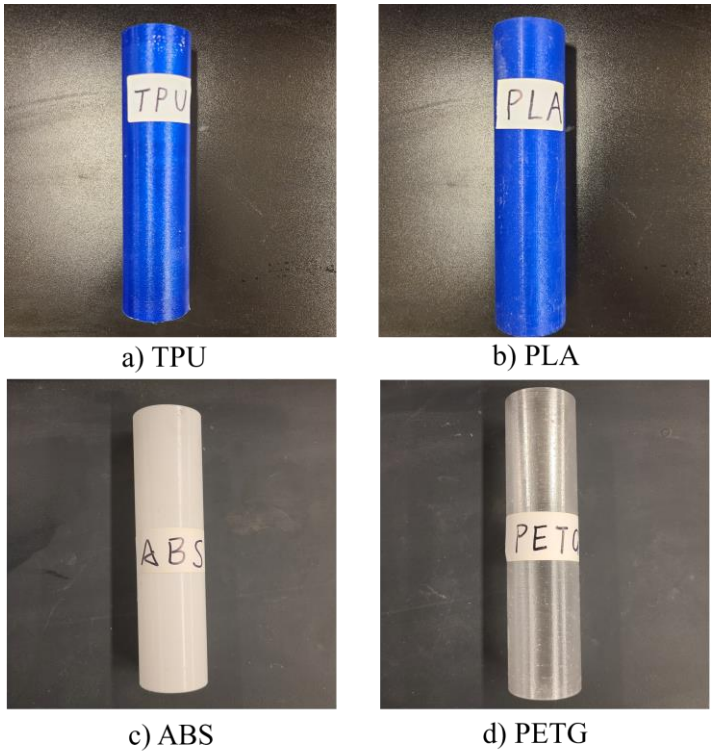

Figure 6.6: Photographs of printed EC cartridges.

6.4. Laboratory testing of EC cartridge performance

6.4.1 Test setup

To assess the performance of the selected cartridges, a single 44.45 mm (1.75″) hole is drilled in a 152.4 mm (6″) × 203.2 mm (8″) face of a Stanstead granite slab that is 152.4 mm (6″) × 203.2 mm (8″) × 406.6 mm (16″). The physical and mechanical properties of Stanstead granite are obtained from testing in CANMET lab in Ottawa, Canada. The test results are shown in Table 6.2 and Table 6.3. The uniaxial compressive strength (UCS) and triaxial tests used axial displacement control of 0.0009 mm/s and the Brazilian tests were carried out using axial load control of 0.10 kN/s. The average UCS is 117.7 MPa and average Brazilian tensile strength is 7.2 MPa.

Table 6.2: Physical and mechanical properties of Stanstead granite

Specimen ID	Specifications			Strength and elastic properties			
	Diameter (mm)	Length (mm)	Density (g/cm^3)	Peak strength (Mpa)	Confinement (Mpa)	Young's modulus (Gpa)	Poisson's ratio
STAC-SG-U1	44.80	101.00	2.67	117.4	0.0	45.0	0.17
STAC-SG-U2	44.80	101.00	2.67	120.2	0.0	45.9	0.11
STAC-SG-U3	44.80	100.90	2.67	115.4	0.0	45.0	0.13
STAC-SG-T1	44.80	100.90	2.67	169.3	5.0	50.4	0.21
STAC-SG-T2	44.90	100.90	2.67	218.2	10.0	54.7	0.19
STAC-SG-T3	44.90	100.90	2.67	268.1	15.0	58.3	0.25

Table 6.3: Brazilian test results for Stanstead granite

Specimen ID	Specifications			Strength	
	Diameter (mm)	Length (mm)	Density (g/cm^3)	Failure load (kN)	Brazilian tensile strength (Mpa)
STAC-SG-B1	44.83	26.93	2.67	14.69	7.75
STAC-SG-B2	44.85	26.96	2.67	15.25	8.02
STAC-SG-B3	44.85	22.32	2.67	10.53	6.70
STAC-SG-B4	44.81	22.31	2.67	11.45	7.29
STAC-SG-B5	44.86	22.32	2.67	9.52	6.05
STAC-SG-B6	44.85	22.33	2.67	11.87	7.55

Fig. 6.7 illustrates the indoor rock slab demolition test setup. The planned borehole size for the test is 44.45 mm (1.75″). The borehole depth was fixed at 4 times the diameter as it is the

minimum depth recommended by the manufacturer. The commercially available EC selected for this investigation is Betonamit Type R. The expansive cement is mixed with water consistently for 3 minutes using a water-to-cement ratio of 0.2, then the mixture is loaded into the borehole at room temperature (25°C). The water temperature is about 20°C. The expansive cement is poured directly into the 3DP cartridges. The open end of the cartridge is then sealed with Tuck sheathing tape to prevent leakage during the loading process. Cartridges are inserted into the borehole horizontally. During the test, temperature variation inside EC, time of first crack (TFC), and minimum demolition time (MDT) were monitored as follows.

1) Time-lapse camera to visually detect the TFC and DMT; photos are taken every 5 minutes.
2) Temperature logger to detect peak temperature of EC.

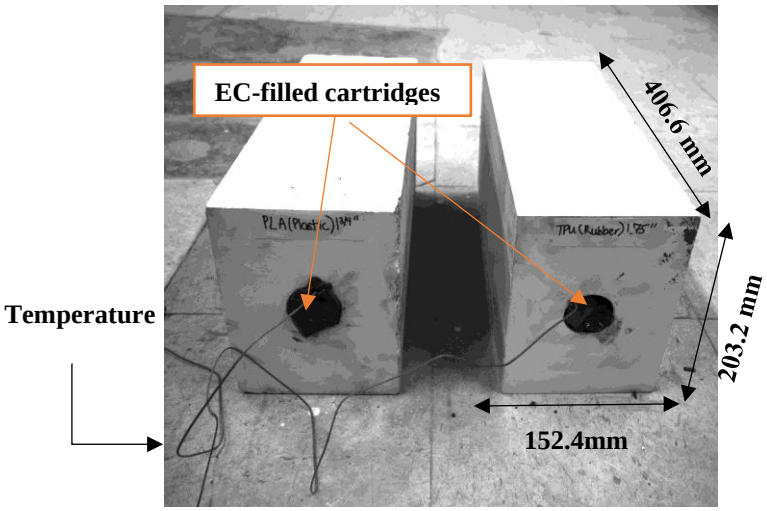

Figure 6.7: Indoor rock slab demolition test setup.

6.4.2 Experimental results

Figure 6.8 demonstrates the rock slab demolition results using EC poured into 44.45 mm diameter borehole by gravity. The slab was painted white so that fractures can be easily identified. The

expansive cement mixture was poured directly into the drill hole vertically. The rock slab was laid down one hour after the cement hardened, allowing the high-resolution camera to capture the crack development around the borehole, as shown in Figure 6.8a. Fig. 6.8b shows the specimen after 6.2 hours loading EC, the first crack appeared around the borehole horizontally. About 5 hours later, the fractured parts of the slab separately completely, as shown in Fig. 6.8c. Therefore, the TFC and DMT of the rock slab was 6.2 hours and 11 hours, respectively.

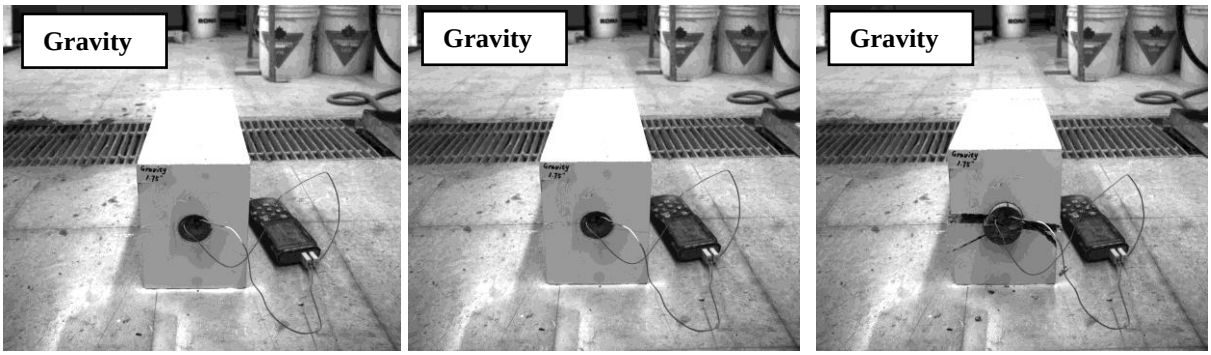

(a) t = 1 hour (b) t = 6.2 hours (c) t = 11 hours

Figure 6.8: Rock slab demolition using EC poured by gravity.

The rock slab fracturing results using EC-filled PLA and TPU cartridges are shown in Figure 6.9. As shown in Fig. 6.9a, the two slabs were loaded by the PLA and TPU cartridges, respectively. As demonstrated in Fig. 6.9b, after 5.5 hours mixing EC, both EC-filled cartridges reacted and slighted bulged out from the borehole. The slab with PLA cartridge cracked first horizontally at 5.5 hours. Then, the fractures developed in both horizontal and vertical directions. As the fractures gradually coalesced in the back, the fractured parts of the slab completely detached at 8.5 hours, as observed in Fig. 6.9c. Thus, the TFC and MDT of the rock slab with the PLA cartridge is 5.5 hours and 8.5 hours, respectively. Once the confinement around PLA cartridge was released after rock demolition, the EC lost its expansive pressure and became powdery gradually. Meanwhile, the

rock slab with TPU cartridge remained intact. There was no visible cracking around the borehole after 24 hours when the test stopped.

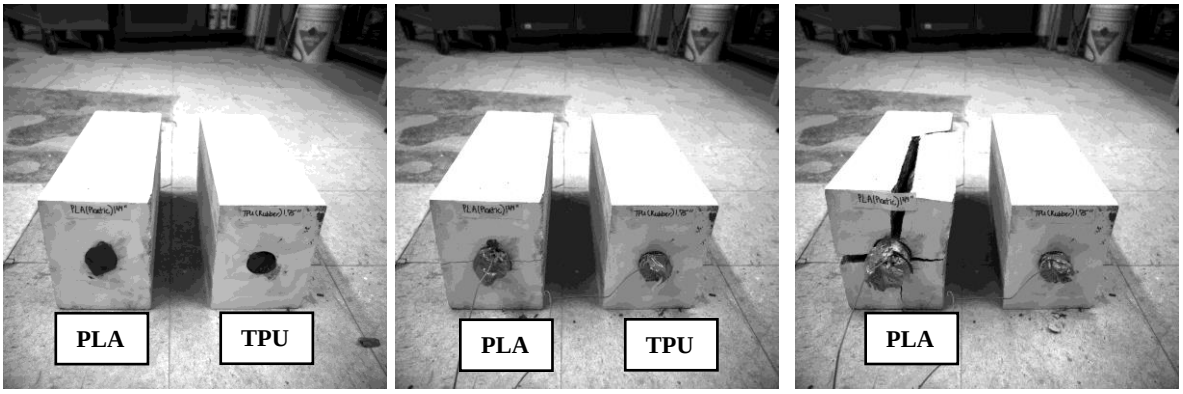

(a) t = 0 (b) t = 5.5 hours (c) t = 8.5 hours

Figure 6.9: EC-filled cartridge test results (PLA vs. TPU).

Figure 6.10 presents slab fracturing results and cartridge conditions after the test. It can be seen from Figure 6.10a that the aperture of the largest vertical crack was up to 6 cm with EC-filled PLA cartridge. Also, "Y" shape fractures were developed on the top of the same slab leading to the fully demolition of the slab, as shown in Figure 6.10b. The fracturing length along the long axis of the panel is up to about 25.5 cm (10″), while the inserted PLA cartridge was only 17.78 cm (7″). The PLA cartridge condition after the test is shown in Figure 6.10c. It is observed that the PLA cartridge was fragmented into small pieces due to EC expansion, while the cartridge made of rubber-like TPU material was still complete in Figure 6.10d. This could be caused by the significant brittleness difference of two materials, as discussed in Section 2.2. Meanwhile, these results could explain the reason why the PLA cartridge performed much better than the TPU one. Once EC expanded when hardening, the PLA cartridge with low elongation at break of 2.8% would crack shortly, and hereby the EC product can be in direct contact with rock medium without affecting the EC performance.

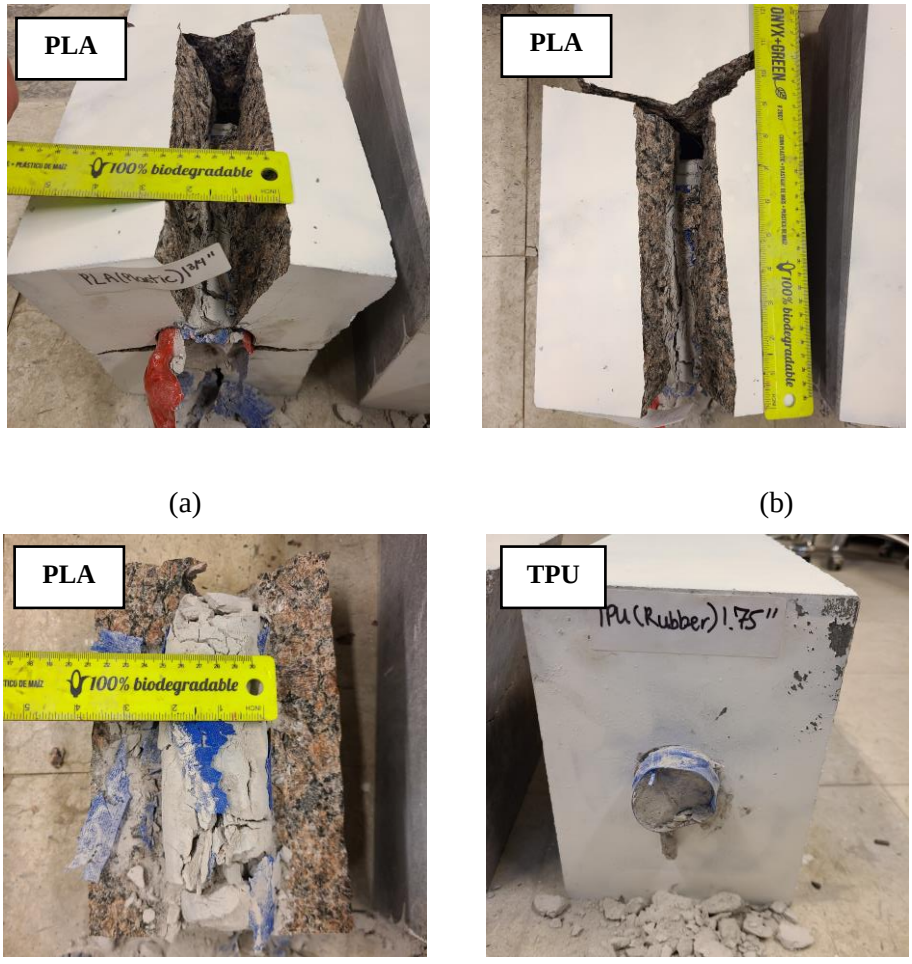

Figure 6.10: Rock slab and cartridge conditions after the test (PLA vs. TPU).

Figure 6.11 presents the timelapse photos of rock demolition test with PETG and ABS cartridges. Fig. 6.11a shows the first sub-vertical crack appearing on the left PETG cartridge slab 8 hours after loading EC. At 10 hours, the ABS cartridge slab experienced the first vertical crack, while vertical and horizontal cracks had been developed in the left slab, as shown in Fig. 6.11b. Two slabs with PETG and ABS cartridges were demolished at 12.5 hours and 16 hours, respectively, as shown in Figs. 6.11c and 6.11d.

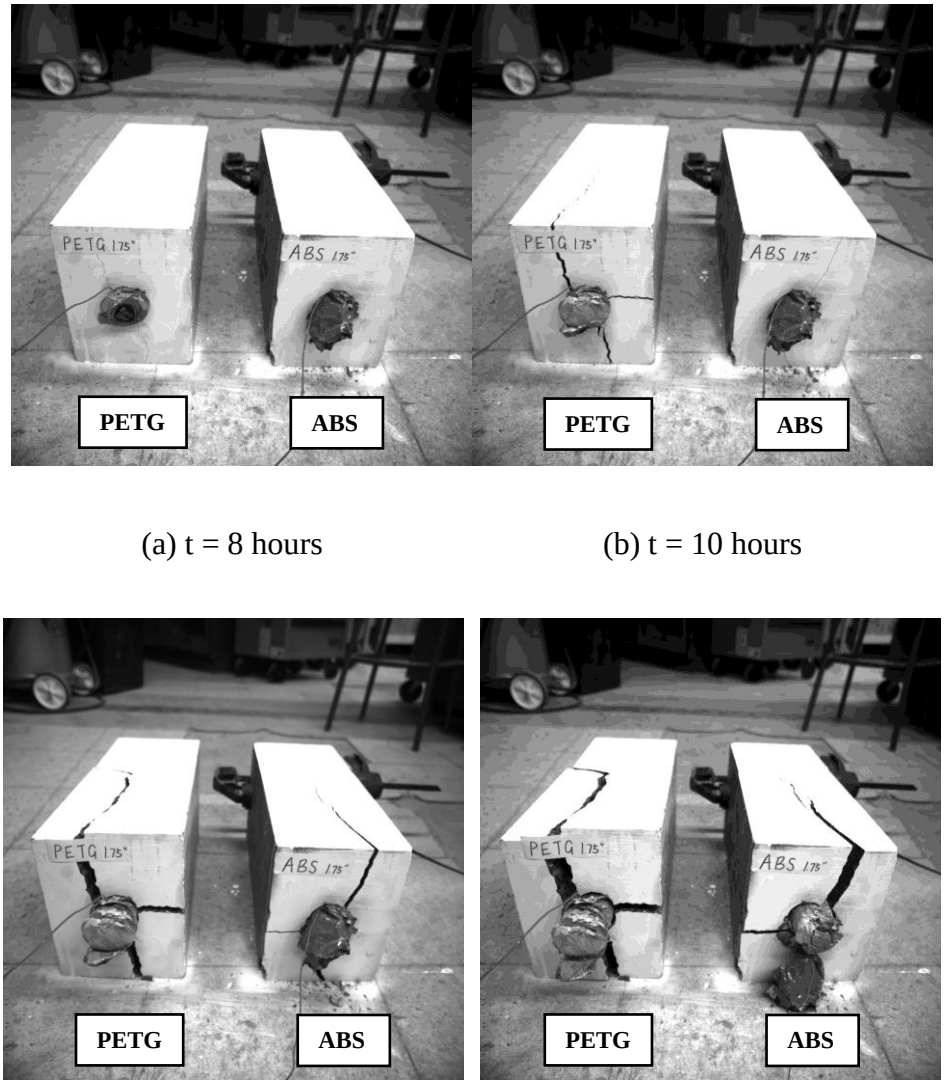

(a) t = 8 hours (b) t = 10 hours

(c) t = 12.5 hours (d) t = 16 hours

Figure 6.11: EC-filled cartridge test results (PETG vs. ABS).

6.4.3 Thermal data analysis

Thermal sensors were employed to monitor the temperature variation during each test. The sensors were inserted into EC mixture directly after pouring EC or after inserting EC-filled cartridges in the borehole. The temperature records are plotted in Fig. 6.12. The EC temperature record in PLA cartridge was cut off at about 6 hours, which could result from sensor detachment after EC bulging

out of the borehole. Of the five curves, the highest temperature peak of 50 ℃ is observed for the TPU cartridge. This indicates the TPU material has the lowest thermal conductivity as most of the heat generated by EC hydro reaction was sealed inside the cartridge. Such heat accumulation would accelerate the EC reaction, so the onset of peak temperature occurs first in TPU curve. However, the peak temperature exceeds the product application temperature limit of 35 ℃, which poses the risk of spouting-out. The curve of PLA cartridge has the second highest peak of 34 ℃, which is higher and shows up earlier than the peak temperature of gravity loading condition (29.4 ℃). This is in line with the test results that TFC and MDT of the slab with PLA cartridge are earlier than those for the slab with gravity loading. Therefore, the PLA cartridge not only partially sealed the heat to speed up the EC reaction, but also the peak temperature did not reach the upper limit of the application requirement, indicating no spout-out risk. For PETG and ABS cartridge, they have similar temperature variation trends. The peak temperature values of about 28 ℃ are lower than the gravity loading condition, revealing that these two materials may hinder the EC performance. This result is also consistent with the time difference of slab fracturing.

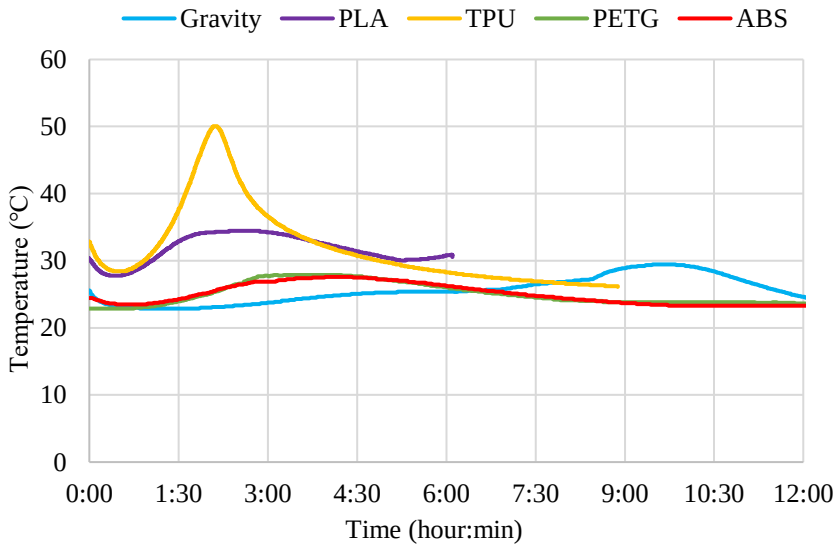

Figure 6.12: Temperature records of EC during tests.

6.4.4 EC cartridge performance discussion

The results from the slab demolition tests are summarized in Table 6.4. The results show that the TFC and MDT of the slabs using PLA cartridge are the shortest. There appears to be a positive correlation between the slab fracturing time and the 3DP material stiffness. The most ductile TPU material is the only one that did not induce any visual cracks on the rock slab. This is attributed to its elongation capacity of 588% at break. On the other hand, the PLA cartridge with the lowest elongation at break of 2.8% fragments once the EC expands, thus, it does not hinder the EC performance. A higher and earlier onset of peak temperature is observed in the EC hosted by PLA cartridge than the one loaded by gravity. This means the usage of PLA cartridge can speed up the EC reaction by partially blocking heat dissipation from the EC into the host rock. It is noteworthy that the peak temperature did not reach the threshold of the application requirement, suggesting little or no risk of spout-out using PLA cartridges. These results reveal that the use of PLA cartridge can boost the efficiency of EC. It significantly shortens the rock breakage time by 30% from 11 hours MDT by gravity loading to 7.6 hours MDT.

Table 6.4: Summary of cartridge test results.

Loading method	Cartridge Material	EC Product	Borehole Size	Seal	Peak Temperature (°C)	TFC	MDT
Gravity	N/A	Betonamit Type R	1.75″	N/A	29.4 °C	6.2	11
Horizontal loading	PLA	Betonamit Type R	1.75″	Sheathing tape	34 °C	5.5	7.6

Horizontal loading	TPU	Betonamit Type R	1.75″	Sheathing tape	50°C	NA	NA
Horizontal loading	ABS	Betonamit Type R	1.75″	Sheathing tape	27.5°C	10	16
Horizontal loading	PETG	Betonamit Type R	1.75″	Sheathing tape	27.9°C	8	12.5

6.5 Field trial

With the help of the novel EC cartridge, EC applications could be expanded to underground mining projects, such as rock corner slashing and excavation of an underground face, where EC is required to be loaded horizontally into boreholes drilled in rock wall. Based on the indoor slab demolition results, the most advantageous PLA cartridge is selected to be the host for EC horizontal loading method. The first field trial of PLA cartridge was conducted at Éléonore mine in northern Quebec, Canada. The test was carried out at a drift intersection at a depth of 530 M below surface. The rock type of the test area is Wacke and its intact rock properties are shown in Table 6.5. Noticeably, its tensile strength is almost twice that of the Stanstead granite in the rock slab. Besides, the ambient temperature in the test area is 10 °C, and the rock surface temperature is 13.5 °C. A previous study by Dowding and Labuz (1982) showed the EC expansive pressure dropped by 38% after 24 h and by 10% after 48 h when ambient temperature decreased from 25°C to 15°C in thick-walled steel cylinder tests. Thus, delayed EC reaction and rock fracturing onset are expected compared to the laboratory conditions.

Table 6.5: Intact host rock property of Wacke rock.

Rock type	Density (g/cm^3)	UCS (MPa)	$Is_{(50)}$ (MPa)	Tensile Strength (MPa)	Young's Modulus (GPa)	Poisson's Ratio

Wacke	2.75	162	6.7	15	39.05	0.14

The test area was painted white over a surface around 1 m × 1.5 m, as shown in Figure 6.13a. Three, 50.8 mm (2”) boreholes were drilled horizontally with lengths of 1 m and vertical spacing of 25 cm – 30 cm. The PLA cartridges were printed with a diameter of 50.3 mm (1.98″). Betonamit Type R was used for the test and the mixing procedure is the same as the indoor slab test. After mixing, EC slurry is poured into PLA cartridge and sealed with sheathing tape before inserting into the borehole, as shown in Figure 6.13b.

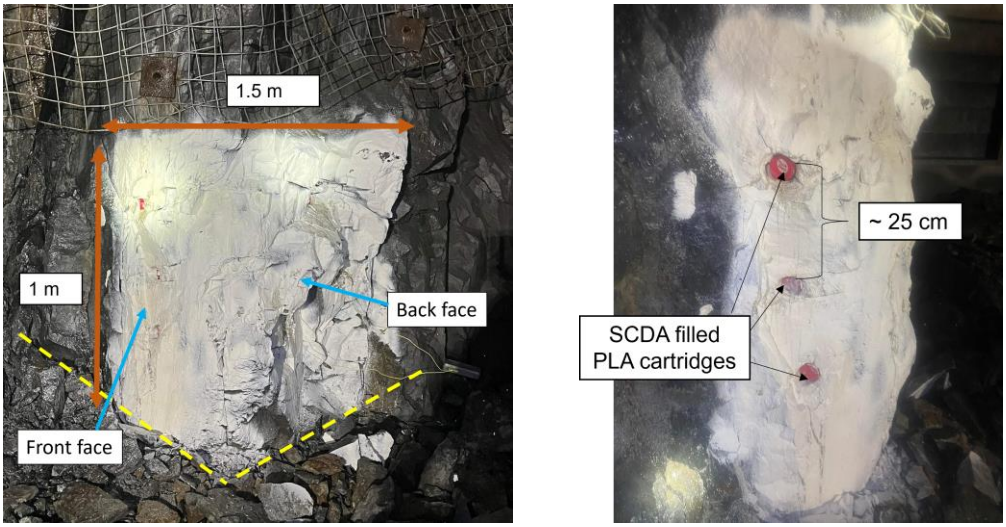

(a) Rock corner test area (b) Borehole loading with cartridges

Figure 6.13: Field trial setup for EC cartridges.

The whole testing process was recorded by a timelapse camera. From the recording, a visual TFC of 17 hours and MDT of 22 hours were identified. Significant fractures coalescing between EC holes up to 80 cm long are shown in Figure 6.14. Although cracking was observed, the fractured block did not detach by itself. It was easily scaled by 25 ~ 30 cm deep into the face after 22 hours

using a scale bar. The TFC and MDT were slower than that in the rock slab demolition test. This is not unexpected as it may be due to the complex underground stress environment, colder temperature, and higher rock strength. Overall, the trial using the developed horizontal loading method is deemed successful.

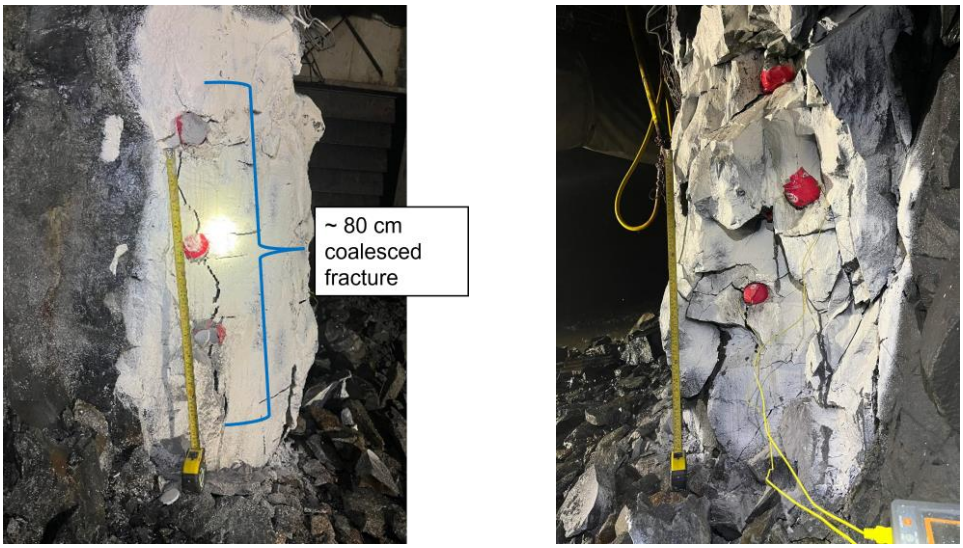

(a) Front face (b) Back face

Figure 6.14: Rock corner slashing results with EC cartridges.

6.6 Conclusion

Field applications of EC can be limited when the EC slurry can only be loaded by gravity in down holes. This research has developed a novel EC cartridge that can greatly reduce the application requirement of EC slurry to expand its applications, as well as enhance the efficiency of rock fracturing due to EC. Four cartridge materials, namely PLA, TPU, ABS and PETG, are tested in laboratory for rock slab demolition with a single EC hole. The PLA host material was found to be superior and implemented in a field trial at an underground mine. The main findings of the study are summarized as follows.

(1) The slab demolition tests show that PLA cartridge improves EC's efficiency for rock breakage. PLA cartridge can reduce the needed rock breakage time by 30% from 11 hours MDT (without cartridge) to 7.6 hours MDT.

(2) A positive correlation is found between the slab fracturing time and the material stiffness. The most ductile TPU cartridge does not crack the rock slab, while the PLA cartridge with the highest stiffness gives the best fragmentation performance.

(3) A higher and earlier onset of the peak temperature is observed in the EC hosted by PLA cartridge compared to the one without cartridge. This implies that PLA cartridge speeds up the EC reaction by partially reducing heat dissipation into host rock medium.

(4) A field test was undertaken in an underground mine to demonstrate the advantage of the novel cartridge method for potentially expanded EC applications. An underground rock intersection was successfully demolished using three 1 m long EC cartridges inserted in horizontal boreholes open at two ends.

References

Akgün, H., & Daemen, J. J. (2000). Influence of degree of saturation on the borehole sealing performance of an expansive cement grout. Cement and concrete research, 30(2), 281-289. https://doi.org/10.1016/S0008-8846(99)00246-X

Calvo, J. G., Carballosa, P., Pedrosa, F., & Revuelta, D. (2022). Microstructural phenomena involved in the expansive performance of cement pastes based on type K expansive agent. Cement and Concrete Research, 158, 106856. https://doi.org/10.1016/j.cemconres.2022.106856

Chen, T., Vennes, I., & Mitri, H. S. (2022). Investigation into Rock Breakage with Expansive Cement Under Biaxial Confinement. Rock Mechanics and Rock Engineering, 55(10), 6263-6277. https://doi.org/10.1007/s00603-022-02988-4

Cho, H., Nam, Y., Kim, K., Lee, J., & Sohn, D. (2018). Numerical simulations of crack path control using soundless chemical demolition agents and estimation of required pressure for plain concrete demolition. Materials and Structures, 51(6), 1-13. https://doi.org/10.1617/s11527-018-1292-y

De Silva, V. R. S., Ranjith, P. G., Perera, M. S. A., Wu, B., & Wanniarachchi, W. A. M. (2018). A low energy rock fragmentation technique for in-situ leaching. Journal of Cleaner Production, 204, 586-606. https://doi.org/10.1016/j.jclepro.2018.08.296

De Silva, V. R. S., Ranjith, P. G., Perera, M. S. A., & Wu, B. (2019). The effect of saturation conditions on fracture performance of different soundless cracking demolition agents (ECs) in geological reservoir rock formations. Journal of Natural Gas Science and Engineering, 62, 157-170. https://doi.org/10.1016/j.jngse.2018.11.013

Dowding, C. H., & Labuz, J. F. (1982). Fracturing of rock with expansive cement. Journal of the Geotechnical Engineering Division, 108(10), 1288-1299. https://doi.org/10.1061/AJGEB6.0001353

Habib, K. M, Shnorhokian S, Mitri H. S (2022) Evaluating the Application of Rock Breakage without Explosives in Underground Construction—A Critical Review of Chemical Demolition Agents. Minerals.12(2):220. https://doi.org/10.3390/min12020220

Habib, K. M., Vennes, I., & Mitri, H. S. (2023). Methodology for the estimation of expansive cement borehole pressure. International Journal of Mining Science and Technology. Volume 33, Issue 1, Pages 73-81. https://doi.org/10.1016/j.ijmst.2022.09.019

Hinze, J., & Brown, J. (1994). Properties of soundless chemical demolition agents. Journal of construction engineering and management, 120(4), 816-827. https://doi.org/10.1061/(ASCE)0733-9364(1994)120:4(816)

Huynh, M. P., & Laefer, D. F. (2009). Expansive cements and soundless chemical demolition agents: state of technology review. In Presented at the 11th Conference on Science and Technology, Ho Chi Minh City Vietnam, October 21-23, 2009.

Jiang, Z., Zheng, W., Li, R., & Guo, C. (2021). A computational model for thick concrete slab demolition using soundless chemical demolition agent. Construction and Building Materials, 303, 124430. https://doi.org/10.1016/j.conbuildmat.2021.124430

Kim, K., Cho, H., Sohn, D., & Lee, J. (2021). The use of expansive chemical agents for concrete demolition: Example of practical design and application. Construction and Building Materials, 272, 121849. https://doi.org/10.1016/j.conbuildmat.2020.121849

Laefer, D. F., Natanzi, A. S., & Zolanvari, S. I. (2018). Impact of thermal transfer on hydration heat of a Soundless Chemical Demolition Agent. Construction and Building Materials, 187, 348-359.

Li, R., Yan, Y., Jiang, Z., Zheng, W., & Li, G. (2021). Impact of hole parameters and surrounding constraint on the expansive pressure distribution and development in soundless chemical demolition agents. Construction and Building Materials, 307, 124992. https://doi.org/10.1016/j.conbuildmat.2018.07.168

Lu, J. X., Shen, P., Sun, Y., & Poon, C. S. (2022). Strategy for preventing explosive spalling and enhancing material efficiency of lightweight ultra high-performance concrete. Cement and Concrete Research, 158, 106842. https://doi.org/10.1016/j.cemconres.2022.106842

Manatunga, U. I., Ranjith, P. G., De Silva, V. R. S., & Wanniarachchi, W. A. M. (2021). Modified non-explosive expansive cement for preconditioning deep host rocks: A review. Geomechanics and Geophysics for Geo-Energy and Geo-Resources, 7(4), 1-30. https://doi.org/10.1007/s40948-021-00292-z

Natanzi, A. S., & Laefer, D. F. (2014). Using chemicals as demolition agents near historic structures. In 9th International Conference on Structural Analysis of Historical Constructions, Mexico City, Mexico, 14-17 October, 2014.

Shang, J., Hencher, S. R., West, L. J., & Handley, K. (2017). Forensic excavation of rock masses: a technique to investigate discontinuity persistence. Rock Mechanics and Rock Engineering, 50(11), 2911-2928. https://doi.org/10.1007/s00603-017-1290-3

Xu, S., Hou, P., Li, R., & Cai, M. (2021). An experimental study on the mechanical properties and expansion characteristics of a novel self-swelling cartridge for rock breakage. Rock Mechanics and Rock Engineering, 54(2), 819-832. https://doi.org/10.1007/s00603-020-02305-x

Yutong, G., Zhiming, J., Chuanyi, D., & Qingbin, Z. (2023). Enhanced effect of self-propagating subsequent heating on the expansive pressure on soundless chemical demolition agent. Construction and Building Materials, 364, 129866. https://doi.org/10.1016/j.conbuildmat.2022.129866

Chapter 7: Conclusions

7.1 Research summary

The method of drilling and blasting with explosives has been the dominant rock fragmentation method in engineering projects such as construction, mining, and oil and gas. As the demand for mineral resources is expected to grow rapidly over the coming decades, rock fragmentation activities will also increase. However, the widely used drilling and blasting method is known to create toxic fumes including green house gas (GHG) emissions, uncontrollable vibrations, fly rocks, noise, and dust. The practice of drilling and blasting method must follow stringent safety and health regulations. With looming concerns over climate change due to the production of GHG emissions, this thesis is part of a multi-phase project that aims to establish a reliable approach for rock breakage in underground mines without the use of explosives. More specifically, it focuses on large-scale experiment design and the investigation of the SCDA performance to break hard rock subjected to biaxial confinement.

- A thorough review of SCDA development and recent applications for rock breakage is carried out in Chapter 2. Earlier literature of SCDA experiments focuses on the SCDA performance in laboratory tests, such as measuring SCDA peak pressure in thick-walled steel cylinder tests, exploring the effect of additives, temperature, and borehole diameter on SCDA performance.
- In terms of rock breakage application, the SCDA method has been initially tried to break surface rock and concrete in civil engineering projects. Several studies report the optimized SCDA hole pattern and spacing design based on laboratory tests and numerical modelling for concrete breakage under no confining stress. Recently, there has been a renewed interest

in SCDA beyond its traditional surface applications due to the merits of SCDA over explosives. The use of SCDA is now anticipated for hard rock roof breaking in coal mines, in-situ leaching, rock fracturing in oil and gas reservoirs, and underground metal mines.

- Based on the literature review, it is believed the proposed SCDA method has great potential as a viable alternative to explosives for underground rock face excavation applications such as underbreak slashing and drift face advance. However, more studies need to conduct to validate such method for large-scale hard rock fragmentation underground. The following challenges that exist in subsurface environments must be addressed.
    - Lack of knowledge and prior hands-on experience with in-situ trials involving the use of SCDA in underground mines where the rock is presumably stiffer and stronger than concrete and rock encountered in surface applications.
    - The underground host rock around the SCDA borehole will be subjected to high biaxial confinement that suppresses the expansion of SCDA and affect the rock fracturing results. However, there is little research that investigates the performance of SCDA for rock breakage under biaxial confinement.
    - It is difficult to use the traditional pumping method for SCDA charging in the holes. A viable loading method of SCDA slurry into underground horizontal, up-tilted boreholes, or wet boreholes has not been established yet.
- In chapter 3, the drillhole pattern design for SCDA method to break a rock face is conducted using numerical modelling code PFC2D based on discrete-element method. Five 60 cm × 60 cm concrete panels with different drillhole patterns are created in PFC2D and loaded with biaxial stresses of 23 MPa and 15 MPa. An SCDA simulation scheme is put forward to represent the SCDA expansive pressure. The diamond-shaped pattern is

found to be superior to others as the applied SCDA pressure leads to more fractures in PFC2D modelling.

- Two patterns including the most promising diamond-shaped pattern are selected for indoor large-scale experiments. Two 1 m × 1 m × 0.25 m high-strength concrete panels are prepared and drilled with the two patterns. The panels are loaded with 23 MPa and 15 MPa using large-scale loading system and charged with SCDA. The results show the first panel had minor cracks and the panel with diamond-shaped drillholes was successfully fractured in 11 hours and 50 mins. The experiments validate the results of numerical modelling and shed light on the use of SCDA to fracture rock-like material under biaxial confinement.
- In Chapter 4, the proposed diamond-shaped pattern is further examined in 1 m × 1 m × 0.25 m Standstead granite panel subjected to 40 MPa and 26 MPa biaxial confinements. The results are compared with the concrete panel. Using larger-diameter SCDA borehole, the initial fracturing of the granite panel occurred at 3 hours. The granite panel completely failed in 7 hours and 18 mins, which is about 4.5 hours earlier than the failure of the concrete panel. Acoustic emission (AE), biaxial loads, and displacement monitoring reveal distinct fracturing process due to SCDA between two panels. The concrete panel experienced continuous out-of-plane creeping, confining pressure loss and gradual AE energy increase, while the granite panel had less out-of-plane displacements and showed a staircase curve of cumulative AE energy release.
- Both concrete and granite tests on diamond-shaped drillholes show that SCDA leads to significant out-of-plane fractures in biaxially loaded panels, but this could not be reflected by PFC2D models due to code limitations. Therefore, 3D modelling code FLAC3D is employed to reconstruct the failure processes of the two panels. FLAC3D model shows

that the diamond-shaped drilling pattern effectively shadows the high confining pressures around SCDA holes by using empty relief or shield holes, which facilitate the expansion of SCDA under high confinements. Poisson's ratio of SCDA materials is calibrated to be 0.15 for FLAC3D models. The simulation results of the panel breakage tests are highly consistent with test observations. FLAC3D modelling confirms the panel failure mechanisms of the two panels. The concrete panel experienced a combination of ductile tensile failures and eventual bridge shear failures, while the granite panel with higher shear strength underwent dominant brittle tensile failures.

- In Chapter 5, a novel V-cut drill hole pattern employing two sets of three SCDA holes angled at 45º from the face is proposed for the rock face breakage application of SCDA. The V-cut uses only small diameter SCDA holes without the needs for empty stress shield holes. It also requires less drilling accuracy than long parallel holes. Therefore, it can be easily applied in tunneling and drifting projects.
- Two Standstead granite panels of 1 m x 1 m x 0.25 m were loaded biaxially corresponding to an in-situ stress state of 1000 m depth in the Canadian shield. Two panels were successfully demolished after 11 hours 53 minutes and 7 hours 29 minutes with the proposed V-cut drilling patten using SCDA. Acoustic emission data shows that the panel test undergoes three phases: SCDA pressure buildup, steady micro-fracture development, and unstable fracture development.
- FLAC3D modelling is also employed to analyze the V-cut panel failure process and the results are comparable to experimental observations. It can be discerned that the SCDA pressure required to initiate panel cracking is 10 MPa. FLAC3D modelling validated the behaviour of the V-cut experiments in terms of observed panel out-of-plane deformation

and tensile failure progressive failure mechanisms. The proposed modeling method can be used to further optimize the SCDA pattern and estimate V-cut field performance in mine-wide models.

- A new SCDA cartridge loading method is put forward in Chapter 6. This work addresses the field charging problem of SCDA slurry into horizontal, up-tilt, or wet boreholes, as well as boreholes open at two ends, which cannot be charged by pouring the slurry by gravity. Various cartridge prototypes are design and produced with 3D printing at low cost and available plastic materials, namely PLA, TPU, ABS and PETG. The performance of each cartridge is investigated in unconfined rock slab demolition tests with single SCDA hole. A positive correlation is found between slab fracturing time and the cartridge material stiffness. The most ductile TPU cartridge does not crack the rock slab, while the PLA cartridge with the highest stiffness gives the best fragmentation performance.
- The slab demolition tests show that PLA cartridge improves SCDA efficiency for rock breakage. PLA cartridge can reduce the needed rock breakage time by 30% from 11 hours MDT (without cartridge) to 7.6 hours MDT due to partial heat containment of the host material.
- A field test was undertaken in an underground mine to demonstrate the advantage of the novel cartridge method for potentially expanded SCDA applications. An underground rock intersection was successfully demolished using three 1 m long SCDA-filled PLA cartridges inserted in horizontal boreholes open at two ends. The proposed cartridge loading method for SCDA not only suits various application requirements beyond the scope of present SCDA surface applications with vertical holes, but significantly improves the rock fracturing efficiency due to SCDA.

7.2 Research conclusions

From the research presented in this thesis, the following conclusions may be drawn.

- A state-of-the art literature review has been conducted on the development and current application range of SCDA method, showing great potential for using SCDA for underground hard rock breakage.
- Large-scale experimental program is designed to test SCDA performance to break high-strength concrete and Stanstead granite panels of 1 m x 1 m x 0.25 subjected to biaxial loads. The rock panel represents a mine drift front subjected to biaxial confinement, and the loading corresponds to a virgin stress level of 1000 m underground in the Canadian shield.
- SCDA drillhole pattern under biaxial stress state is optimized based on PFC2D modelling. Diamond-shaped pattern is found to have the maximum fracturing efficiency.
- With the diamond-shaped pattern, biaxially confined panels from concrete and granite are successfully demolished in a relatively short period of time.
- FLAC3D modelling shows the diamond pattern facilitates the panel fracturing under high confinements, because empty holes around SCDA holes effectively shield the confining pressures.
- Distinct failure mechanisms of the concrete and rock panels with the diamond pattern are discerned in FLAC3D models based on Mohr-Column yielding criterion.
- V-cut drill hole pattern that requires less boreholes and drilling accuracy is proposed for the rock face advance using SCDA. Two Stanstead granite panels under high biaxial stress are successfully demolished using V-cut.

- Based on FLAC3D modelling, the SCDA pressure required to initiate the cracking of V-cut granite panel is 10 MPa.
- A feasible SCDA loading method using PLA cartridge is developed. Such method solves the problem of charging SCDA slurry into horizontal, uptilted or wet boreholes, as well as boreholes open at two ends that might be encountered in underground mines.
- PLA cartridge can improve SCDA efficiency for rock breakage by 30% due to partial heat containment of the host material.

7.3 Technical-economic considerations of SCDA

The focus of the present thesis is on the mechanical performance of SCDA and how it can be utilized to fracture a biaxially loaded rock panel. While it may be premature, the following discussion sheds light on the potential economic benefits of SCDA as a means for hard rock breakage in mines and tunnels. Needless to say, traditional methods of drilling and blasting are most suited for large scale production in surface and underground mines. Hence, rock fragmentation with explosives remains most effective for such applications.

That said, this research has revealed several important economic aspects about the use of SCDA for hard rock breakage. First, the application of SCDA for small scale tasks in underground mines such as slashing a corner at an intersection or creating crater in the sidewall for use as a safety bay in a mine development is far more convenient to do with SCDA than with blasting with explosives. The use of blasting in such small-scale applications is likely to create excavation overbreak and cause damage to the host rock. Furthermore, the use of SCDA does not require that mining activities be halted for a certain period (usually 2 hours) for ventilating the excavation area. Thus, it can be claimed that unlike blasting with explosive energy, SCDA does not create overbreak nor

damage to the wall rock, and this is due to the docile nature of rock breakage. It can also be claimed that SCDA are economical in the sense that they do not require additional ventilation.

In addition to potential cost savings on ventilation, the use of SCDA for underground construction can also improve project timelines. The application of SCDA can be carried out 24 hours a day as there is no need to vacate the work area. This could lead a paradigm shift in project scheduling going from two 10-hour shifts to three 8-hour shifts, an increase in production time of 20%.

Furthermore, SCDA does not produce noise nor vibrations. This is an especially important feature in shallow excavations such as subway tunnels passing underneath existing urban infrastructure. The fact that there is no dust, vibration, nor noise associated with SCDA lends to suggesting lower risk of accidents and improved worker safety on the job site. With increased safety and efficiency, projects can be completed faster and with less disruption to surrounding areas.

Overall, the use of SCDA could provide a cost-effective and efficient solution for underground construction, with the potential for economic benefits over blasting with explosive energy.

7.4 Contribution to original knowledge

This thesis has contributed to advancing explosive-free rock breakage method using SCDA. Through the examination of SCDA method for rock panel breakage under high biaxial confinement, this work has demonstrated the feasibility of face rock breakage in underground mines without explosives. This work lays the foundation for potential SCDA application in underground hard rock mines and tunnels when the use of explosives is to be avoided, restricted, or prohibited. The contributions in detail are as follows.

- Developed a PFC2D modelling scheme to simulate progressive SCDA expansion and optimize SCDA drillhole pattern.

- Conducted large-scale indoor tests on panels subjected to biaxial loads which mimics the stress state of a mining front in laboratory.
- Investigated the SCDA performance under biaxial confinements with the proposed drillhole patterns.
- Observed significant panel out-of-plane cracking and bulging deformation due to SCDA under biaxial loading. This new finding expands current knowledge of how SCDA works under biaxial confinement.
- Proposed and examined V-cut drillhole pattern for the rock face breakage application of SCDA.
- Examined panel failure mechanisms with diamond and V-cut patterns via FLAC3D modelling.
- Developed a novel cartridge loading method for SCDA slurry into boreholes to reduce the application requirement of SCDA and improve SCDA rock breakage efficiency.

7.5 Suggestions for future research

The research done for this thesis has uncovered several research questions that can be investigated further in extensive studies. The list of recommendations for future research to expand on the work completed in this study is included below.

- This thesis comprehensively investigated the feasibility of SCDA method for rock face breakage in laboratory. Field trials are required to conduct in underground mines to finalize the practical guidelines and hands-on instructions of this method.
- Potential SCDA applications in underground mines based on the developed approaches in this thesis can be explored in future studies.

- This study employed a large-scale biaxial loading system to test the intact Stanstead panel under biaxial stresses up to 40 MPa and 26 MPa, which corresponds to a virgin stress condition of 1000 m underground in the Canadian shield. The validated FLAC3D model can further be used in a parametric study on the optimal SCDA drillhole pattern and spacing for different mining depths (confining stresses) and rock mass properties.
- To set the stage for future research involving in-situ tests, several mine drift front models can be built with the established FLAC3D modelling scheme in this thesis. The performance of several SCDA drill hole patterns in an underground mine where the mining face is subjected to true constraints from the host rock can be examined.
- This study examines the performance of SCDA indoor in room temperature. However, the temperature in an underground mine varies with depth and season, which may significantly impact the performance of SCDA. It would be interesting to explore how the SCDA performance could be affected by change of the rock temperature in underground mines.
- It would be useful to eventually conduct an efficiency evaluation of the SCDA method, and the following aspects can be assessed. 1) the quantity of SCDA used per meter square of the mining face, 2) estimated fragment size, and 3) out-of-plane deformations. This information could serve as a foundation for the implementation of SCDA method in underground mines.

References

Al-Bakri, A., & Hefni, M. (2021). A review of some nonexplosive alternative methods to conventional rock blasting. Open Geosciences, 13(1), 431-442.

Arshadnejad, S., Goshtasbi, K., & Aghazadeh, J. (2011). A model to determine hole spacing in the rock fracture process by non-explosive expansion material. International Journal of Minerals, Metallurgy, and Materials, 18(5), 509-514.

ASTM (2004) Standard Specification for Expansive Hydraulic Cement. In Annual Book of ASTM Standards; 845 Standard; West Conshohocken, PA, USA, 2004; pp. 390–393.

Buffington, G. L. (2000). The art of blasting on construction and surface mining sites. In ASSE Professional Development Conference and Exposition. OnePetro.

Chen, T., Vennes, I., & Mitri, H. S. (2022). Investigation into Rock Breakage with Expansive Cement Under Biaxial Confinement. Rock Mechanics and Rock Engineering, 55(10), 6263-6277.

Cho, H., Nam, Y., Kim, K., Lee, J., & Sohn, D. (2018). Numerical simulations of crack path control using soundless chemical demolition agents and estimation of required pressure for plain concrete demolition. Materials and Structures, 51(6), 1-13.

Christmann, P., & Lefebvre, G. (2022). Trends in global mineral and metal criticality: the need for technological foresight. Mineral Economics, 1-12.

Conti, J., Holtberg, P., Diefenderfer, J., LaRose, A., Turnure, J. T., & Westfall, L. (2016). International energy outlook 2016 with projections to 2040. USDOE Energy Information Administration, Washington, DC, USA. Office of Energy Analysis.

D’Hugues, P., Bourg, S., & Menard, Y. (2022). From mineral processing to waste management and recycling: common challenges and needs for innovation in France. Mineral Economics, 35(3), 563-567.

De Silva, R. V., Pathegama Gamage, R., & Anne Perera, M. S. (2016). An alternative to conventional rock fragmentation methods using SCDA: a review. Energies, 9(11), 958.

De Silva, V. R. S., Ranjith, P. G., Perera, M. S. A., Wu, B., & Rathnaweera, T. D. (2017). Investigation of the mechanical, microstructural and mineralogical morphology of soundless cracking demolition agents during the hydration process. Materials Characterization, 130, 9-24.

De Silva, V. R. S., Ranjith, P. G., Perera, M. S. A., Wu, B., & Rathnaweera, T. D. (2018). A modified, hydrophobic soundless cracking demolition agent for non-explosive demolition and fracturing applications. Process Safety and Environmental Protection, 119, 1-13.

De Silva, V. R. S., Ranjith, P. G., Perera, M. S. A., & Wu, B. (2019a). The effect of saturation conditions on fracture performance of different soundless cracking demolition agents (SCDAs) in geological reservoir rock formations. Journal of Natural Gas Science and Engineering, 62, 157-170.

De Silva, V. R. S., & Ranjith, P. G. (2019b). Intermittent and multi-stage fracture stimulation to optimise fracture propagation around a single injection well for enhanced in-situ leaching applications. Engineering Fracture Mechanics, 220, 106662.

De Silva, V. R. S., & Ranjith, P. G. (2020). A study of rock joint influence on rock fracturing using a static fracture stimulation method. Journal of the Mechanics and Physics of Solids, 137, 103817.

Drake, B., Koroznikova, L., Tuck, M., & Durkin, S. (2020). Application of thermal fragmentation in Australian hard rock underground narrow-vein mining. Mining, Metallurgy & Exploration, 37(1), 219-229.

Gad, E. F., Wilson, J. L., Moore, A. J., & Richards, A. B. (2005). Effects of mine blasting on residential structures. Journal of Performance of Constructed Facilities, 19(3), 222-228.

Habib, K. M. (2022). Development of explosive-free method for the breakage of hard rock using soundless chemical demolition agents, PhD Thesis, McGill University (Canada).

Habib, K. M, Shnorhokian S, Mitri H. S (2022) Evaluating the Application of Rock Breakage without Explosives in Underground Construction—A Critical Review of Chemical Demolition Agents. Minerals.12(2):220.

Habib, K. M, Vennes, I., & Mitri, H. S. (2023). Methodology for the estimation of expansive cement borehole pressure. International journal of mining science and technology. Volume 33, Issue 1, Pages 73-81.

Harada, T., Idemitsu, T., Watanabe, A., & Takayama, S. I. (1989). The design method for the demolition of concrete with expansive demolition agents. In Fracture of Concrete and Rock (pp. 47-57). Springer, New York, NY.

Hinze, J., & Brown, J. (1994). Properties of soundless chemical demolition agents. Journal of construction engineering and management, 120(4), 816-827.

Huynh, M. P., & Laefer, D. F. (2009). Expansive cements and soundless chemical demolition agents: state of technology review. In Presented at the 11th Conference on Science and Technology, Ho Chi Minh City Vietnam, October 21-23, 2009.

Huo, X., Shi, X., Qiu, X., Zhou, J., Gou, Y., Yu, Z., & Ke, W. (2020). Rock damage control for large-diameter-hole lateral blasting excavation based on charge structure optimization. Tunnelling and Underground Space Technology, 106, 103569.

Huang, Z., Zhang, S., Yang, R., Wu, X., Li, R., Zhang, H., & Hung, P. (2020). A review of liquid nitrogen fracturing technology. Fuel, 266, 117040.

Ish-Shalom, M., & Bentur, A. (1975). Properties of type K expansive cement of pure components III. Hydration of pure expansive component under varying restraining conditions. Cement and Concrete Research, 5(2), 139-152.

Ikkurthi, V. R., Tahiliani, K., & Chaturvedi, S. (2002). Simulation of crack propagation in rock in plasma blasting technology. *Shock Waves*, *12*(2), 145-152.

Itasca Consulting Group, Inc. (2021) PFC — Particle Flow Code, Ver. 7.0. Minneapolis: Itasca.

Jiang, Z., Zheng, W., Li, R., & Guo, C. (2021). A computational model for thick concrete slab demolition using soundless chemical demolition agent. Construction and Building Materials, 303, 124430.

Kuznetsova, N., Zhgun, D., & Golovanevskiy, V. (2022). Plasma blasting of rocks and rocks-like materials: An analytical model. International Journal of Rock Mechanics and Mining Sciences, 150, 104986.

Kim, K., Cho, H., Sohn, D., & Lee, J. (2021). The use of expansive chemical agents for concrete demolition: Example of practical design and application. Construction and Building Materials, 272, 121849.

Laefer, D. F., Natanzi, A. S., & Zolanvari, S. I. (2018). Impact of thermal transfer on hydration heat of a Soundless Chemical Demolition Agent. Construction and Building Materials, 187, 348-359.

Li, R., Yan, Y., Jiang, Z., Zheng, W., & Li, G. (2021). Impact of hole parameters and surrounding constraint on the expansive pressure distribution and development in soundless chemical demolition agents. Construction and Building Materials, 307, 124992.

Liu, S., Liu, Z., Cui, X., & Jiang, H. (2014). Rock breaking of conical cutter with assistance of front and rear water jet. Tunnelling and Underground Space Technology, 42, 78-86.

Liu, S., Cui, Y., Cui, S., Li, Z., Zhou, F., & Wang, H. (2021). Experimental investigation on rock fracturing performance under high-pressure foam impact. Engineering Fracture Mechanics, 252, 107838.

Liu, H., Li, W., Guan, W., Zhao, H., Junhui, Y., & Yingyuan, W. (2022). Mechanistic Study of a Microwave Field-Controlled Static Crushing Agent for Efficient Rock Breaking. ACS omega, 7(33), 29344-29355.

Manatunga, U. I., Ranjith, P. G., De Silva, V. R. S., & Wanniarachchi, W. A. M. (2021). Modified non-explosive expansive cement for preconditioning deep host rocks: A review. Geomechanics and Geophysics for Geo-Energy and Geo-Resources, 7(4), 1-30.

Natanzi, A. S., & Laefer, D. F. (2014). Using chemicals as demolition agents near historic structures. In 9th International Conference on Structural Analysis of Historical Constructions, Mexico City, Mexico, 14-17 October, 2014.

Natanzi, A. S., Laefer, D. F., & Connolly, L. (2016). Cold and moderate ambient temperatures effects on expansive pressure development in soundless chemical demolition agents. Construction and Building Materials, 110, 117-127.

Natanzi, A. S., Laefer, D. F., Kakali, G., & Iman Zolanvari, S. M. (2019). Temperature-Induced Chemical Changes in Soundless Chemical Demolition Agents. Journal of Materials in Civil Engineering, 31(7), 04019098.

Natanzi, A. S., Laefer, D. F., & Zolanvari, S. I. (2020). Selective demolition of masonry unit walls with a soundless chemical demolition agent. Construction and Building Materials, 248, 118635.

Vrontisi, Z., Charalampidis, I., & Paroussos, L. (2020). What are the impacts of climate policies on trade? A quantified assessment of the Paris Agreement for the G20 economies. Energy Policy, 139, 111376.

Odell, S. D., Bebbington, A., & Frey, K. E. (2018). Mining and climate change: A review and framework for analysis. The extractive industries and society, 5(1), 201-214.

Qiu, Z., Ji, Y., Zhang, F., & Yan, G. (2021). Experimental Investigation and Numerical Modeling of Elastic Modulus Variation with Stress during Hydration and Expansion Process of Static Cracking Agent. Applied Sciences, 11(9), 3955.

Sainoki, A., & Mitri, H. S. (2014). Numerical simulation of rock mass vibrations induced by nearby production blast. Canadian geotechnical journal, 51(11), 1253-1262.

Stoxreiter, T., Martin, A., Teza, D., & Galler, R. (2018). Hard rock cutting with high pressure jets in various ambient pressure regimes. International Journal of Rock Mechanics and Mining Sciences, 108, 179-188.

Shang, J., Hencher, S. R., West, L. J., & Handley, K. (2017). Forensic excavation of rock masses: a technique to investigate discontinuity persistence. Rock Mechanics and Rock Engineering, 50(11), 2911-2928.

Tang, Y., Yuan, L., Xue, J., & Duan, C. (2017). Experimental study on fracturing coal seams using CaO demolition materials to improve permeability. Journal of Sustainable Mining, 16(2), 47-54.

Tang, W., Zhai, C., Xu, J., Sun, Y., Cong, Y., & Zheng, Y. (2021). The influence of borehole arrangement of soundless cracking demolition agents (SCDAs) on weakening the hard rock. International Journal of Mining Science and Technology, 31(2), 197-207.

Tang, W., Zhai, C., Xu, J., Yu, X., Sun, Y., Cong, Y., ... & Zhu, X. (2022). Numerical simulation of expansion process of soundless cracking demolition agents by coupling finite difference and discrete element methods. Computers and Geotechnics, 146, 104699.

Timoshenko, S., & Goodier, J. N. Theory of elasticity. 1951. New York, 412, 108.

Wang, S., Mitri, H., Li, H., Li, D., & Wang, W. (2018). Study of SCA-induced rock crack propagation under different stress conditions using a modified cohesive element method. Advances in Civil Engineering, 2018.

Wang, S., Liu, Z., Zhang, K., & Zheng, H. (2022a). Damage Mechanism and Stress Distribution of Gypsum Rock Pillar Subjected to Blasting Disturbance. Sustainability, 14(9), 5010.

Wang, L., Duan, K., Zhang, Q., Li, X., & Jiang, R. (2022b). Study of the Dynamic Fracturing Process and Stress Shadowing Effect in Granite Sample with Two Holes Based on SCDA Fracturing Method. Rock Mechanics and Rock Engineering, 1-17.

Xu, J., Zhai, C., Ranjith, P. G., Sun, Y., Qin, L., Ma, H., ... & Ma, Z. (2019). Investigation of non-explosive expansion material in roof caving field application. International Journal of Rock Mechanics and Mining Sciences, 120, 50-57.

Xu, S., Hou, P., Li, R., & Cai, M. (2021). An experimental study on the mechanical properties and expansion characteristics of a novel self-swelling cartridge for rock breakage. Rock Mechanics and Rock Engineering, 54(2), 819-832.

Xu, S., Hou, P., Li, R., & Suorineni, F. T. (2022). An improved outer pipe method for expansive pressure measurement of static cracking agents. International Journal of Mining Science and Technology, 32(1), 27-39.

Zhao, X., Huang, B., & Xu, J. (2019). Experimental investigation on the characteristics of fractures initiation and propagation for gas fracturing by using air as fracturing fluid under true triaxial stresses. Fuel, 236, 1496-1504.